

**A Comparative In Vitro Study of the
Flow Characteristics Distal to
Mechanical and Natural Mitral Valves**

Amber Rae Mace

A thesis submitted to the Faculty of the Virginia
Polytechnic Institute and State University in partial
fulfillment of the requirements for the degree of

Master of Science

in

Engineering Mechanics

December 16, 2002

Dr. Demetri P. Telionis, Committee Chairman

Dr. Pavlos P. Vlachos

Dr. J. W. Grant

Dr. R. Lee Pyle

Keywords: Mechanical heart valves, mitral leaflets, chordae tendineae,
St. Jude Medical, vorticity, DPIV

Copyright 2002, Amber Rae Mace

ABSTRACT

A Comparative In Vitro Study of the Flow Characteristics Distal to Mechanical and Natural Mitral Valves

Amber Rae Mace

Mechanical heart valve (MHV) flows are characterized by high shear stress, regions of recirculation, and high levels of turbulent fluctuations. It is well known that these flow conditions are hostile to blood constituents, which could lead to thromboembolism. In the ongoing effort to reduce long-term complications and morbidity, it is imperative that we better understand the flow characteristics of the natural valve as well as that of the mechanical valve. In this study, we overcome many of the limitations imposed by other measurement techniques by employing a powerful, high-speed Time-Resolved Digital Particle Image Velocimetry (TRDPIV) system to map the flow field. We compare the flows downstream from a St. Jude Medical bileaflet MHV, a porcine mitral valve (MV), and a combination of both valves to simulate the technique of chordal preservation. Instantaneous velocity fields and vorticity maps are presented, which provide detailed information about the development of the flow. Time-averaged velocity, vorticity, and turbulent kinetic energy measurements are also discussed. Asynchronous leaflet behavior was observed in all cases involving the mechanical valve. Extensive vortex formation and propagation are present distal to the MHV, which leads to high levels of jet dispersion. The porcine mitral jet exhibits lateral oscillatory behavior, but it does not disperse like the MHV. In the MHV/porcine combination system, the native tissue limits vortex propagation and jet dispersion. The results presented provide insight on the hemodynamic characteristics of natural and MHVs, reveal the detrimental character of asynchronous leaflet opening, document the mechanism of vortex formation and interaction distal to the valve, and illustrate the importance of chordal preservation. These results may improve MHV replacement clinical practice and/or motivate and aid the design of MHVs that better mimic natural mitral flow patterns.

TABLE OF CONTENTS

CHAPTER 1	1
1 INTRODUCTION AND ANATOMICAL REVIEW	1
1.1 MOTIVATION	1
1.2 THE MITRAL VALVE APPARATUS	3
1.3 MITRAL VALVE DISEASE, REPAIR, AND REPLACEMENT	8
1.4 ARTIFICIAL HEART VALVE PROSTHESES	9
CHAPTER 2	11
2 LITERATURE REVIEW	11
2.1 AHV FLOW FIELD STUDIES	11
2.1.1 EXPERIMENTAL WORK	11
2.1.2 LIMITATIONS.....	13
2.1.3 RELATED DPIV STUDIES	14
2.2 INFLUENCE OF NATIVE MITRAL TISSUE, CLINICAL RESULTS.....	17
2.3 CONTRIBUTION.....	22
CHAPTER 3	23
3 EXPERIMENTAL FACILITIES AND METHODS	23
3.1 LEFT VENTRICULAR SIMULATOR.....	23
3.2 SETUP AND CONFIGURATIONS	25
3.3 DATA ACQUISITION AND ADDITIONAL INSTRUMENTATION.....	26
CHAPTER 4	28
4 EXPERIMENTAL RESULTS AND DISCUSSION	28
4.1 INSTANTANEOUS RESULTS.....	28
4.1.1 BILEAFLET MHV	28
4.1.2 PORCINE MV	34
4.1.3 CHORDAL PRESERVATION	40
4.2 TIME-AVERAGED RESULTS	45
4.2.1 VELOCITY AND VORTICITY	45
4.2.2 ADDITIONAL PLANES OF DATA	48
4.2.3 TURBULENT KINETIC ENERGY	53
4.2.4 VELOCITY PROFILES DISTAL TO THE VALVES	61
4.3 DISCUSSION	65
4.3.1 LEAFLET MOTIONS.....	65

4.3.2	VORTEX SHEDDING	72
4.3.3	MITRAL JET DISPERSION	77
CHAPTER 5	79
5	CONCLUSIONS AND FUTURE WORK	79
REFERENCES	81
VITA	87

LIST OF FIGURES

FIGURE 1.1: ANATOMY OF THE HEART.	4
FIGURE 1.2: (A) DIAGRAM OF THE CARDIAC SKELETON, (B) THE MITRAL LEAFLETS AND ANNULUS. (ST. JUDE MEDICAL, 2000)	5
FIGURE 1.3: (A) DIAGRAM ILLUSTRATING THE TWO MITRAL LEAFLETS, ANTERIOR AND POSTERIOR, (B) MITRAL VALVE SHOWING THREE SCALLOPED PORTIONS OF THE POSTERIOR LEAFLET. (ST. JUDE MEDICAL, 2000).....	5
FIGURE 1.4: (A) VIEW OF ANTERIOR LEAFLET SHOWING THE MITRAL LEAFLET ROUGH ZONE AND INSERTION OF CHORDAE TENDINEAE. SCALE INDICATES 5-MM. (RANGANATHAN ET AL.,1976) (B) DIAGRAM OF MITRAL VALVE, ILLUSTRATING THE ARRANGEMENT OF THE CHORDAE TENDINEAE. A-ANTERIOR CUSP, M-MEDIAL CUSP, P-POSTERIOR CUSP, L-LATERAL CUSP. 1. MAJOR FIXING CHORDA TO ANTERIOR CUSP. 2. LATERAL FIXING CHORDA TO ANTERIOR CUSP. 3. COMMISSURAL CHORDA. 4. MAJOR FIXING CHORDAE LATERAL AND MEDIAL CUSPS. 5. COMMISSURAL CHORDA. 6. LATERAL FIXING OF POSTERIOR CUSP. 7. MAJOR FIXING OF POSTERIOR CUSP. (YACOUB, 1976)	6
FIGURE 1.5: MOTION OF BEADS PLACED ON THE FREE EDGES OF ANTERIOR AND POSTERIOR CUSPS RECORDED AT A SLOW SINUS RHYTHM OF 51 BPM. DO-DIASTOLIC OPENING, DC-DIASTOLIC CLOSURE, DR – DIASTOLIC REBOUND, AO – ATRIAL OPENING, VC – VENTRICULAR CLOSURE. (TSAKIRIS, 1976)	7
FIGURE 1.6: FOUR ARTIFICIAL HEART VALVE DESIGNS, FROM LEFT TO RIGHT: CAGED BALL VALVE, TILTING DISC VALVE, BILEAFLET VALVE, AND PORCINE BIOPROSTHETIC VALVE. (CAMP, 1997)	9
FIGURE 2.1: (B) VELOCITY AND (C) VORTICITY MAPS DURING THE FULLY OPEN PHASE FOR THE 450 MS TIME POINT. (SUBRAMANIAN ET AL., 2000).....	15
FIGURE 2.2: (A) VELOCITY FIELD DISTAL TO THE VALVE DURING PEAK SYSTOLE (LEAFLETS TIPS AT $y = \pm 0.3$ CM). (B) VORTICITY FIELD DISTAL TO THE VALVE DURING PEAK SYSTOLE. DASHED CONTOURS: CCW ROTATION, SOLID LINES: CW ROTATION. (BLUESTEIN ET AL., 2000).....	16
FIGURE 2.3: TURBULENT PLATELET PATHS THROUGH AREAS OF HIGHEST STRESSES AROUND THE LEAFLET: ABOVE THE LEAFLET (TOP) AND BELOW (BOTTOM), LEADING TO ENTRAPMENT WITHIN THE SHED VORTICES IN THE LEAFLET’S WAKE. THE CORRESPONDING VELOCITY VECTORS ARE SHOWN (PATHS ARE COMPUTED FROM 165 MS TO 419 MS AFTER PEAK SYSTOLE). (BLUESTEIN ET AL., 2000).	16
FIGURE 2.4: SKETCHES ILLUSTRATING THE 2-D FLOW PATTERNS FOR THE ST. JUDE MEDICAL BILEAFLET VALVE IN THE ANATOMIC POSITION FROM THE VERTICAL LONG AXIS VIEW THROUGH THE VALVE CENTERLINE DURING PEAK DIASTOLE. (FONTAINE ET AL., 1996) 19	19
FIGURE 2.5: MRI IMAGES ILLUSTRATING HEALTHY REDIRECTION OF THE MITRAL JET TOWARD THE AORTIC VALVE. (LAAS ET AL., 2000)	20

FIGURE 2.6: MRI IMAGES SHOWING THE LOSS OF ASYMMETRIC REDIRECTION AFTER IMPLANTATION OF A BILEAFLET MHV. (LAAS ET AL., 2000)	20
FIGURE 2.7: MAGNETIC RESONANCE VELOCITY MAPPING REVEALS ASYMMETRIC FLOW PATTERNS WITHIN THE LV. (E) FLOW THROUGH THE AORTIC VALVE IN SYSTOLE, (F) REDIRECTION OF THE MITRAL JET AROUND THE ANTERIOR LEAFLET IN EARLY DIASTOLE. (KILNER ET AL., 2000)	21
FIGURE 3.1: BASIC SCHEMATIC OF THE LEFT VENTRICULAR SIMULATOR.	23
FIGURE 3.2: SCHEMATIC OF THE LEFT VENTRICULAR CHAMBER WITH THE BILEAFLET MHV AND PORCINE MITRAL VALVE MOUNTED ONTO THE ATRIAL INFLOW PIPE.	24
FIGURE 3.3: (A) ST. JUDE MEDICAL BILEAFLET MHV. (B) EXCISED PORCINE MITRAL VALVE APPARATUS.	25
FIGURE 3.4: SCHEMATIC OF A TYPICAL DPIV SETUP.....	26
FIGURE 3.5: SCHEMATIC SHOWING THE ORIENTATION OF THE ILLUMINATED PLANES WITH RESPECT TO THE BILEAFLET MHV.	27
FIGURE 4.1: UNSTEADY VORTICITY DISTRIBUTIONS FOR THE BILEAFLET MHV AT TWO TIME INSTANTS, $T = 0.10$ s AND $T = 0.15$ s.....	30
FIGURE 4.2: UNSTEADY VORTICITY DISTRIBUTIONS FOR THE BILEAFLET MHV AT TWO TIME INSTANTS, $T = 0.20$ s AND $T = 0.25$ s.....	31
FIGURE 4.3: UNSTEADY VORTICITY DISTRIBUTIONS FOR THE BILEAFLET MHV AT TWO TIME INSTANTS, $T = 0.30$ s AND $T = 0.35$ s.....	32
FIGURE 4.4: UNSTEADY VORTICITY DISTRIBUTIONS FOR THE BILEAFLET MHV AT ONE TIME INSTANT, $T = 0.50$ s.....	33
FIGURE 4.5: UNSTEADY VORTICITY DISTRIBUTIONS FOR THE PORCINE MITRAL VALVE AT TWO TIME INSTANTS, $T = 0.10$ s AND $T = 0.15$ s.	36
FIGURE 4.6: UNSTEADY VORTICITY DISTRIBUTIONS FOR THE PORCINE MITRAL VALVE AT TWO TIME INSTANTS, $T = 0.20$ s AND $T = 0.25$ s.	37
FIGURE 4.7: UNSTEADY VORTICITY DISTRIBUTIONS FOR THE PORCINE MITRAL VALVE AT TWO TIME INSTANTS, $T = 0.30$ s AND $T = 0.35$ s.	38
FIGURE 4.8: UNSTEADY VORTICITY DISTRIBUTIONS FOR THE PORCINE MITRAL VALVE AT ONE TIME INSTANT, $T = 0.50$ s.....	39
FIGURE 4.9: UNSTEADY VORTICITY DISTRIBUTIONS FOR THE CHORDAL PRESERVATION CASE AT TWO TIME INSTANTS, $T = 0.10$ s AND $T = 0.15$ s.	41
FIGURE 4.10: UNSTEADY VORTICITY DISTRIBUTIONS FOR THE CHORDAL PRESERVATION CASE AT TWO TIME INSTANTS, $T = 0.20$ s AND $T = 0.25$ s.	42
FIGURE 4.11: UNSTEADY VORTICITY DISTRIBUTIONS FOR THE CHORDAL PRESERVATION CASE AT TWO TIME INSTANTS, $T = 0.30$ s AND $T = 0.35$ s.	43
FIGURE 4.12: UNSTEADY VORTICITY DISTRIBUTIONS FOR THE CHORDAL PRESERVATION CASE AT ONE TIME INSTANT, $T = 0.50$ s.	44
FIGURE 4.13: TIME-AVERAGED VORTICITY DISTRIBUTIONS FOR THE BILEAFLET MHV AND PORCINE VALVE CASES.....	46

FIGURE 4.14: TIME-AVERAGED VORTICITY DISTRIBUTION FOR THE CHORDAL PRESERVATION CASE.....	47
FIGURE 4.15: TIME-AVERAGED VORTICITY DISTRIBUTIONS FOR THREE PLANES, BILEAFLET MHV, $x = 0, 15,$ AND 30	50
FIGURE 4.16: TIME-AVERAGED VORTICITY DISTRIBUTIONS FOR THREE PLANES, PORCINE MITRAL VALVE, $x = 0, 15,$ AND 30	51
FIGURE 4.17: TIME-AVERAGED VORTICITY DISTRIBUTIONS FOR TWO PLANES, CHORDAL PRESERVATION, $x = 0$ AND 15	52
FIGURE 4.18: TIME-AVERAGED TURBULENT KINETIC ENERGY DISTRIBUTIONS FOR THE BILEAFLET MHV AVERAGED OVER 100 FRAMES (TOP) AND 200 FRAMES (BOTTOM).....	55
FIGURE 4.19: TIME-AVERAGED TURBULENT KINETIC ENERGY DISTRIBUTIONS FOR THE BILEAFLET MHV AVERAGED OVER 500 FRAMES.....	56
FIGURE 4.20: TIME-AVERAGED TURBULENT KINETIC ENERGY DISTRIBUTIONS FOR THE PORCINE VALVE AVERAGED OVER 100 FRAMES (TOP) AND 200 FRAMES (BOTTOM).....	57
FIGURE 4.21: TIME-AVERAGED TURBULENT KINETIC ENERGY DISTRIBUTIONS FOR THE PORCINE VALVE AVERAGED OVER 500 FRAMES.....	58
FIGURE 4.22: TIME-AVERAGED TURBULENT KINETIC ENERGY DISTRIBUTIONS FOR THE CHORDAL PRESERVATION CASE AVERAGED OVER 100 FRAMES (TOP) AND 200 FRAMES (BOTTOM).....	59
FIGURE 4.23: TIME-AVERAGED TURBULENT KINETIC ENERGY DISTRIBUTIONS FOR THE CHORDAL PRESERVATION CASE AVERAGED OVER 500 FRAMES.....	60
FIGURE 4.24: ILLUSTRATION OF MHV ORIENTATION AND TYPICAL Y/D LOCATIONS WHERE THE VELOCITY PROFILES ARE CALCULATED	61
FIGURE 4.25: TIME-AVERAGED VELOCITY PROFILES FOR FIVE Y/D LOCATIONS DISTAL TO THE BILEAFLET MHV (TOP) AND PORCINE MITRAL VALVE (BOTTOM)	63
FIGURE 4.26: TIME-AVERAGED VELOCITY PROFILES FOR FIVE Y/D LOCATIONS DISTAL TO THE COMBINATION CASE (TOP) AND PROFILES AT $Y/D = 2.5$ FOR THREE TEST CASES (BOTTOM)	64
FIGURE 4.27: FLOW VISUALIZATION IMAGES ILLUSTRATING MITRAL JET DEVELOPMENT IN A CASE WITH SYMMETRIC MITRAL LEAFLET OPENING.....	66
FIGURE 4.28: FLOW VISUALIZATION IMAGES ILLUSTRATING MITRAL JET DEVELOPMENT IN A CASE WITH SYMMETRIC MITRAL LEAFLET OPENING.....	67
FIGURE 4.29: UNSTEADY VORTICITY DISTRIBUTIONS FOR TWO BILEAFLET MHVs AT $T = 0.20$ S: ASYMMETRIC LEAFLET OPENING (TOP) AND SYMMETRIC LEAFLET OPENING (BOTTOM).....	68
FIGURE 4.30: TIME-AVERAGED VORTICITY DISTRIBUTIONS FOR TWO BILEAFLET MHVs: ASYMMETRIC LEAFLET OPENING (TOP) AND SYMMETRIC LEAFLET OPENING (BOTTOM).....	69
FIGURE 4.31: ILLUSTRATION OF THE EFFECT OF THE VORTEX SHED FROM THE LEFT LEAFLET ON THE MITRAL JET BEHAVIOR.....	70
FIGURE 4.32: MAXIMUM VELOCITY POINTS AT VARIOUS Y/D LEVELS ILLUSTRATE HOW THE MITRAL JETS SHIFT Laterally.....	71

FIGURE 4.33: UNSTEADY VORTICITY DISTRIBUTIONS WITH STREAMLINES AT TWO TIME INSTANTS, $T = 0.20$ s AND $T = 0.30$ s.....	75
FIGURE 4.34: UNSTEADY VORTICITY DISTRIBUTIONS WITH STREAMLINES AT $T = 0.35$ s.	76
FIGURE 4.35: DISPERSION OF THE MITRAL JETS FOR THE TEST CASES STUDIED.	78
FIGURE 4.36: AVERAGE MITRAL JET DISPERSION LEVELS BASED ON SIX Y/D LEVELS.	78

**The more I study nature, the more I stand amazed
at the work of the Creator.**

Louis Pasteur

ACKNOWLEDGEMENTS

I'm so thankful that this thesis is finally finished! It seems like projects usually take longer than you originally plan, and this work certainly followed suit. Sometimes I thought I was never going to finish! Through all the ups and downs, God gave me so many people that loved me along the way and were so patient with me. Though I hate to admit it, I did complain quite a bit! Fortunately, it's all over now, and looking back, I see that I made things harder than they had to be. I guess that's part of the learning process. Okay, on to thanking.

Thanks to the Department of Engineering Science and Mechanics for allowing me to stay here at Virginia Tech to pursue this Masters Degree and for providing support along the way. I truly enjoyed my assistantship assignments in the Busting Lab working with Bob Simonds, George Lough, Marc Schultz, and Don Ohanehi. I extend my sincere appreciation to Loretta Tickle for her sweet and helpful spirit. You always had a smile and word of encouragement for me whenever I would stop by to steal a piece of chocolate. I definitely missed you when you moved on to your well-deserved retirement! Thanks to Joyce Smith for all of her help with defense and thesis details and of course, candy too! I've also enjoyed visiting with Lisa Smith and Vanessa McCoy many times to "talk." To those in the ESM Machine Shop, it's always a pleasure to work with you and see you around the building. Thanks for all your support and smiling faces.

To my advisors, Dr. Demetri P. Telionis and Dr. Pavlos P. Vlachos, I could not have achieved this degree without you. You both have always believed without a doubt that I could do it even when I didn't. Dr. Telionis, you've been my advisor since I first came to Virginia Tech, and I hope you've enjoyed seeing me grow up and mature both intellectually and personally. I am privileged to be a recipient of your insight, wit, and wisdom. Sometimes I thought I was never going to get out of your office without one more research path to explore, but we finally narrowed things down and have something to show for it. Your passion for learning (and arguing about fluid mechanics) is inspiring. Thank you again for everything. Pavlos, your knowledge and constant pursuit of it continue to amaze me. I will most remember the times you listened to my frustrations through tears when something seemed too difficult or I

felt stupid because I didn't understand something. Our talks kept me moving forward and often restored my belief that I really could conquer my hidden fears and lack of confidence in my abilities. Thank you for pushing me to move forward and for all of the time and energy you spent working with me. I hope that I made you proud to be one of my advisors.

Thanks to Dr. R. Lee Pyle for his assistance from senior design until now. I appreciate the time and energy you spent in getting us acquainted with "real" hearts. I couldn't have performed my research without the valves provided or your assistance. Dr. Grant, I've enjoyed having you as one of my professors, and I greatly appreciate you serving on my committee and for your thoughts and comments on my work.

Olga, I've been so blessed to have you in the lab with me. I would have gone crazy without another woman to talk to! We've been working together for quite a while now, and as I look back, we've become friends. I take away many memories from staying up all night taking data to conferences to giving me rides home. Thanks for all of your support not only with school but also in my life. You have been so excited about the baby and have listened to every detail. You've motivated me so many times to work harder and be better. I wish you all the best in your future endeavors.

To all those in the Fluids Lab, you made it a great place to work. Each of you has helped me in some way or another during my time here. Whether it was helping me with data, giving me Matlab and computer assistance, or making me laugh, I couldn't have made it without you. I miss my French guy Claude and all of our discussions (and arguments too). Thankfully, there's email to keep in touch across the world!

I extend many thanks to my friends who have been supportive and encouraging along the way. I cannot express enough appreciation for Tsu-sheng Roger Chang. I'm not even going to attempt to write about all you've done for me. Suffice it to say that you've been more like a brother to me than a friend.

To my family, you have supported me my entire life, and I'm so grateful for that. You've been behind me all the way in my endeavors great and small and have made countless sacrifices.

Mom, you've always told me I could do anything if I put my mind to it, and you were right! Your perseverance and courage are an inspiration to me. I'm so glad I can always call home when I need you. Thanks to my Uncle Hughie for pushing me to "just do it" all the way from Arizona. I wish that my Granddaddy could have lived long enough to see me achieve this goal. I know he's proud of me anyway.

Kevin, my sweetie, you've been by my side for ten years now. You've seen me grow from a young girl into a woman. We made it through those seemingly endless years of long distance, and sometimes I forget how blessed I am to have you with me each and every day. I'm so thankful that of all the women on earth, God chose me to be your wife. I'm privileged to spend the rest of my life with you, and I look forward to the adventures of life and faith together. Thank you for loving me for who I am and not what I do just like God does. Thank you for keeping me young at heart and carefree like a child. Thank you for being my diamond. I'm so honored to bring you our baby girl, Charis Rae.

And baby Charis Rae, you've motivated me more than you could ever imagine...

And finally, to save the best for last, I must thank God for bringing me through this chapter of life. Father God, I thank You for knowing me inside and out and for loving me anyway. Since we first met, You have been growing me in countless ways, and I'm thankful for your patience with me. Your creation never ceases to amaze me, and I stand in awe of Your creative talent and infinite power. Thank You for teaching me so much through this whole thesis experience. I'll never look at the heart the same way again! Thank You for Your Spirit who fills my life with joy and peace. Jesus, I thank You that one of the reasons you came to earth was so that we could "have life and have it to the full" (John 10:10). Through your life and sacrifice, I can truly experience real life now and forever. No words can express what my heart wants to say, but I know You understand. I'm eternally grateful that Your love for me is beyond my understanding.

**Lovingly Dedicated to
My Granddaddy, Hugh H. Lovelady, Sr.,
From Your Angel Child**

Chapter 1

1 Introduction and Anatomical Review

1.1 Motivation

In spite of the great advancements achieved in the realm of mechanical heart valve (MHV) development, today's valve designs continue to generate high shear stress flows, regions of recirculation, and high levels of turbulent fluctuations. It is well known that these flow conditions are hostile to blood constituents, thereby increasing the risk of valve-induced platelet and/or hemolytic events leading to thromboembolism [61]. This threat necessitates the use of anticoagulant therapy, which imposes yet more risks. In the ongoing effort to reduce long-term complications and morbidity by improving valve designs, it is imperative that we better understand the flow characteristics of the natural valve as well as that of the mechanical valve.

The mitral valve has been a subject of much study for years. In the late fifteenth century, Leonardo da Vinci made outstanding advances in his detailed anatomical studies of the heart. He compared the mitral valve and its subvalvular tension apparatus in the left ventricle to a romanian basilica, noting the importance of the continuity relationship among valve constituents. Centuries later, after much technological advancement, it is routine not only to repair mitral valve lesions but also to replace the diseased or defective valve by implanting a prosthetic one, either mechanical or biological.

With the advent of extracorporeal circulation, the mitral valve became more accessible, allowing for the repair of diseased valves to a greater extent than ever before. As experience with reconstructive surgeries increased, it quickly became evident that total mitral valve replacement (MVR) would be desirable in certain cases. The first artificial heart valve was implanted in 1952 [10], and by the early '60s, the first commercially available replacement mitral valve became available [17]. Today, approximately 100,000 mitral valves

are replaced per year worldwide, 60,000 in America alone, making it the most commonly replaced valve in the heart [2, 10]. In the 1960s, operative mortality ranged from 18 to 40 percent and decreased to approximately 10 percent in the 1980s [50].

In the past five decades, vast progress has been made not only in the area of implantation techniques and procedures but also in the design of the artificial valve itself. Many valve designs, both mechanical and biological, have been discarded, redesigned, and/or re-evaluated as new technology continues to emerge. The replacement of damaged or defective heart valves is a safe, routine, universally accepted surgical procedure. Although this is the case, current research efforts indicate that hemolysis, thrombosis, and anticoagulation side effects remain a problem for mechanical valves, whereas longevity remains a challenge for bioprostheses [6]. In fact, hemolytic and thromboembolic events account for approximately 70% of all complications associated with mechanical valves, even when patients follow anticoagulant therapies [18]. While the present mortality rate is approximately 5 percent, there has been difficulty in reducing mortality from mitral valve procedures to that of other cardiac procedures such as aortic valve replacement or coronary artery bypass grafting [50]. The pulsatility of the flow, the unsteady motion of the leaflets, and the interaction of the jets with the leaflets and chordae tendineae generate intrinsically complicated flow fields. Consequently, a more detailed study of the hemodynamics involved is essential in order to gain insight into the effects of various valve designs and implantation procedures on blood flow. Studies such as this may serve to fuel the ongoing effort to create new and improved artificial mitral valves.

In the past two decades, total MVR with chordal preservation has reemerged in clinical studies as surgeons research the characteristics and effects of mitral apparatus continuity. Original MVR techniques called for the complete excision of the diseased mitral valve, chordae tendineae, and papillary muscles. During the 1990s, the technique of chordal preservation during MVR grew to be widely accepted. In the realm of clinical studies, there exists countless investigations, which indicate the benefits of preserving the continuity of the mitral apparatus. Some of these include an increase in exercise capacity, the avoidance of low output syndrome, and an overall increase in postoperative survival. However, very

few studies have been documented with regard to how chordal preservation affects, in detail, the fluid dynamics of left ventricular flow.

In order to aid in the development and/or redesign of artificial mitral valves so that their resulting flows more closely resemble normal valve hemodynamics, further investigation of the flow characteristics of both the natural and mechanical valve must be performed. The goal of this work is to examine and analyze in vitro the downstream flow characteristics of a mechanical mitral valve and a natural mitral valve along with its subvalvular apparatus. This will be accomplished through a comparison study between three valve configurations, namely, a porcine mitral valve, a bileaflet mechanical heart valve, and a combination of both aforementioned valves using the powerful diagnostic technique of Time Resolved Digital Particle Image Velocimetry (TRDPIV).

1.2 The mitral valve apparatus

Before delving into the fluid dynamics associated with the mitral valve, we must first review the basic anatomy and physiology of the region of interest, namely the mitral valve apparatus and left ventricular chamber. The shape, geometry, and motions associated with the mitral valve directly impact the flow downstream. Having a basic knowledge of this multifaceted region will aid in analyzing and understanding the resulting flow field.

The heart weighs 7-15 ounces and is a little larger than the size of a fist. If a person lives a relatively long life, his heart may have expanded and contracted more than 3.5 billion times. Daily, the average heart beats 100,000 times, pumping about 2,000 gallons of blood. [52]. The left ventricle (LV), as shown in Figure 1.1, is a thick-walled muscular chamber that receives oxygenated blood from the left atrium through the mitral valve and pumps it to the rest of the circulatory system via the aorta. The mitral valve apparatus, also displayed in Figure 1.1, is structurally unique and quite complex. It consists of the annulus, leaflets, chordae tendineae, and papillary muscles. It is located below, behind, and to the left of the aortic valve. The mitral valve sustains the greatest peak load of pressure during the cardiac

cycle, equal to the left ventricular peak systolic pressure minus left atrial pressure. Amazingly, the mitral valve undergoes this tremendous level of cyclic loading about 37 million times per year.

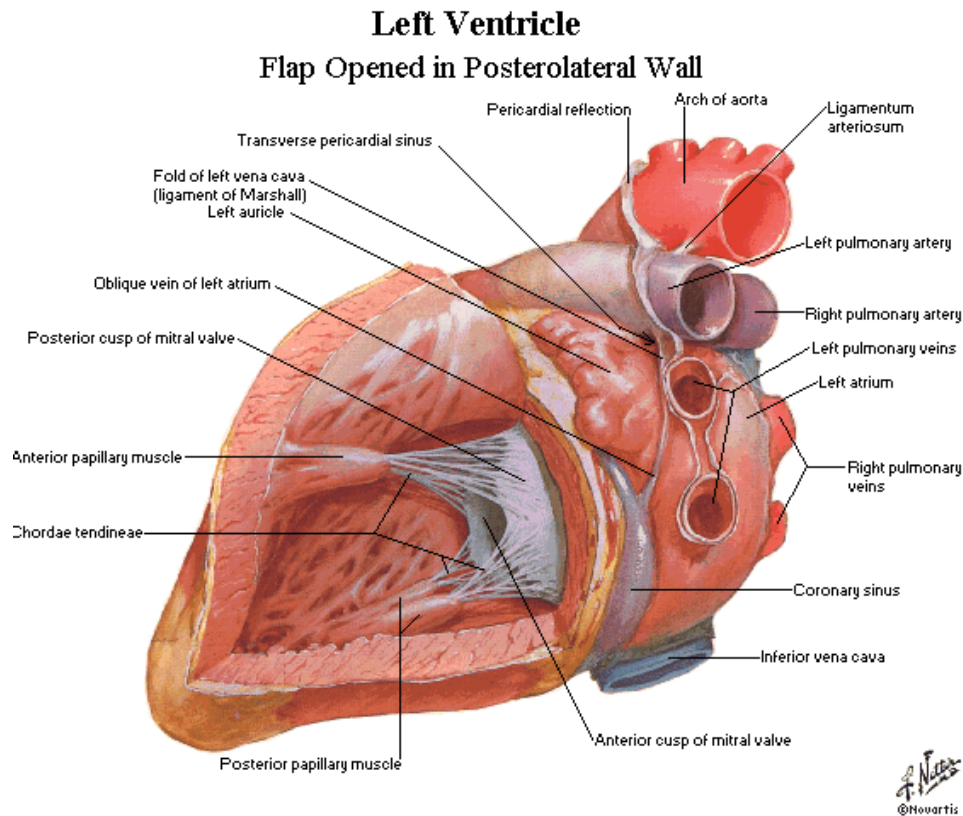


Figure 1.1: Anatomy of the heart.

The “aorto-ventricular membrane,” also known as the cardiac skeleton (Figure 1.2a), is a bridge of fibrous tissues (left and right trigones), which separates the atria from the ventricles and also divides the LV into a mitral inflow tract and an aortic outflow tract. The attachment of the left atrium to the aorto-ventricular membrane at the left trigone defines the mitral valve orifice. As seen in Figure 1.2b, the annulus of the valve, a fibromuscular ring, is fixed medially to the central cardiac skeleton at the aortic root. A normal mitral annulus measures about 10 cm in circumference [3]. The posterior portion of the annulus is muscular and has contractile properties. During ventricular systole, the annulus becomes more D-shaped, and in the latter half of systole, it increases in diameter. In ventricular diastole, the annulus assumes a circular shape.

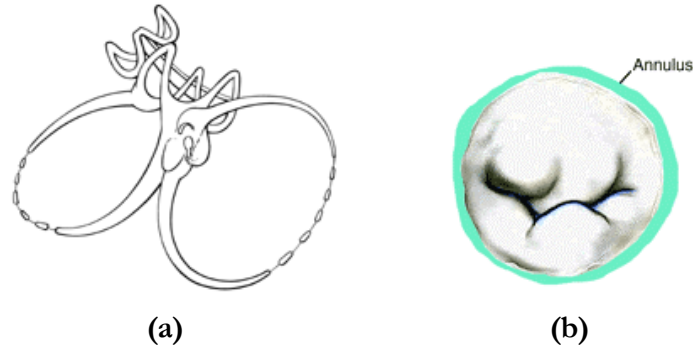


Figure 1.2: (a) Diagram of the cardiac skeleton, (b) The mitral leaflets and annulus. (St. Jude Medical, 2000)

The mitral leaflets (sometimes called cusps), as seen in Figure 1.3a, form a continuous veil of tissue around the mitral orifice of which the basal portion is attached to the annulus. Lying closer to the aortic valve, the semicircular-shaped anterior leaflet forms the boundary of the left ventricular outflow tract. Although it is the larger of the two leaflets, it occupies only 35% of the annular circumference. The posterior leaflet (Figure 1.3b) lies closer to the ventricular wall and is triscalloped in structure with a large middle scallop and two equal-sized scallops on either side. This leaflet accounts for the remaining 65% of the annular circumference because of its longer, more narrow attachment area [3].

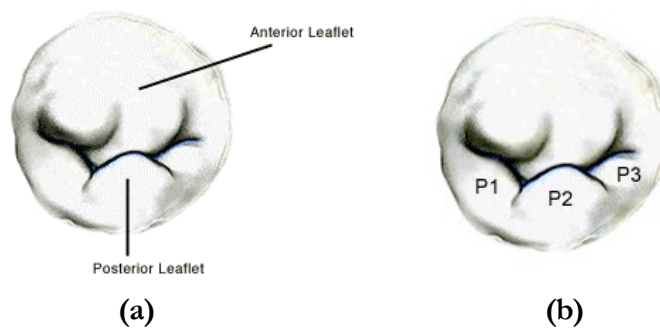


Figure 1.3: (a) Diagram illustrating the two mitral leaflets, anterior and posterior, (b) Mitral valve showing three scalloped portions of the posterior leaflet. (St. Jude Medical, 2000)

The total surface area of the leaflets is approximately two times as much as the mitral orifice which allows for much overlap. The following three zones can be identified on the leaflet surface: a rough zone forming the distal portion, a clear zone, and a basal zone. Originating from the rough zones are the chordae tendineae (CT), fibrous string-like structures which serve to prevent the mitral leaflets from prolapsing into the atrium. Two primary papillary muscles, the anterolateral and posteromedial, support the chordae tendineae and leaflets. The chordae begin at the tip of the papillary muscle and insert along the leaflets' rough zones to form an intricate web of opaque tissue as seen in Figure 1.4a. Approximately 25 chordae tendineae insert into the mitral valve, many of which branch into secondary and tertiary chordae [40]. A generalized arrangement of the chordae tendineae with respect to the leaflets and papillary muscles can be seen in Figure 1.4b.

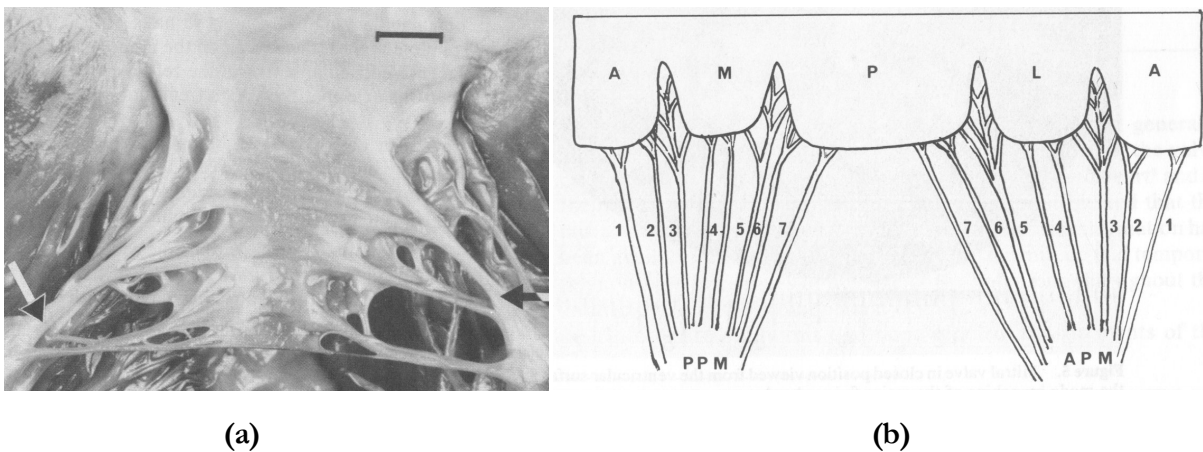


Figure 1.4: (a) View of anterior leaflet showing the mitral leaflet rough zone and insertion of chordae tendineae. Scale indicates 5-mm. (Ranganathan et al.,1976) (b) Diagram of mitral valve, illustrating the arrangement of the chordae tendineae. A- anterior cusp, M-medial cusp, P-posterior cusp, L-lateral cusp. 1. Major fixing chorda to anterior cusp. 2. Lateral fixing chorda to anterior cusp. 3. Commissural chorda. 4. Major fixing chordae lateral and medial cusps. 5. Commissural chorda. 6. Lateral fixing of posterior cusp. 7. Major fixing of posterior cusp. (Yacoub, 1976)

During ventricle filling, the mitral leaflets undergo oscillating motions that include opening, partial closing, reopening, fluttering, and closing. Due to their size, shape, and function, the anterior and posterior leaflet motions are not identical. These leaflet oscillations will have a direct effect on the mitral jet as it enters and develops within the left ventricle. The cusp motion for a normal mitral valve can be seen in Figure 1.5. The vertical axis represents the instantaneous linear distance between individual reference positions and the leaflet markers (anterior-upper, posterior-lower). During diastolic closure, the motion of both cusps is characterized by opening, immediate reclosure, a short pause, and a resumption of closure at a slower speed. After a small rebound, the cusps remain motionless at their semi-closed positions until atrial opening. The valve is closed by the combined effect of atrial and ventricular contractions at the end of diastole.

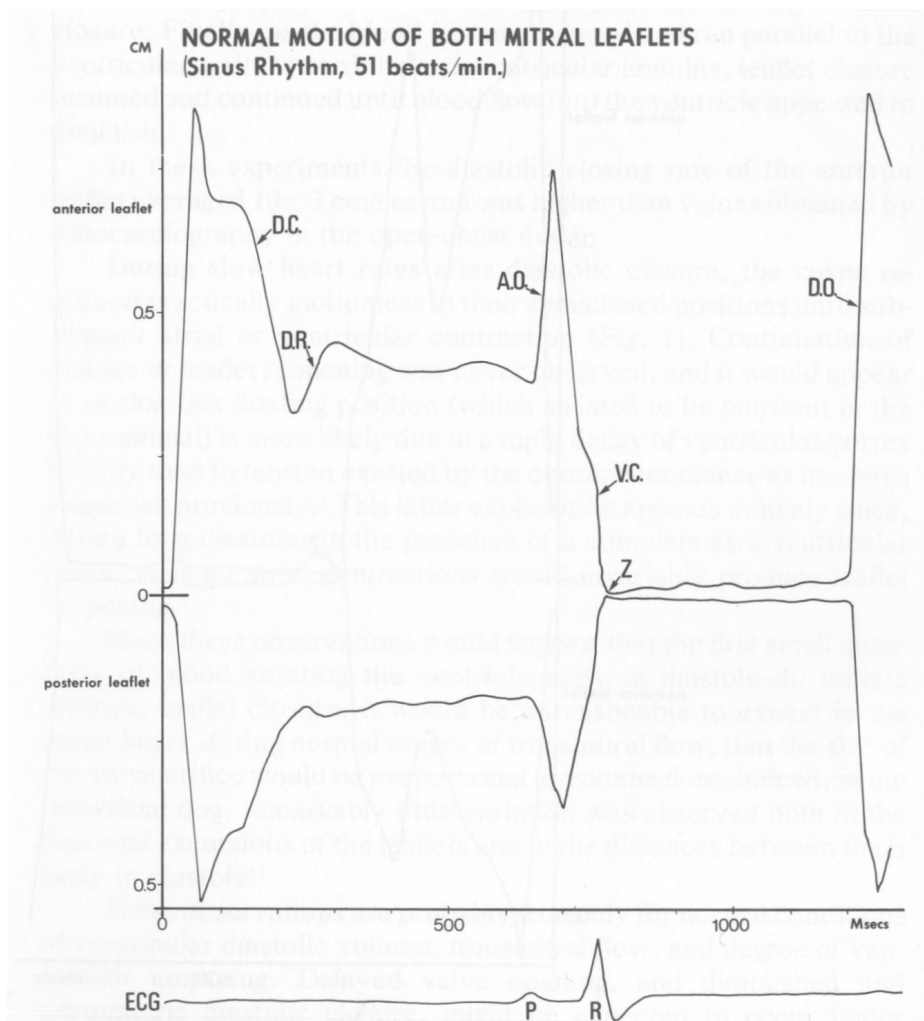


Figure 1.5: Motion of beads placed on the free edges of anterior and posterior cusps recorded at a slow sinus rhythm of 51 bpm. DO-diastolic opening, DC-diastolic closure, DR – diastolic rebound, AO – atrial opening, VC – ventricular closure. (Tsakiris, 1976)

The purpose of this brief section was simply to orient the reader anatomically to the region of interest. A more in depth and detailed description is beyond the scope of this work as entire textbooks have been written about this subject. From what is presented here, we see that the mitral valve apparatus is a complicated structure consisting of several parts, each of which influences hemodynamic flow characteristics. It is evident that the mitral valve apparatus, when healthy, is quite an engineering marvel. Problems arise when the leaflets or parts of the subvalvular apparatus become defective or damaged.

1.3 Mitral valve disease, repair, and replacement

Of the four valves in the human heart, the mitral valve is the most commonly diseased. Although there are several specific causes of heart valve disease, they are generally divided into one of two categories, either congenital or acquired disease. Those diseases and/or defects present at birth, some which may possibly be corrected early in life, are classified as congenital disorders. The acquired diseases or defects that negatively affect the heart valves include infective endocarditis, rheumatic fever, and progressive degeneration. Valve damage remains the outcome no matter what the cause of the disease. This damage typically results in either a stenotic or regurgitant valve. Stenosis is characterized by fusion of the commissures between the leaflets which leads to obstruction of blood flow, thereby causing the heart to work harder to pump a normal supply of blood. With a regurgitant valve, the leaflets are loose or damaged so that they do not close tightly, allowing blood to leak in the opposite direction of normal flow. Various forms of calcification may also occur which lead to improper valve function. If not treated, eventually the overworked heart "begins to fail, causing shortness of breath, dizziness, chest pain, fatigue, and fluid retention" [26].

The course of treatment obviously depends on the extent of valvular disease, which can range from mild to moderate to severe. First, a heart murmur is typically heard through a stethoscope, and then a diagnosis is made from tests such as an electrocardiogram, chest X-ray, echocardiogram, or cardiac catheterization. Some levels of disease require surgical intervention where one or more valves may be repaired or replaced. Many times the

decision to repair or replace cannot be made until the valve is visualized during the actual surgery. Normally, a surgeon will make every effort to use repair techniques such as valvuloplasty, commissurotomy, or annuloplasty in order to save the natural valve. If this is not possible, then the valve will be replaced with an artificial prosthesis.

1.4 Artificial Heart Valve Prostheses

The normal function of heart valves is necessary for the maintenance of a normal to active lifestyle. In order for those with diseased valves to return to a more healthy, normal lifestyle, their defective valves must be replaced. Artificial heart valve (AHV) prostheses are intended to fully replace the natural valve and must endure strenuous conditions for the remainder of the patient's life. By 1980, approximately 30 different AHV designs were being produced around the world [10]. Four of the most popular types of valves are shown in Figure 1.6. Currently, three options exist for replacing heart valves: mechanical prosthetics, bioprosthetics, and transplants.

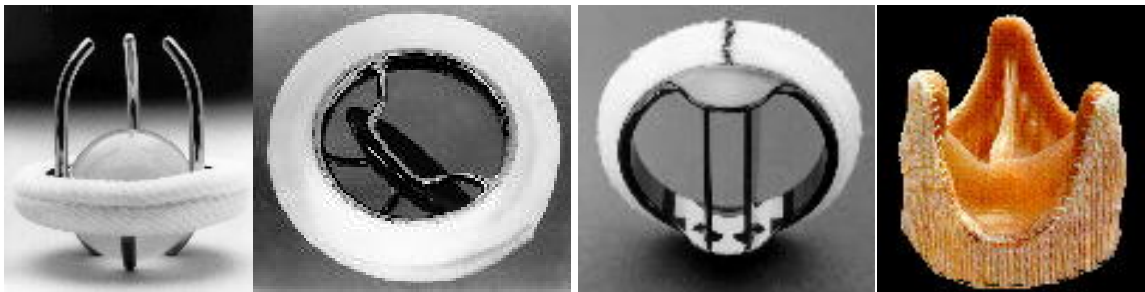


Figure 1.6: Four artificial heart valve designs, from left to right: caged ball valve, tilting disc valve, bileaflet valve, and porcine bioprosthetic valve. (Camp, 1997)

Mechanical heart valves (MHVs) are capable of restoring normal blood flow through the heart and are known for their hardness, strength, and durability. However, these valves typically alter the heart's biofluid mechanics as they disrupt normal flow patterns of the natural heart valves. MHVs can also induce hemolysis and thrombosis, due to high shear, as well as serve as excellent substrates for bacterial infection. Patients with MHVs must take

anticoagulants for the rest of their lives, which imposes other risks and side effects. Bioprosthetic heart valves (BHVs), or transplants from other mammals, typically pigs, successfully replace human valves and do not significantly deviate from normal valve hemodynamics. Unfortunately, BHVs lack the longevity of their mechanical counterparts. The third alternative, a transplant from an organ donor, becomes a living part of the surrounding heart tissue, but it must overcome immune system rejection. Since this is highly unlikely, transplant valves are not often used in MVR. Today, the preferred method among surgeons is to replace the diseased valve with a bileaflet mechanical heart valve.

Chapter 2

2 Literature Review

2.1 AHV Flow Field Studies

Countless efforts have been made to learn more about the biofluid dynamics of AHVs ranging from computational to experimental to clinical studies. Since the approach of this work is experimental, the majority of the studies discussed will also be from the same perspective, with some related clinical results included as well.

2.1.1 Experimental Work

Flow downstream from a bileaflet MHV is characterized by the dramatic dispersion of the mitral jet as three individual jets issue distal to the valve, interact, and entrain surrounding fluid in a sudden expansion area. Flow disturbances generated from the leaflets form intrinsically complicated, turbulent flow fields which include the shedding of vortical structures. Considering the risk of thromboembolic complications, MHV patients require life-long anticoagulants, in contrast to patients receiving bioprosthetic valves. A review of articles published since 1979 by Edmunds [18] demonstrated that thrombotic and bleeding complications account for about 50% of valve-related problems in patients with BHV and approximately 75% in patients with MHV. Apparently, the flow through pivoted leaflets of MHVs induces a combination of flow characteristics that are clearly conducive to clot formation. Pockets of very slow flow downstream of some sections of the MHVs are created, but within very small regions in the neighborhood of the MHVs, the flow of blood is forced to do exactly the opposite--accelerate to high speeds, creating regions of high shear. Shear levels of 100 to 130 dyn/cm² for durations that are fractions of a second are enough to induce platelet damage [30, 58]. Platelet activation requires somewhat higher levels, namely, 300 to 1000 dyn/cm², while even higher shear stress levels induce hemolysis [39]. MHVs can also induce very high levels of Reynolds stresses. In fact, Maymir et al. [34]

found that regurgitant jet flows may generate high-speed jets in the atrium that are accompanied by Reynolds stresses on the order of 20,000 dyn/cm².

Ventricle filling and vortical effects were investigated by Bellhouse and his co-workers [4, 5] beginning in 1969 . Reul et al. [45] studied the fluid mechanics of the natural mitral valve and its subvalvular apparatus by examining the flow patterns and motions of a porcine valve both with and without an elastic left ventricular model. For the case using the model, they observed strong vortices during peak flow that grew to be fully developed in the first deceleration phase. Without the ventricle, no vortices were present at peak flow, and at the onset of deceleration, a small vortex formed downstream of the valve. Also using flow visualization, Chandran and his colleagues [11] examined the effect of geometry and orientation on the flow field past MHVs and found that for the bileaflet prosthesis in the anatomical position, greater flow through the central orifice forms a pair of counter-rotating vortices in mid-diastole. They also stated that vortex formation distal to the valve is a function of the size and shape of the flow chamber downstream.

Woo and Yoganathan [59] conducted velocity and shear stress measurements for pulsatile flow in mechanical mitral prostheses using Laser Doppler Velocimetry (LDV). Bruss et al. [9] reported on the velocity fields of four MHV prostheses by implementing the technique of Laser Doppler Anemometry (LDA). Schoephoerster and Chandran [48] also used LDA to make velocity and turbulence measurements past mitral valve prostheses. Bileaflet velocity profile results for the anatomical position showed a wide jet of three peaks with the majority of the flow entering the ventricle through the two outer orifices. Vortex formation was limited to the anterior half of the LV due to the wide jet, and areas of flow stagnation and recirculation were observed in regions near the right and left ventricular walls. Garitey et al. [21] made extensive pressure measurements and used pulsed ultrasound Doppler velocimetry to record the velocity field. Their results (anatomical orientation) showed the dispersion of three jets toward the posterior and anterior ventricular walls with stagnation occurring before the apex, along with zones of recirculating flow near the mitral inlet. Both Reif et al. [44] and Gross et al. [22] have also observed vortex shedding in the wake experimentally. In 1995, Walker and his team [54]

used magnetic resonance velocity imaging techniques to measure blood velocity downstream of prosthetic heart valves and identified regions of high velocity, shear layers, and areas of stagnation.

2.1.2 Limitations

All of these studies were conducted in confined chambers, namely either rigid or flexible ventricle models, sized as nearly as possible to the anatomical dimensions. As a result, many recirculating patterns are due to the effects of the walls. One of the aims of this work is to remove the wall effects and focus on the vortices that are due exclusively to the mitral jets. It should also be emphasized that the redirection of the flow as shown by Kilner et al. [31] in a curved and expanding sack like the ventricle, as it develops under healthy physiological conditions, minimizes the generation of turbulence. The intrinsic features of a pulsing jet's spatial and temporal development are significantly complicated, and thus better understanding could be achieved if studied in a simplified chamber.

In addition, these studies were carried out using either a non-quantitative method (flow visualization) or a point-by-point measurement technique such as LDV that only measures velocity at one point. Such systems require tedious and careful traversing of the measurement volume to reconstruct the entire flow field and even then, this is accomplished in a time-averaged manner. To reconstruct instantaneous data of pulsatile flow fields, one can employ phase trigger methods but must first ensure repeatability and ignore the random spatio-temporal character of turbulent flows. A main drawback of magnetic resonance imaging is its inability to obtain accurate measurements in regions of high turbulence intensity [54]. A method that bypasses such difficulties is Digital Particle Image Velocimetry (DPIV), which captures the velocity field at each instant in an entire plane and depending on the system, is capable of providing sufficient temporal and spatial resolution to investigate the turbulent characteristics of the flow. Traditional Particle Image Velocimetry (PIV) originated in the early 1980s (reviews by Hasselinc [25] and Adrian [1] provide a detailed discussion), but it was the work of Willert and Gharib [57], Westerweel, 55] and Huang and Gharib [29] that established the digital implementation of PIV.

While DPIV has many advantages over other measurement techniques, some systems also have limitations of their own. The efforts of the abovementioned authors, as well as many other studies that followed, focus on a single-exposure, double-frame digital cross correlation approach. In addition, they focus on high-resolution (1Kx1K pixels) cameras that sample with up to 30 fps resulting in a sampling frequency of the flow field of only 15Hz. This is the major limitation of the DPIV systems that are commercially available. A recent study by Browne et al. [7] compared the techniques of LDV and DPIV in mapping two-dimensional flow fields distal to a bileaflet MHV. They obtained significantly different results between the methods in areas of unsteady flow and attributed the limitations of PIV to the low frequency of data acquisition, namely 10 Hz, and lack of computer memory for increased sample size. These are serious limitations for the analysis of turbulent flows, where high frequency fluctuations are present. High-speed imaging reveals that leaflet opening occurs within a time of 0.10 s. With a standard DPIV system that utilizes a frequency of 30 Hz, only three frames could be captured during this time interval. The system developed in our facility has overcome these difficulties by integrating a high-power pulsing laser with special type of optics and a unique CMOS (Complementary Metal Oxide Semiconductor) camera, capable of acquiring up to 1000 fps. This creates a DPIV system with 1 kHz sampling frequency. By using this TRDPIV system, resolving the flow phenomena during leaflet opening, for example, would allow for the capture of 100 frames of information, representing an increase of two orders of magnitude.

2.1.3 Related DPIV Studies

Subramanian et al. [51] performed a DPIV study on the pulsatile flow within the lumen of an optically clear bileaflet MHV. During the fully open phase, as seen in Figure 2.1, the velocity profile showed three peaks across the valve lumen, with the central peak having higher velocity than the two outer orifice jets. Further downstream, however, the lateral jets had higher peak velocity values. They also observed vortex flows of low velocity downstream of the leaflets' trailing edges, as well further downstream, later in the cardiac cycle. Asynchronous leaflet motion, not due to valve malfunction, was also detected. Donnerstein and Allen [16] quantified this phenomenon in vivo by analyzing closing sounds

and determined that the MHV did function properly. A DPIV study by Brucker [8] suggested that asynchronous motion causes a significant increase in the maximum shear rate, which would lead to more blood damage and larger regions of stagnation. A goal of the present work is to examine the effects of asymmetric leaflet motion on the far field of the mitral jet.

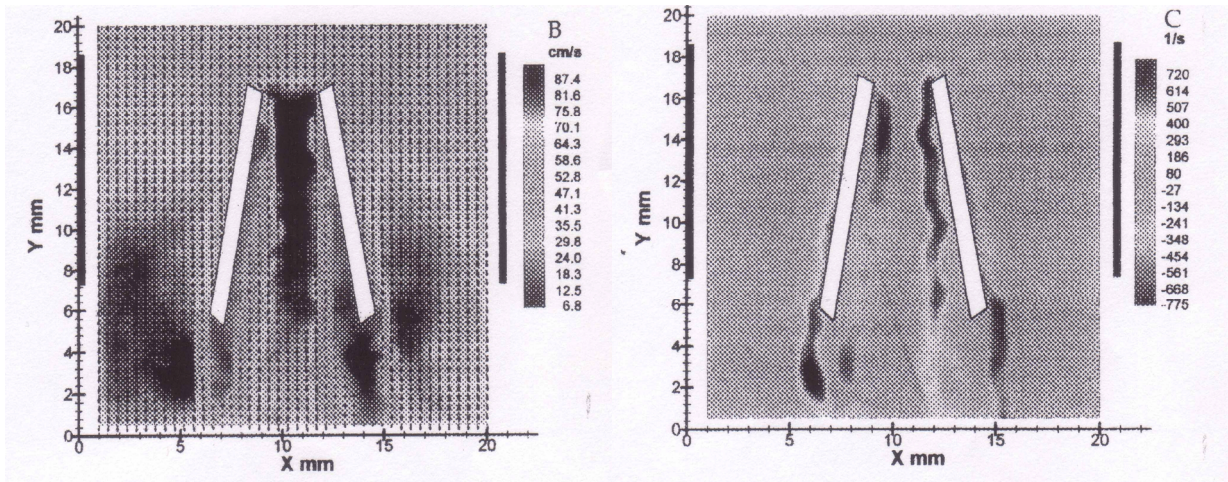


Figure 2.1: (b) Velocity and (c) Vorticity maps during the fully open phase for the 450 ms time point. (Subramanian et al., 2000)

In 2000, Bluestein et al. [6] performed an extensive experimental and numerical study that linked vortex shedding to free emboli formation. A numerical simulation of unsteady turbulent flow through a bileaflet MHV in the aortic position was compared with quantitative flow visualization using DPIV. Both numerical and DPIV results were in agreement. Periodic vortex shedding in the wake of the leaflets as well as a recirculation region below one leaflet were observed. DPIV velocity and vorticity measurements, shown in Figure 2.2, reveal visible fluctuations in the wake downstream of the two leaflets. High levels of vorticity and strong vortical structures were also generated.

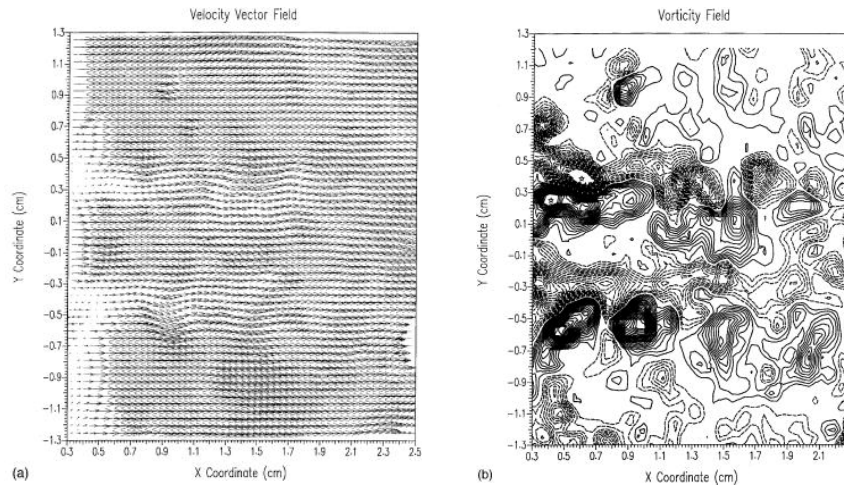
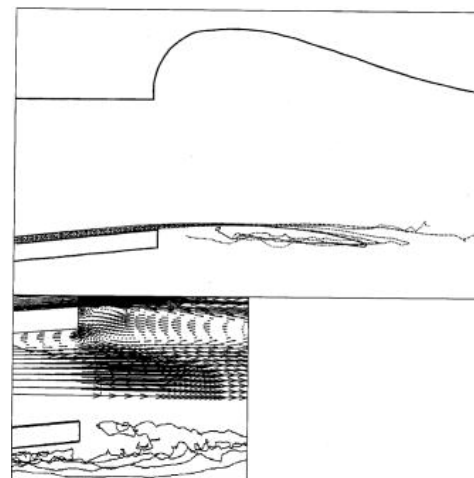


Figure 2.2: (a) Velocity field distal to the valve during peak systole (leaflets tips at $y = \pm 0.3$ cm). (b) Vorticity field distal to the valve during peak systole. Dashed contours: CCW rotation, solid lines: CW rotation. (Bluestein et al., 2000)

Platelet paths were computed around the leaflets by seeding the flow above and below the leaflets as illustrated in Figure 2.3. To determine the turbulent platelet paths, a stochastic model was used so that with each iteration, a different path resulted. Particle paths revealed that platelets exposed to the highest flow stresses around the leaflets were repeatedly trapped in the small-scale shed vortices. Along these paths of high deformation and turbulent stresses, platelets are more likely to be damaged and/or activated, which causes them to lose their disk shape, thereby increasing their collision frequency. It is then more probable that the platelets will form aggregates.

Figure 2.3: Turbulent platelet paths through areas of highest stresses around the leaflet: above the leaflet (top) and below (bottom), leading to entrapment within the shed vortices in the leaflet's wake. The corresponding velocity vectors are shown (paths are computed from 165 ms to 419 ms after peak systole). (Bluestein et al., 2000).



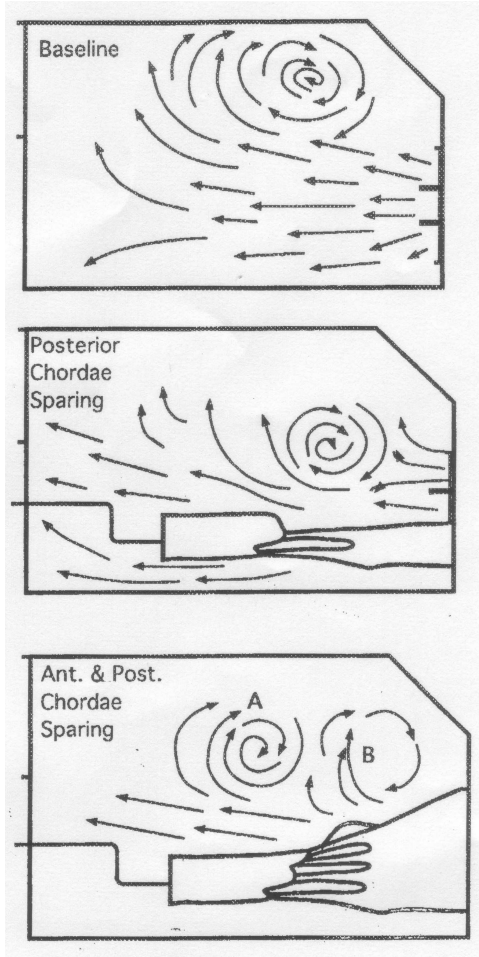
These findings led Bluestein et al. to postulate that the shed vortices provide flow conditions which favor the formation of larger platelet aggregates, thereby activating the positive feedback reactions of coagulation. Ultimately this could lead to free emboli formation, elevating the risk of systemic embolism. As discussed above, it has been well documented that valve-induced high shear flows along with vortex shedding also occur in the wake of the bileaflet MHV in the mitral position. It is then only natural to speculate that the vortices shed from the mitral valve may create similar flow conditions, which would trap damaged blood components. It is necessary to study the mitral jet flow to examine the validity of this assumption.

2.2 Influence of Native Mitral Tissue, Clinical Results

Another important factor which influences mitral jet development is the presence of the native leaflet tissue, chordae tendineae (CT), and papillary muscles. Their effect on the hemodynamic performance is often overlooked. In 1962, Lillehei [33] was the first to devise a mitral valve replacement (MVR) procedure which provided for the preservation of the papillary muscles and chordae tendineae. In early work with the Starr-Edwards ball valve, he observed a period of low cardiac output after implantation despite seemingly excellent valve function. If the patient were able to survive this critical clinical stage, he would most likely proceed to a full recovery. Previously, physiologic studies by Wiggers and Katz [56] and Rushmer [47] proposed that the continuity of the mitral annulus, mitral leaflets, chordae tendineae, and papillary muscles played a crucial role in the function of the left ventricle. It appeared that this hypothesis was correct as Lillehei observed patient after patient with low ventricular output whose MVR included the complete excision of the mitral leaflets, chordae, and papillary muscles. As a result, series of experimental studies were conducted in which Starr-Edwards valves were inserted in situ with the preservation of the mitral leaflets, chordae tendineae, and papillary muscles. It was found that with the proper surgical technique, the function of the prosthetic valve was not affected by the presence of the natural structures of the mitral apparatus.

In November 1962, Lillehei began preserving the continuity of the mitral apparatus. In most cases, the anterior leaflet of the mitral valve was excised leaving a rim of valve tissue (2-3 mm) attached to the mitral annulus. This excision of the anterior leaflet was necessary as most patients' anatomies did not allow for the insertion of the ball valve. As for the posterior leaflet, excision was done as close to the leaflet as possible, thereby preserving the entire set of posterior chordae and often some of the chordae from each end of the anterior leaflet. In Lillehei's previous cases without preservation techniques, the mortality rate was a relatively high 37 percent. In patients with CP, there were no occurrences of low output syndrome, and the mortality rate dropped to 14 percent. One would think that such a dramatic decrease in mortality rates would draw much attention to Lillehei's technique of CP, thus warranting thorough clinical studies and possible implementation as regular practice. Soon after, however, there appeared in the literature strong opposition to the technique from prominent surgeons and physicians [12, 41-43,46]. Only one report during this early era, from Seidel and Gross [49], confirmed the benefits of preserving the integrity of the chordae tendineae. Though published in a national journal, it was ignored. It wasn't until 1979 that these benefits were "rediscovered" by Dr. Donald Miller [36]. Following soon after, David [13] and Hetzer [28] also witnessed the positive effect of chordal preservation. From then on, the idea of chordal integrity began to be studied vigorously as it was an important issue for surgeons and physicians. A plethora of clinical studies have been documented regarding the positive effects of preserving some or all of the chordae; however, very few have been conducted which examine the effect of leaflets and CT on flow dynamics past the artificial valve [14, 15, 20, 23, 24, 27, 28, 37].

One such experimental study was performed by Fontaine et al. [19] and explored the effects of the mitral subvalvular apparatus on prosthetic valve function. The influence of CP on transvalvular and left ventricular flow patterns was assessed using 2-D planar flow visualization, pulsed wave Doppler velocity measurements, 2-D echocardiography, and selected color Doppler flow mapping. For the anatomical case with complete preservation, the inflow jet was centrally directed toward the apex and was laterally constricted by the



tissue, shown in Figure 2.4. The flow then quickly expanded downstream of the anterior leaflet. Two patterns of recirculation were also observed in the outflow tract.

Using magnetic resonance imaging (MRI), Joachim Laas [32] and his colleagues from the Clinic of Cardiothoracic Surgery in Germany captured in vivo intraventricular flow patterns through a sufficient MV and a bileaflet MHV. Figure 2.5 shows five images which display the inflow and outflow patterns for the mitral jet. The left ventricle is located in the upper right portion of the image, and the mitral jet appears as a stream of white.

Figure 2.4: Sketches illustrating the 2-D flow patterns for the St. Jude Medical bileaflet valve in the anatomic position from the vertical long axis view through the valve centerline during peak diastole. (Fontaine et al., 1996)

For the normal condition, the blood flow enters and exits the LV smoothly as it makes a distinct and total change in direction towards the aortic valve as shown by Figure 2.5. It appears as if the mitral jet is initially directed along the posterior wall smoothly and keeps its coherence throughout the heart cycle which would minimize turbulence. It is thought that this preferred jet direction stems from a “rudder” effect induced by the anterior leaflet. With the bileaflet substitute, shown in Figure 2.6, the flow completely deviates from normal conditions as it expands greatly through the three valve orifices and diffuses into the ventricle. This lateral dispersion of the jet causes it to lose much of its coherence and momentum.

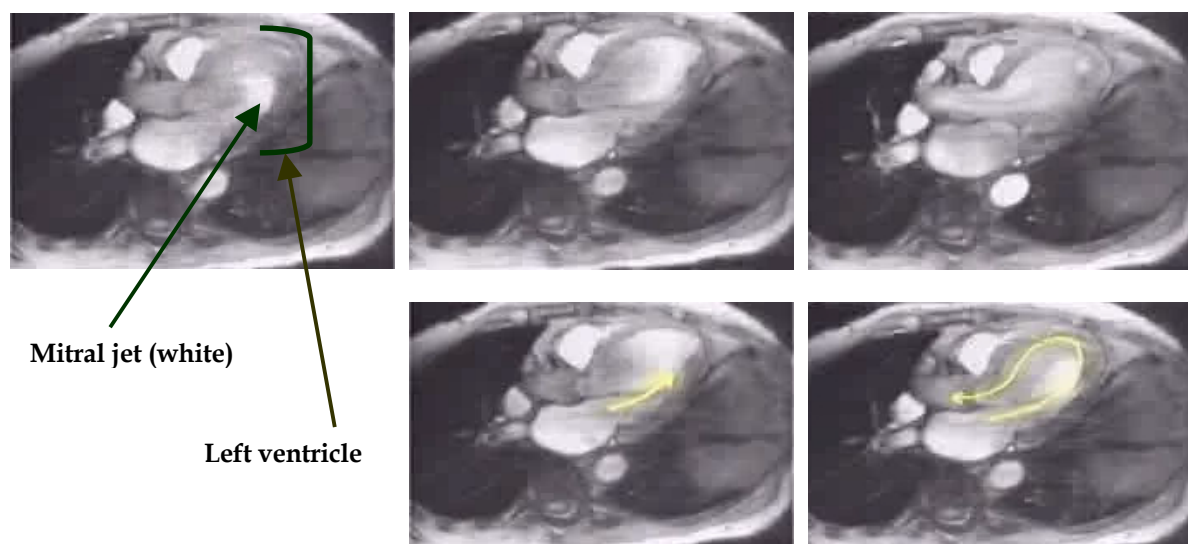


Figure 2.5: MRI Images illustrating healthy redirection of the mitral jet toward the aortic valve. (Laas et al., 2000)

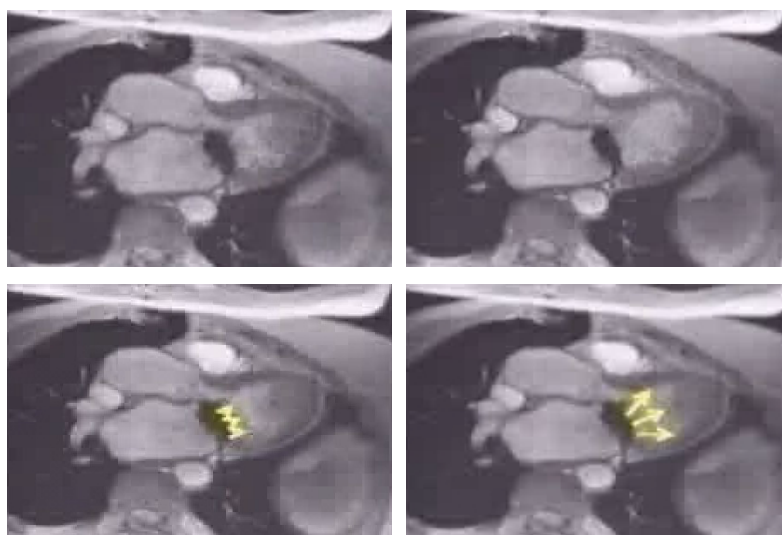


Figure 2.6: MRI images showing the loss of asymmetric redirection after implantation of a bileaflet MHV. (Laas et al., 2000)

Recently Kilner et al. [31] employed magnetic resonance velocity mapping to visualize and study the filling patterns in human atrial and ventricular cavities. A most interesting conclusion was that the geometrical arrangements of the atria and the ventricles asymmetrically redirect the flow along sinous, chirally oriented paths as shown by Figure 2.7. The volume of blood was completely redirected toward the outflow tract, which suggests that the dissipative interaction between entering, recirculating and outflowing streams is minimized.

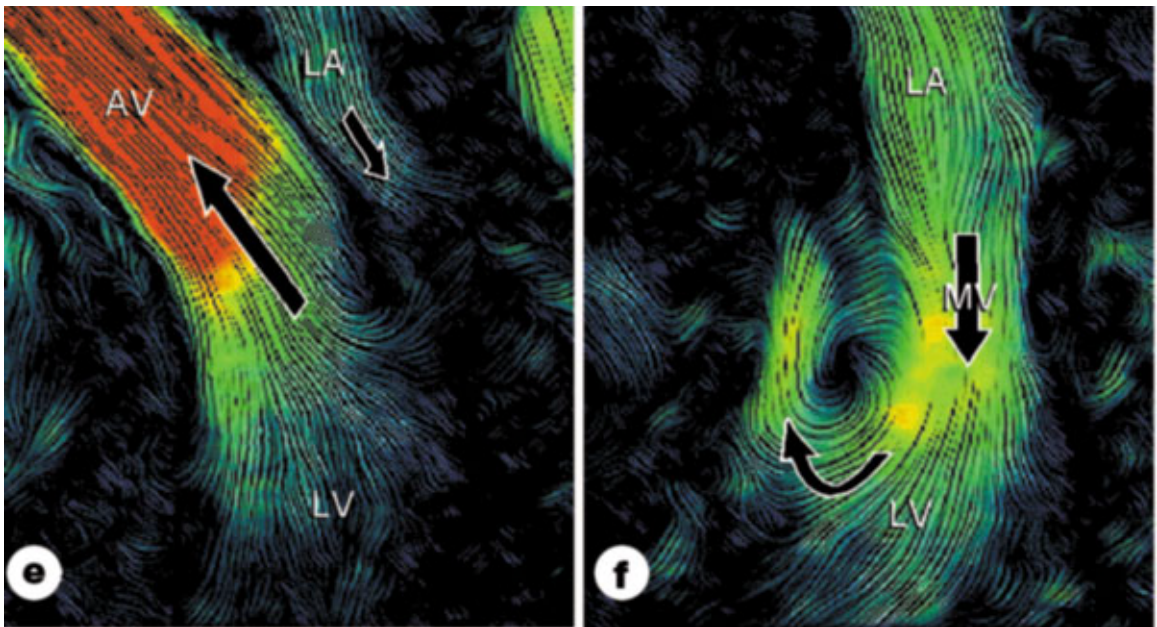


Figure 2.7: Magnetic resonance velocity mapping reveals asymmetric flow patterns within the LV. (e) Flow through the aortic valve in systole, (f) Redirection of the mitral jet around the anterior leaflet in early diastole. (Kilner et al., 2000)

According to these studies, it appears that the heart pumps blood along a preferred pathway that minimizes energy losses, particularly during vigorous exercise. The purpose of the CT has long been thought to provide the mechanism that serves to anchor the mitral leaflets, thereby preventing them from involuting into the left atrium under systolic pressure. Along with this known function, is it possible that the mitral leaflets and CT also

act as a flow control mechanism to direct the mitral jet in such a way that preserves its coherence and momentum, thus facilitating redirection towards the aortic valve? It is important to compare the far-field coherence of mitral jets and the measurement of the spreading of jets issuing from various valve configurations. This would confirm that the most efficient operation would reduce spreading and preserve the kinetic energy of the jet while later allowing the flow to be redirected towards the aortic exit.

2.3 Contribution

We have seen that throughout the years, much effort has been exerted to study the fluid mechanics of mechanical heart valves as well as that of the natural mitral valve apparatus. A plethora of information has been generated, which has greatly influenced AHV designs, implantation procedures, and valve repair techniques. In spite of these advances, problems and questions still remain as to the mechanisms and functions that allow for the intrinsically complex flow field in the wake of heart valves. Ideally, a MHV would accurately mimic the flow patterns in the natural heart without excessive damage to blood elements. This goal has not yet been realized.

The present work contributes to the overall effort by providing further insight into the flow fields past both mechanical and natural mitral valves individually as well as a combination of both types of valves. While a variety of sensors are available to explore the flow, by using a specially developed, high frequency TRDPIV system, we provide adequate temporal and spatial resolution to investigate the turbulent flow character, thus overcoming many limitations of other systems. The measurements obtained provide detailed information regarding the character of the flow such as levels of vorticity, jet dispersion, vortex shedding, and leaflet motion behavior for each of the cases evaluated. These results can be utilized to make clinical advancements in MVR techniques and to further the development and design of AHVs.

Chapter 3

3 Experimental Facilities and Methods

3.1 Left Ventricular Simulator

The current experiment was performed in the heart simulator facility in the Fluid Mechanics Laboratory at Virginia Tech. In order to study the fluid mechanics of blood flow through heart chambers and valves, we constructed a simulation machine. A schematic of the simulator can be seen in Figure 3.1.

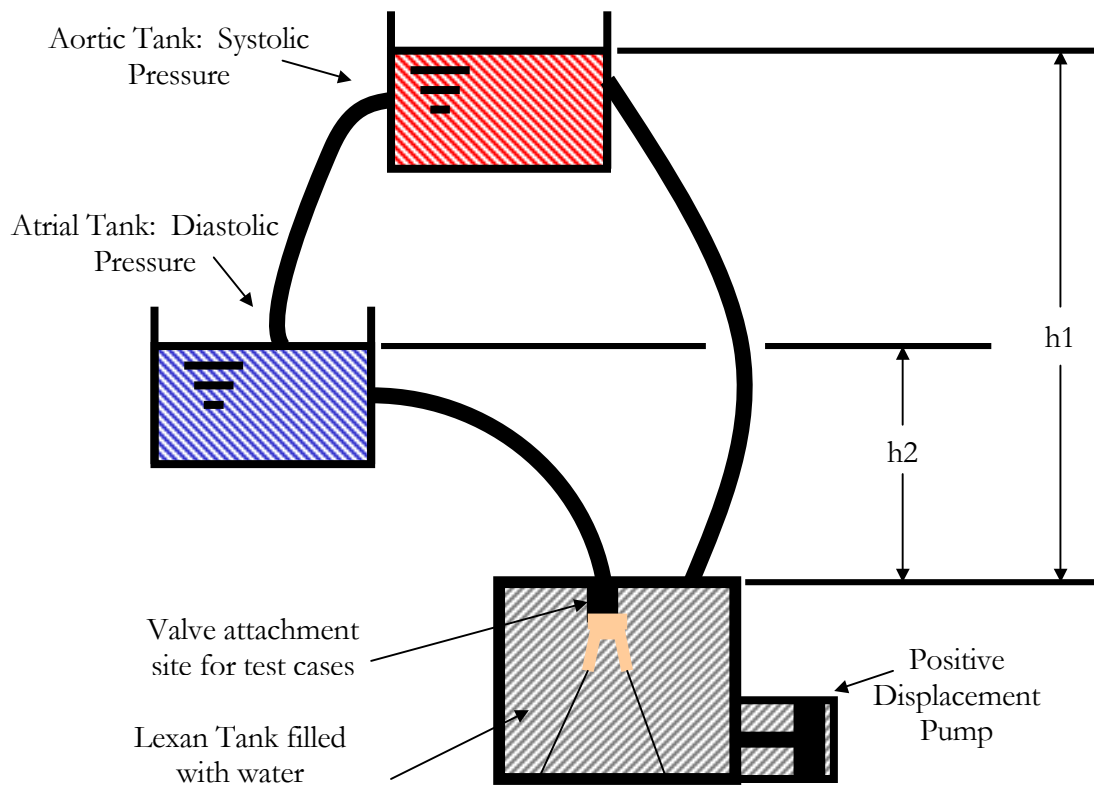


Figure 3.1: Basic schematic of the left ventricular simulator.

Comparable simulators have been constructed in the past. The machine can dynamically adjust the volume of the chamber and therefore the heartbeat, stroke volume and ejection fraction. These tasks are accomplished via a piston with adjustable travel, driven by a motor with variable frequency. The elevation of delivery and receiving tanks controls systolic and diastolic pressures. When the piston forces more fluid in the tank, the systolic phase of the motion is simulated. The mitral valve closes and the aortic valve opens to allow flow into the aorta and up to the aortic tank, working against the head of the upper tank. As the piston withdraws, the diastole begins, and flow enters through the mitral valve.

The left ventricular tank is rectangular with flat rigid walls. Lexan was employed to provide for excellent optical access without the distortion induced by curved walls. Usually, a flexible, left ventricular model is placed in the tank [38]. However, in this study we focus specifically on the behavior of the mitral valve jet and not the ventricular wall motion effects. The system was modified to examine the flow distal to mitral leaflets and CT by removing the flexible LV and allowing the flow to enter directly into the tank as shown in Figure 3.2. The tank's volume is 150 times greater than the volume of our left ventricular model thus eliminating any end effects introduced by the walls.

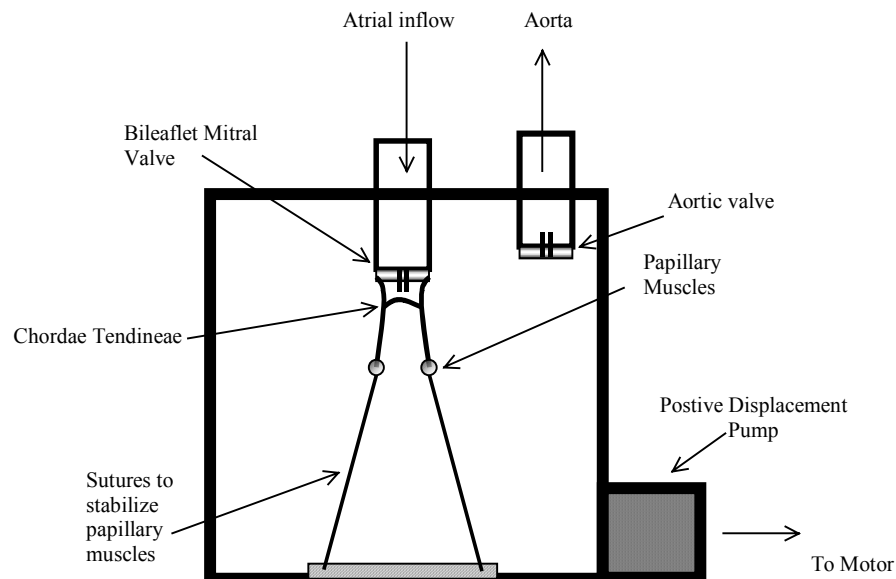
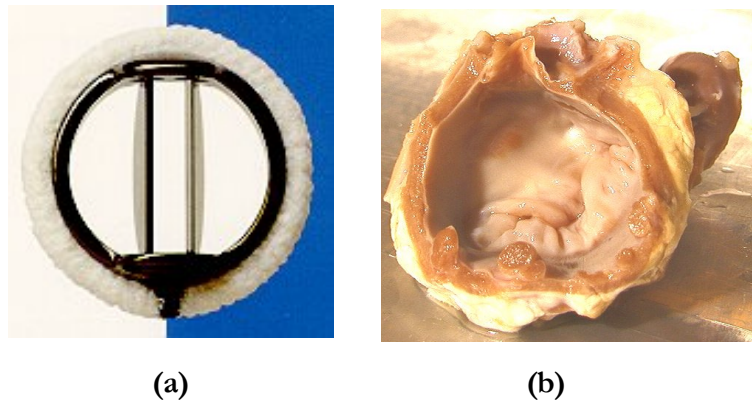


Figure 3.2: Schematic of the left ventricular chamber with the bileaflet MHV and porcine mitral valve mounted onto the atrial inflow pipe.

3.2 Setup and Configurations

We tested a biological valve, a mechanical heart valve and a combination that simulates the implant of a MHV with preserved chordae. A 31-mm St. Jude Medical bileaflet heart valve served as the baseline test case in this work, since it is the valve most commonly implanted today. An explanted (no fixatives) porcine mitral valve along with its CT and papillary muscles served as the natural valve. Both valves are shown in Figure 3.3. To stabilize the subvalvular apparatus, the papillary muscles were secured to a movable frame at the bottom of the tank using sutures. The simulation of CP was done by implanting the St. Jude valve inside the excised porcine mitral valve annulus. All valves tested were clamped onto the cylindrical end of the atrial inflow pipe. Both anterior and posterior leaflets and their CT were preserved in all tests. For cases using the MHV, the interrogation plane was aligned perpendicular to the pivot axis of the mechanical leaflets to capture the flow patterns corresponding to the anatomical position.

Figure 3.3: (a) St. Jude Medical bileaflet MHV. (b) Excised porcine mitral valve apparatus.



Water served as the working fluid in all tests. Dynamic similarity with the biological conditions was preserved by operating at a mean Reynolds number of 3000, based on the mitral valve diameter of 31-mm. During the experiment a cardiac output of 4.75 liters/min was maintained. In order to better understand the spatio-temporal development of the flow, we increased the time between two consecutive cycles by employing a low heart rate of 50 bpm. Flow rate was measured using a Transonic Flowprobe (Transonic Systems, Inc., Ithaca, NY) coupled with an ultrasonic flow meter (model T110, Transonic Systems, Inc.,

Ithaca, NY). Digital data acquisition was performed using 16-bit analog to digital conversion with 1 kHz sampling rate.

3.3 Data Acquisition and Additional Instrumentation

Time-Resolved Digital Particle Image Velocimetry (TRDPIV) was employed to carry out the task of instantaneous plane velocity measurements. In order to illuminate the area of interest, a powerful 60 Watt copper-vapor pulsing laser (beam diameter of 42-mm) was coupled with special beam-guiding and sheet-forming optics, which deliver a plane sheet of 2-mm thickness as shown in Figure 3.4. Accurate flow tracing (no response lag to any turbulent fluctuations) was accomplished by seeding the flow with neutrally buoyant particles, having a diameter of approximately 10- μ m. A high-speed Phantom v.4 CMOS (Complementary Metal Oxide Semiconductor) video camera (1000 fps, 512 \times 512 pixel resolution) was synchronized with the laser to capture the instantaneous positions of the particles. In the present experiment, a sampling frequency of 1000 Hz was used. Data were acquired for two seconds, thus generating 2000 frames. This system is two orders of magnitude faster than commercially available DPIV systems. The data are then processed, employing different software packages to return the instantaneous velocity fields.

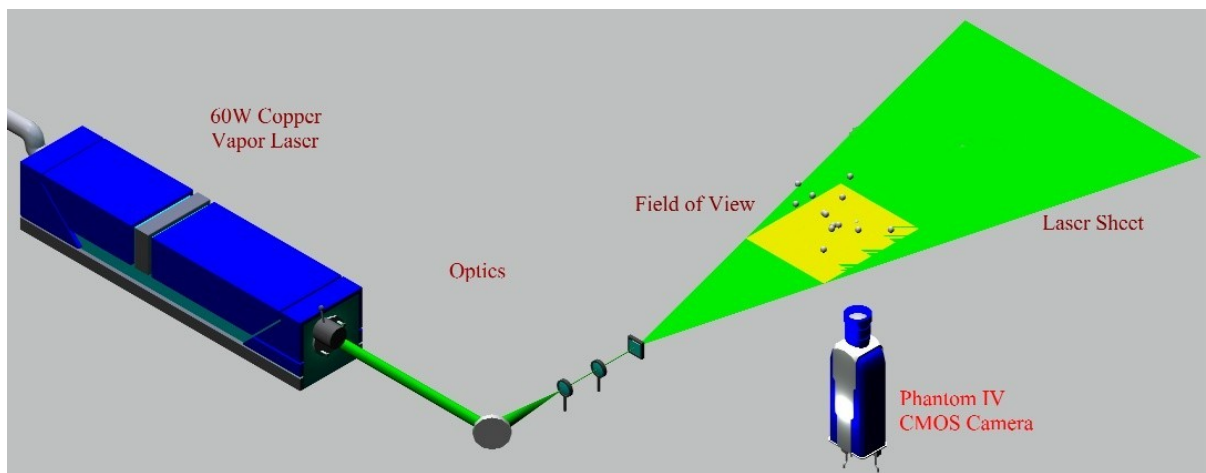


Figure 3.4: Schematic of a typical DPIV setup.

Five planes with areas of $15.36 \text{ cm} \times 15.36 \text{ cm}$ were interrogated at intervals of 15-mm across the valves as shown in Figure 3.5. Each plane of data is parallel to the direction of the jet. The task of the velocity evaluation was performed using conventional cross-correlation between the particle image patterns of two consecutive frames. The interrogation window size of 8×8 pixels and 50% overlap resulted in approximately 127×127 vectors. The overall accuracy of the method is on the order of $\pm 1\%$ of full-scale velocity. A total of 16000 vectors with a grid spacing of 1100 microns are used to describe the flow field.

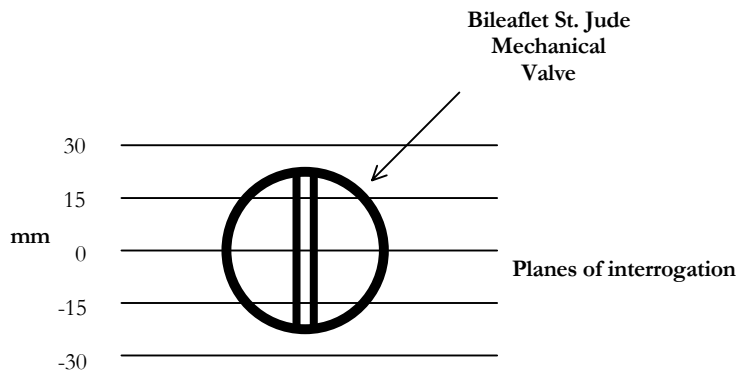


Figure 3.5: Schematic showing the orientation of the illuminated planes with respect to the bileaflet MHV.

Chapter 4

4 Experimental Results and Discussion

In this section, results from each of the test cases are presented along with a discussion of the findings. Although we are unable to do so within the context of this document, it is necessary to animate the sequence of 2000 time instants in order to fully grasp the complexity of the flow field. These animations are available to the reader as .avi files along with the thesis. For the three cases tested, sequences of only seven frames that capture the instantaneous development of the jet field in time are presented. The instantaneous data shown are also from the center plane, $x = 0$. In these figures, the mitral jet initiates from the bottom of each frame and moves upward. The horizontal and vertical axes are scaled according to the diameter of the MHV (31-mm). It should be noted that the porcine valve blocks part of the field and for the two cases where the porcine leaflets and the chordae are in the test section, the DPIV data are limited to a region above $Y/D = 1.3$, with $Y/D = 1$ being the location of the edges of the MHV leaflets in the fully open position. The vectors represent the velocity with their length being proportional to the velocity magnitude. The color scale on the right indicates vorticity levels with yellow to red indicative of positive (counterclockwise-oriented) vorticity and blue indicative of negative (clockwise-oriented) vorticity. To make accurate comparisons between the three test cases, the figures were generated using the same vector length and color scales.

4.1 Instantaneous Results

4.1.1 Bileaflet MHV

In Figures 4.1 through 4.4, we observe seven time instants which reveal the initiation of the mitral jet, the expansion of the high-speed region, and the development of vortices that peel off on the sides of the jet. Regions of high shear stress are generated as the jet interacts with the mechanical valve leaflets, as indicated by the alternating red and blue

regions at the jet inlet. As it penetrates the chamber, the high-speed jet begins to roll the vorticity into counter-rotating vortical structures. It should be noted that the level of vorticity within these vortices is very high (290 1/s) as indicated by the bright red and blue regions. In addition, this high-level vortex vorticity is seen in each of the time instants, indicating that vorticity remains strong through the cycle.

A more careful examination of these figures indicates that the flow consists essentially of two jets. At $T = 0.10$ s, we see a strong, coherent vortex being shed from the right leaflet but not from the left. At the next instant, the right leaflet vortex has grown larger and is joined by the first vortex shed from the left leaflet as shown by the red circular region at $T = 0.15$ s. This vortex also induces opposite sign vorticity as indicated by the adjacent blue region. Moreover, the jet on the left is delayed and issues in the chamber only after the jet on the right has penetrated up to a distance of $Y/D = 2.8$. By $T = 0.20$ s, two individual jets are clearly separate from one another with vortices being shed from each. This behavior is attributed to asynchronous opening of the leaflets. Indeed, high-speed camera data indicate that the opening of the left leaflet follows the opening of the right. In reality, three jets must be present due to the geometry of the MHV itself, but it seems that they are masked because of the asynchronous leaflet behavior. It is possible that a slight inclination could give rise to such an asymmetric operation, but previous studies have also observed this same phenomenon [8, 9, 16, 51]. Consistency and repeatability were observed with respect to the asynchronous opening of the valve, which indicates that it is not a random process.

Throughout the remainder of the cycle, the width of the jet continues to grow over time as the vortices develop further and fluid is entrained into the system. For time instances $T = 0.25$ through $T = 0.35$ s, four distinct vortices are present in the flow field. Overall, it appears that the two lateral orifice jets are stronger as the jet issuing from the center orifice is not well defined. For the time instances shown, the lateral dispersion of the jet is widest at $T = 0.50$ s, where it ranges from $X/D = -1.2$ to $X/D = 1.4$.

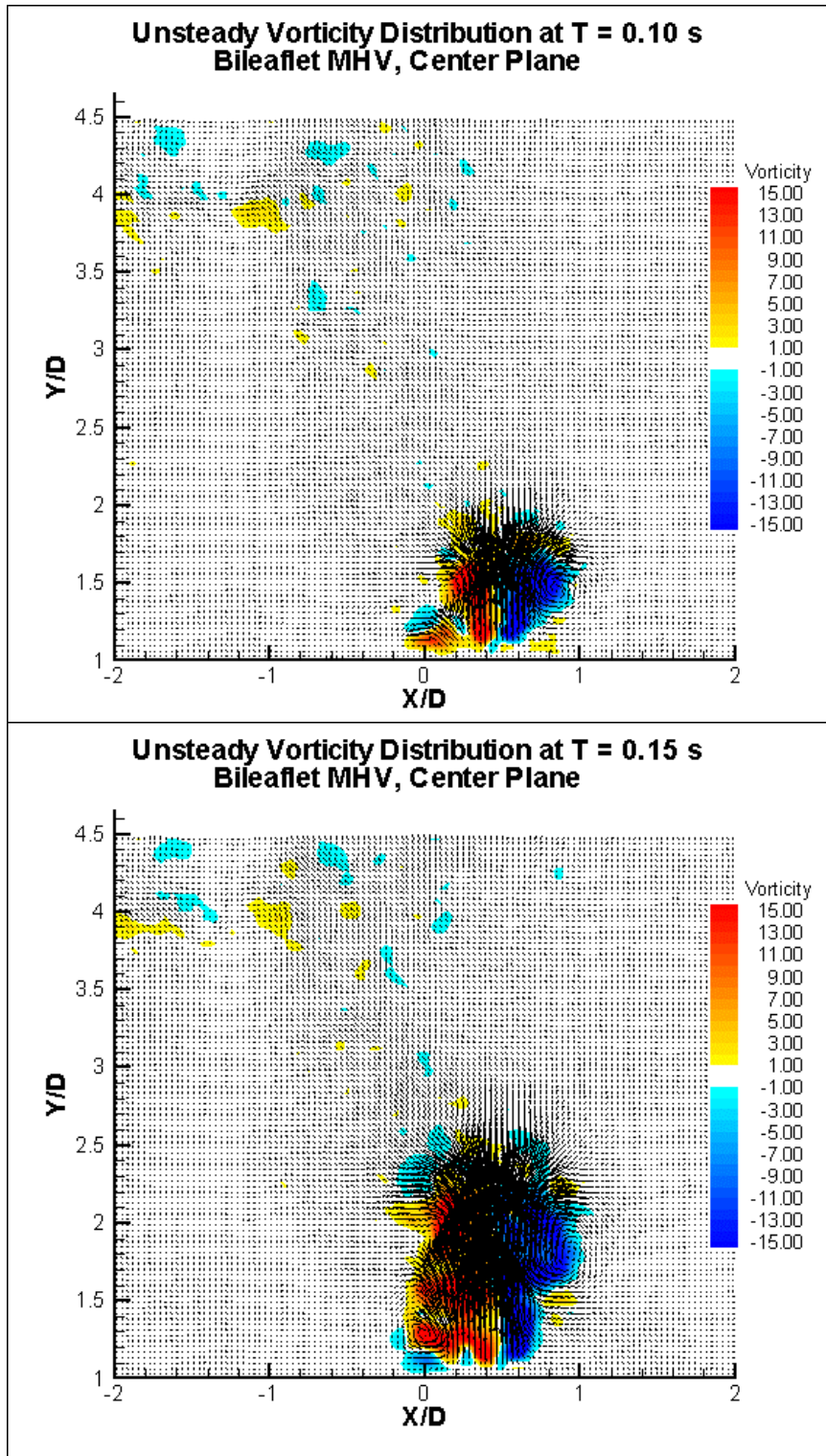


Figure 4.1: Unsteady Vorticity Distributions for the bileaflet MHV at two time instants, $T = 0.10$ s and $T = 0.15$ s.

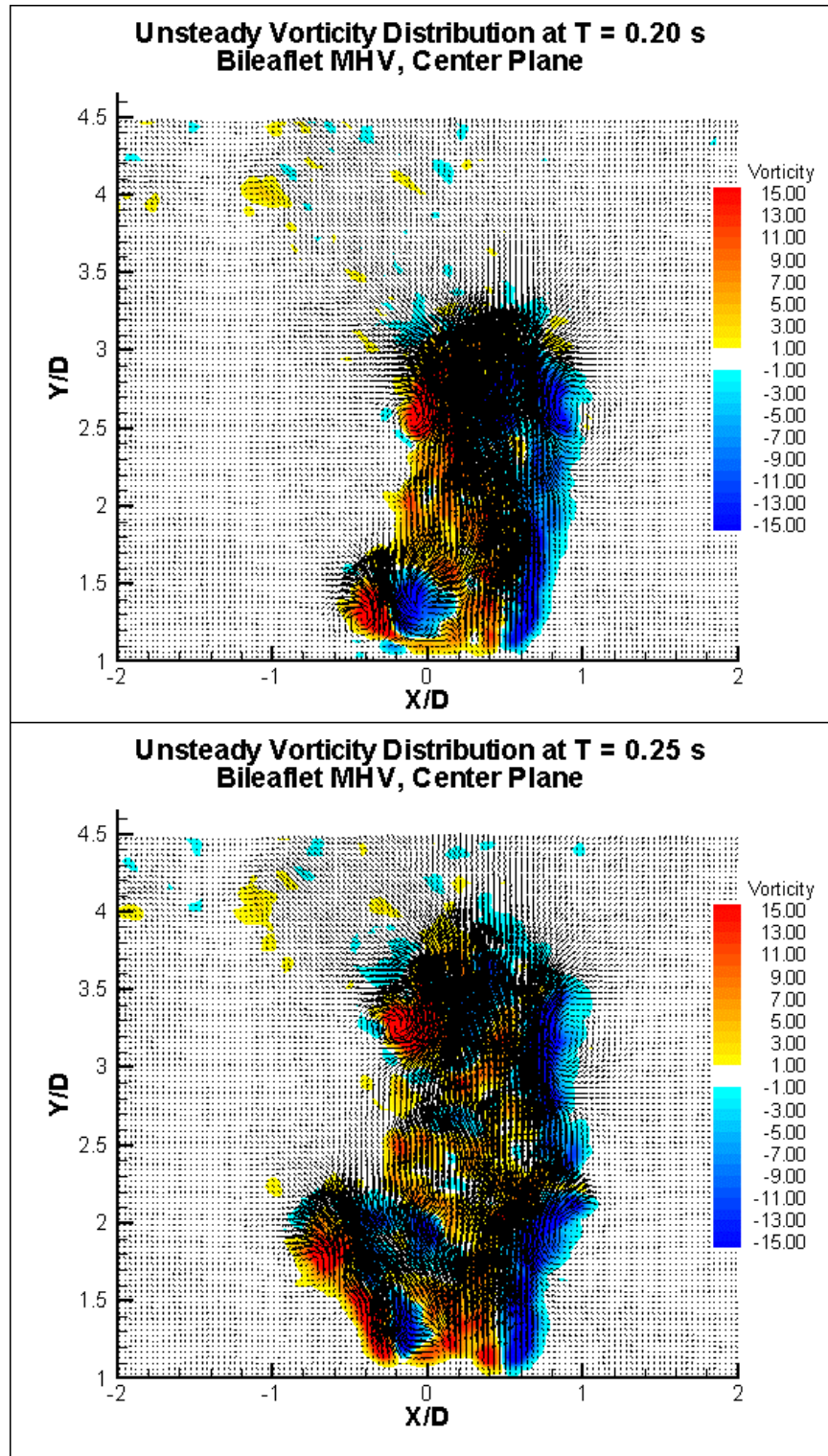


Figure 4.2: Unsteady Vorticity Distributions for the bileaflet MHV at two time instants, $T = 0.20$ s and $T = 0.25$ s.

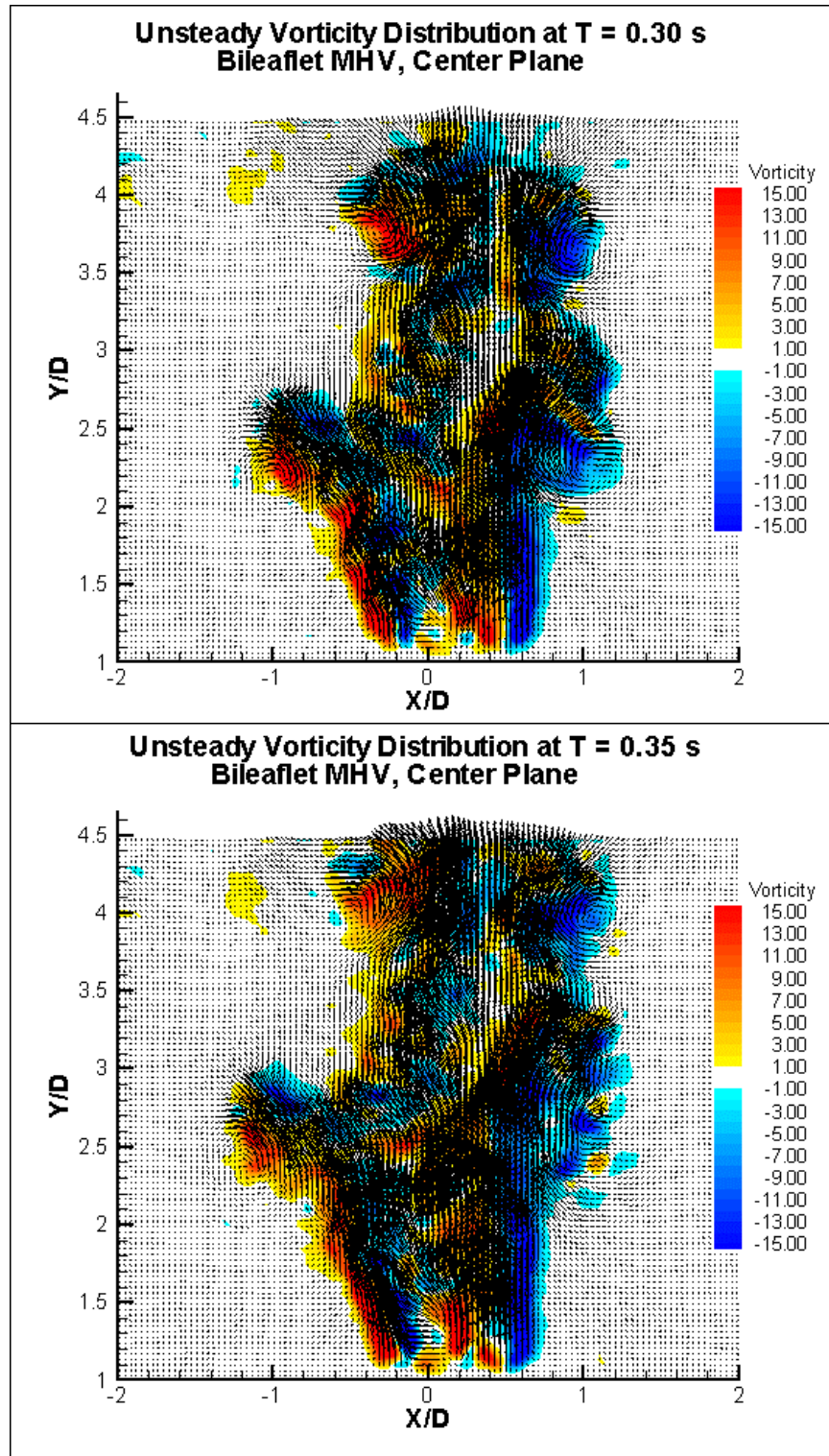


Figure 4.3: Unsteady Vorticity Distributions for the bileaflet MHV at two time instants, $T = 0.30$ s and $T = 0.35$ s.

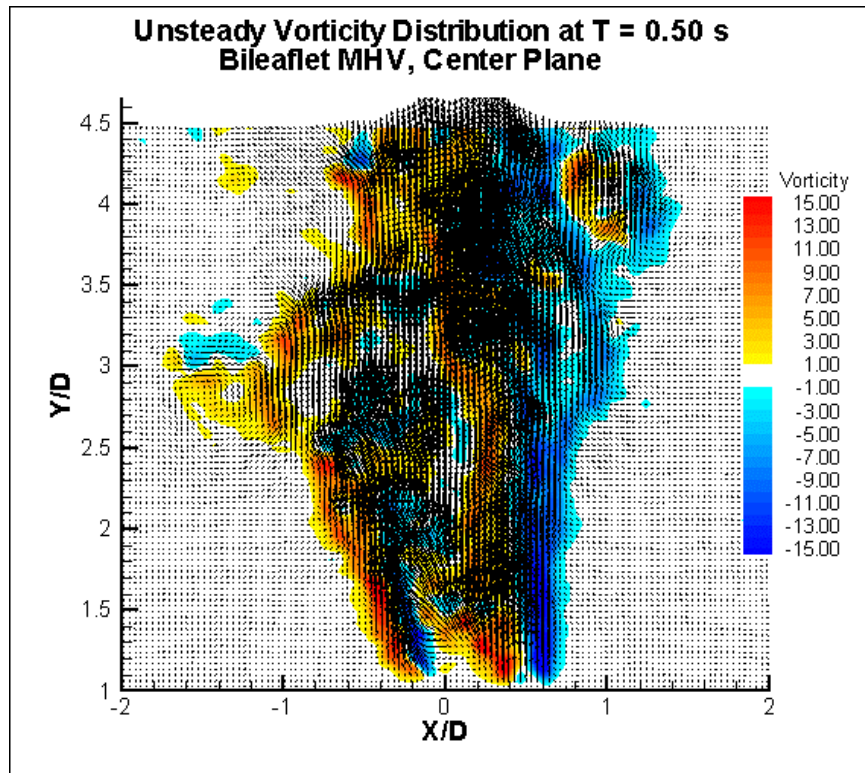


Figure 4.4: Unsteady Vorticity Distributions for the bileaflet MHV at one time instant, T = 0.50s.

4.1.2 Porcine MV

Figures 4.5 through 4.8 show the development of the mitral jet for the natural porcine valve and its subvalvular apparatus. It is now evident that the formation and proliferation of vortices is limited in this case. The jet enters with higher velocity than the MHV and penetrates further into the chamber to a distance of $Y/D = 3.0$ during the first time instant. Throughout the cycle, the levels of vorticity in this case are comparable to that of the MHV, but at one point during the cycle, there exists a very high level of vorticity, 350 $1/s$. This is due to the fact that the porcine jet has a higher velocity than its mechanical counterpart.

In addition, it appears as if a more prominent vortex sheds from the anterior leaflet; however, it is thought that the sutures which anchor the papillary muscles initially mask the posterior vortex somewhat. For the bileaflet valve, as seen in Figure 4.1 ($T = 0.10$ s), a vortex is immediately shed from the right leaflet at a distance of $Y/D = 1.5$, whereas for the porcine valve, the vortex is located at $Y/D = 2.2$. At the second time instant, two symmetric counter-rotating vortices are present at $Y/D = 2.9$ with the negatively oriented vortex slightly further downstream. Interestingly, at $T = 0.20$ s, the positively oriented vortex has propagated downstream faster than its counterpart; in fact, during the same amount of time, it moved twice as fast. Overall, the vortex shedding present in this case is minimal in comparison to the bileaflet MHV as the vortices do not further develop and proliferate throughout the entire heart cycle as seen in Figures 4.1 through 4.4. Between time instants $T = 0.20$ s and $T = 0.30$ s for the porcine valve, the vortices have diminished considerably and are almost completely gone.

Rather than experiencing asynchronous leaflet motion, the porcine valve jet as a whole exhibits more of a wavelike behavior. This motion is more easily seen when all 2000 time instants are animated, but one is able to detect it in the time instants presented. The wavy motion is best observed at $T = 0.30$ s and $T = 0.50$ s, where the vectors and vorticity regions on either side of the jet appear to undulate. It is also interesting to note how the porcine leaflets are able to control the flow after the initial penetration of the jet. When the

flow impulsively enters the chamber, the leaflets undergo a large initial displacement, which allows for a wider jet at the onset of the cycle. This can be seen in Figures 4.5 and 4.6. Once the leaflets reach their steady state condition, the flow assumes a more narrow, directed pathway through the chamber for the remainder of the cycle, as shown in Figure 4.8. Toward the end of the cycle, when the jet is less forceful, a distinct vertical line can be seen oscillating between the positive and negative levels of vorticity. Throughout the jet progression, while the jet oscillates back and forth laterally, it does not disperse in this direction, as does the bileaflet MHV. The width of the jet is much more contained, and for the present time instances, the widest spreading ranges from $X/D = -0.6$ to $X/D = 0.9$ at $T = 0.15$ s. In addition, at the last time instant, the velocity is much higher and is concentrated toward the center of the flow whereas in the MHV case, the jet has dissipated energy laterally.

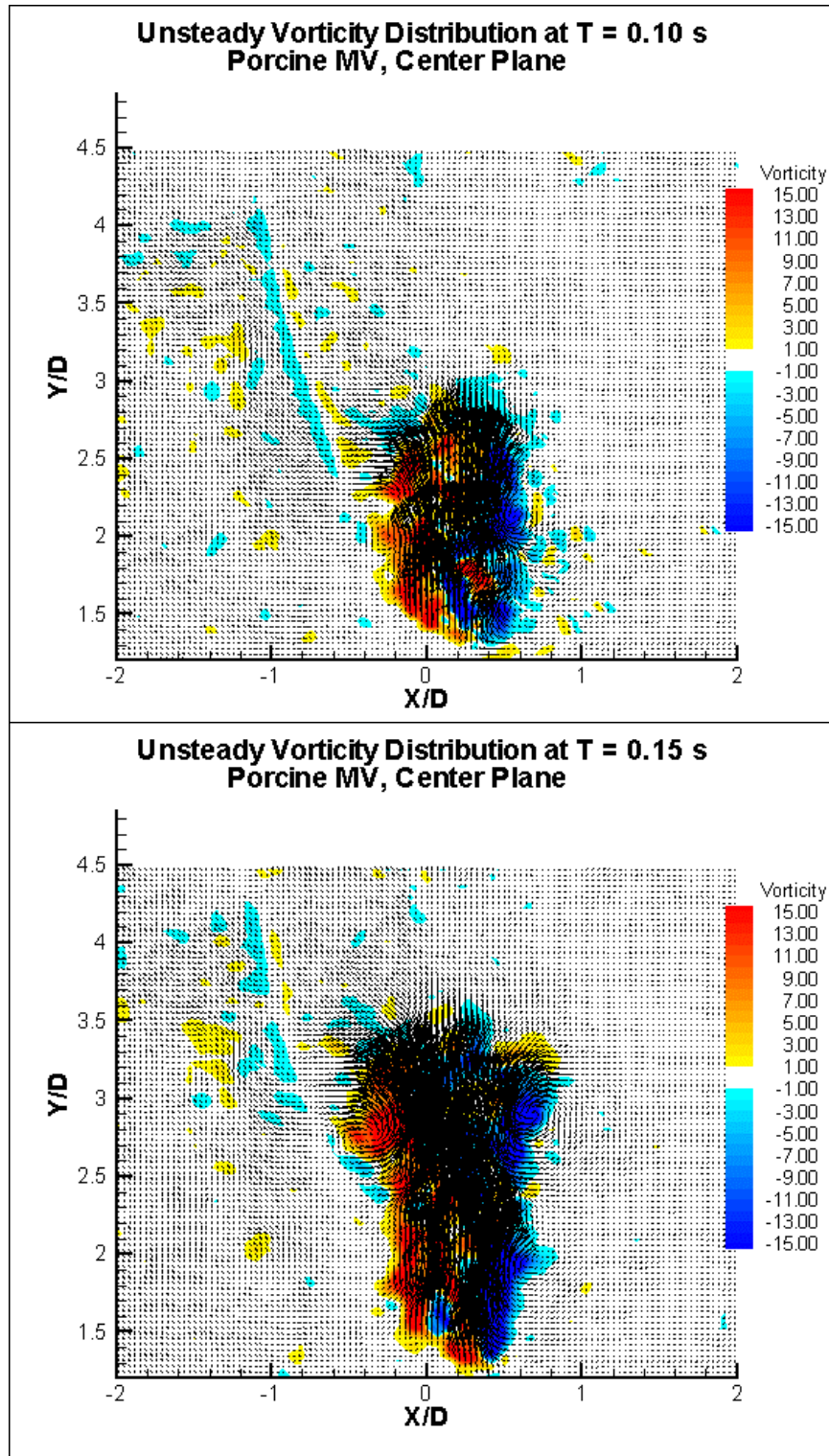


Figure 4.5: Unsteady Vorticity Distributions for the porcine mitral valve at two time instants, $T = 0.10$ s and $T = 0.15$ s.

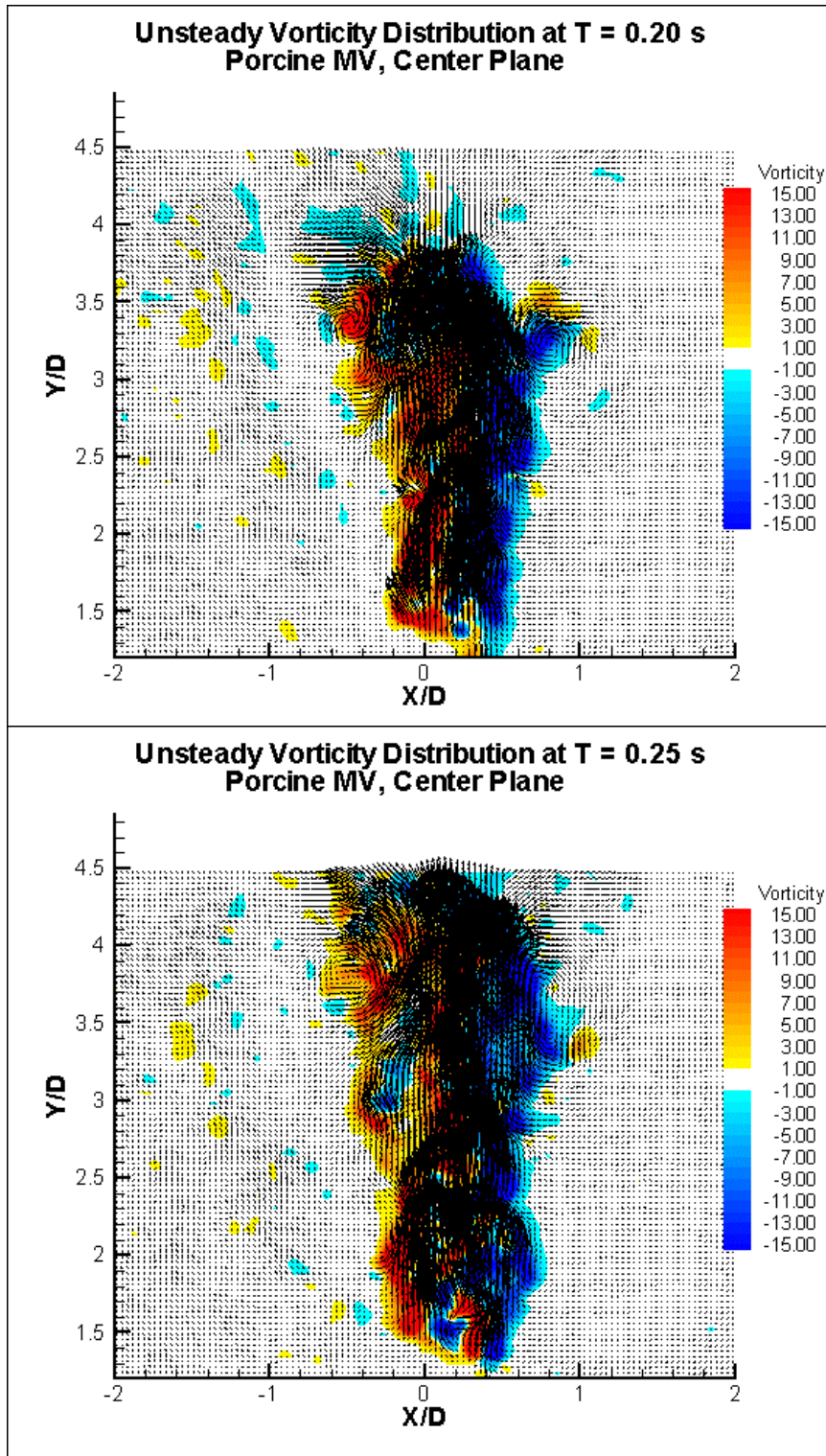


Figure 4.6: Unsteady Vorticity Distributions for the porcine mitral valve at two time instants, $T = 0.20$ s and $T = 0.25$ s.

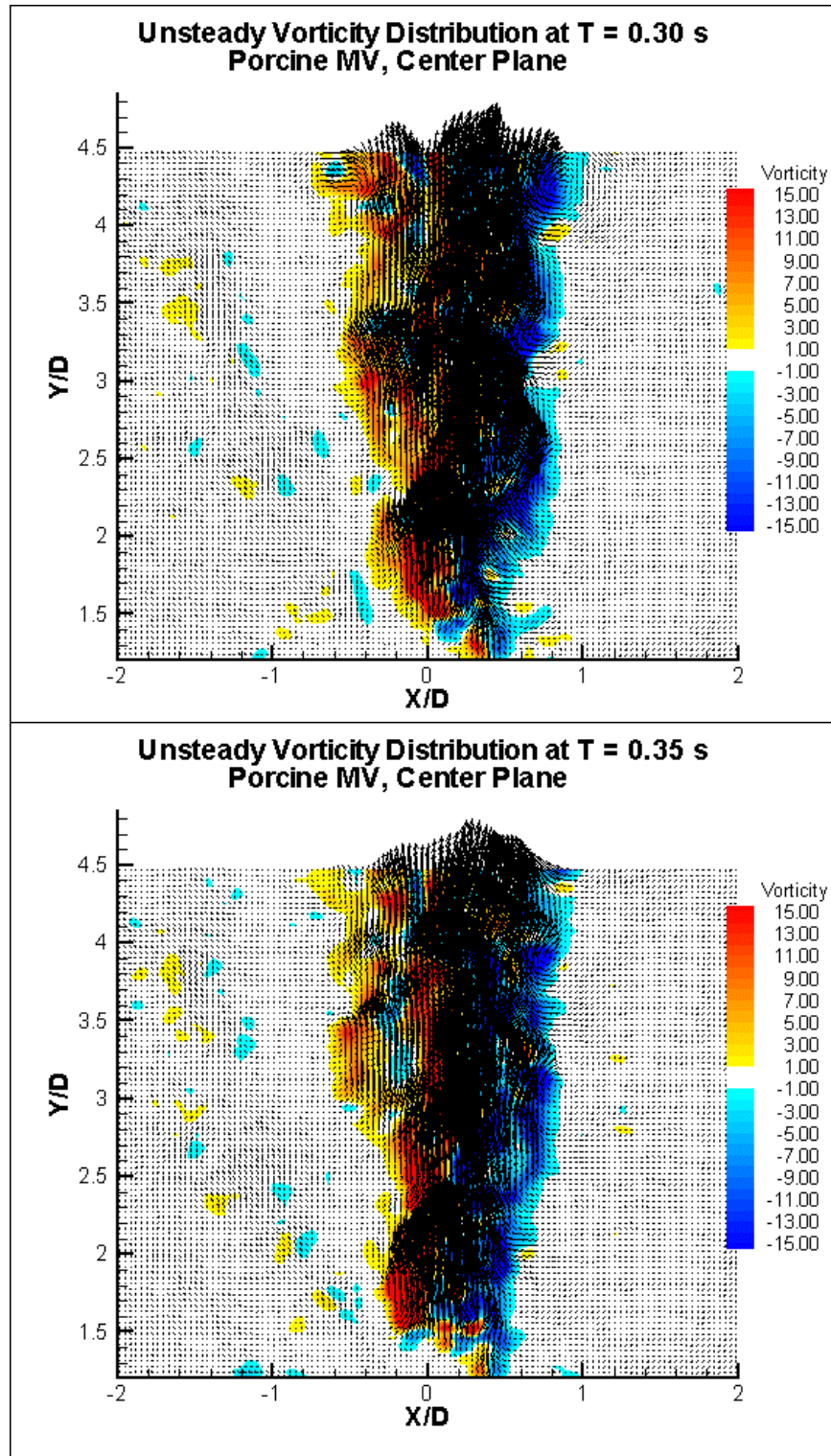


Figure 4.7: Unsteady Vorticity Distributions for the porcine mitral valve at two time instants, $T = 0.30$ s and $T = 0.35$ s.

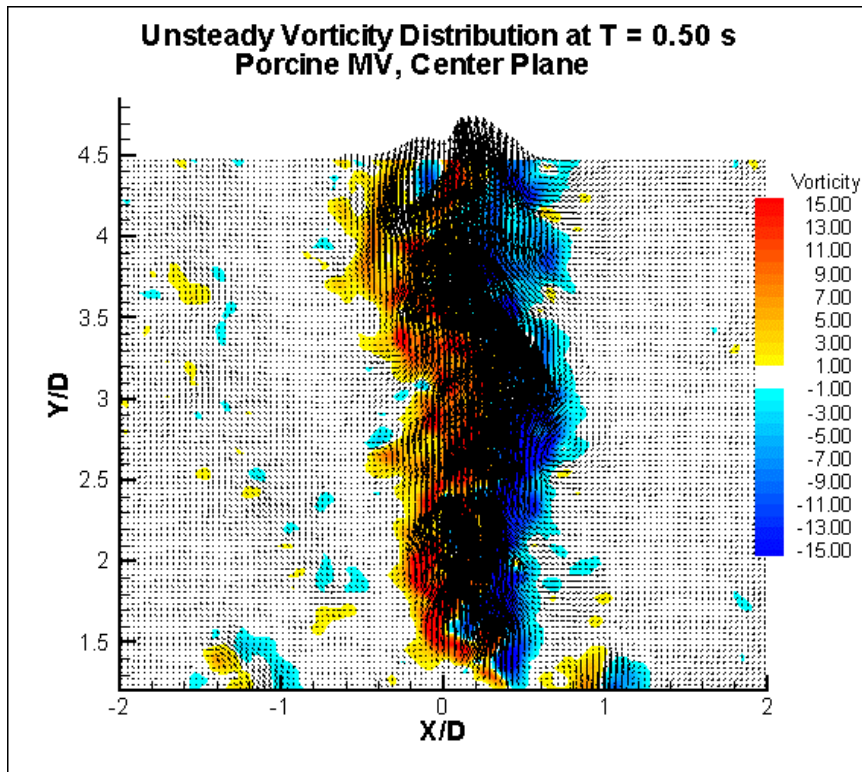


Figure 4.8: Unsteady Vorticity Distributions for the porcine mitral valve at one time instant, $T = 0.50$ s.

4.1.3 Chordal Preservation

In Figures 4.9 through 4.12, we observe the mitral jet behavior for the test case simulating CP, namely the bileaflet MHV implanted into an excised mitral valve apparatus. Intuition tells us that the results for this case would lie somewhere between the first two cases presented, and indeed, that is what we observe. Qualitatively, the appearance of the combination jet more closely resembles that of the porcine jet, as it is more confined with minimal spreading. At the first time instant, $T = 0.10$ s, the vortex development is delayed in comparison to the MHV. For the bileaflet valve, as seen in Figure 4.1, a vortex is immediately shed from the right leaflet at a distance of $Y/D = 1.5$, but in the combination, the vortex is located at $Y/D = 1.9$. Due to its higher speed, the jet also penetrates further into the chamber ($Y/D = 2.8$), at a level almost equal to the penetration level of the porcine MV. Two counter-rotating vortices are observed at the first time instant, but the level of vorticity within them is slightly less than that of the MHV alone. In the remaining time instants, it is more difficult to locate the vortices in the field because they are weaker and less coherent. By $T = 0.25$ s, there are no longer vortices present in the flow field. The presence of the native tissue does not fully suppress the generation of vortices from the mechanical leaflets, but the natural valve certainly affects on the overall flow behavior. It appears that the presence of the mitral leaflets and chordae tendineae act as an acceleration region downstream of the MHV. Distal to the valve, we observe wavelike patterns indicative of the superposition between the free stream and the shed vortices. While the jet does not exhibit the same oscillatory behavior as the porcine jet, it is similar, especially when viewing all 2000 time instants. Among the time instants shown, $T = 0.35$ s best captures the wavelike motion. Overall, the jet is more smoothly directed and contained than the bileaflet case. The widest dispersion is limited to the range of $X/D = -0.9$ to $X/D = 0.9$, as seen in Figure 4.12.

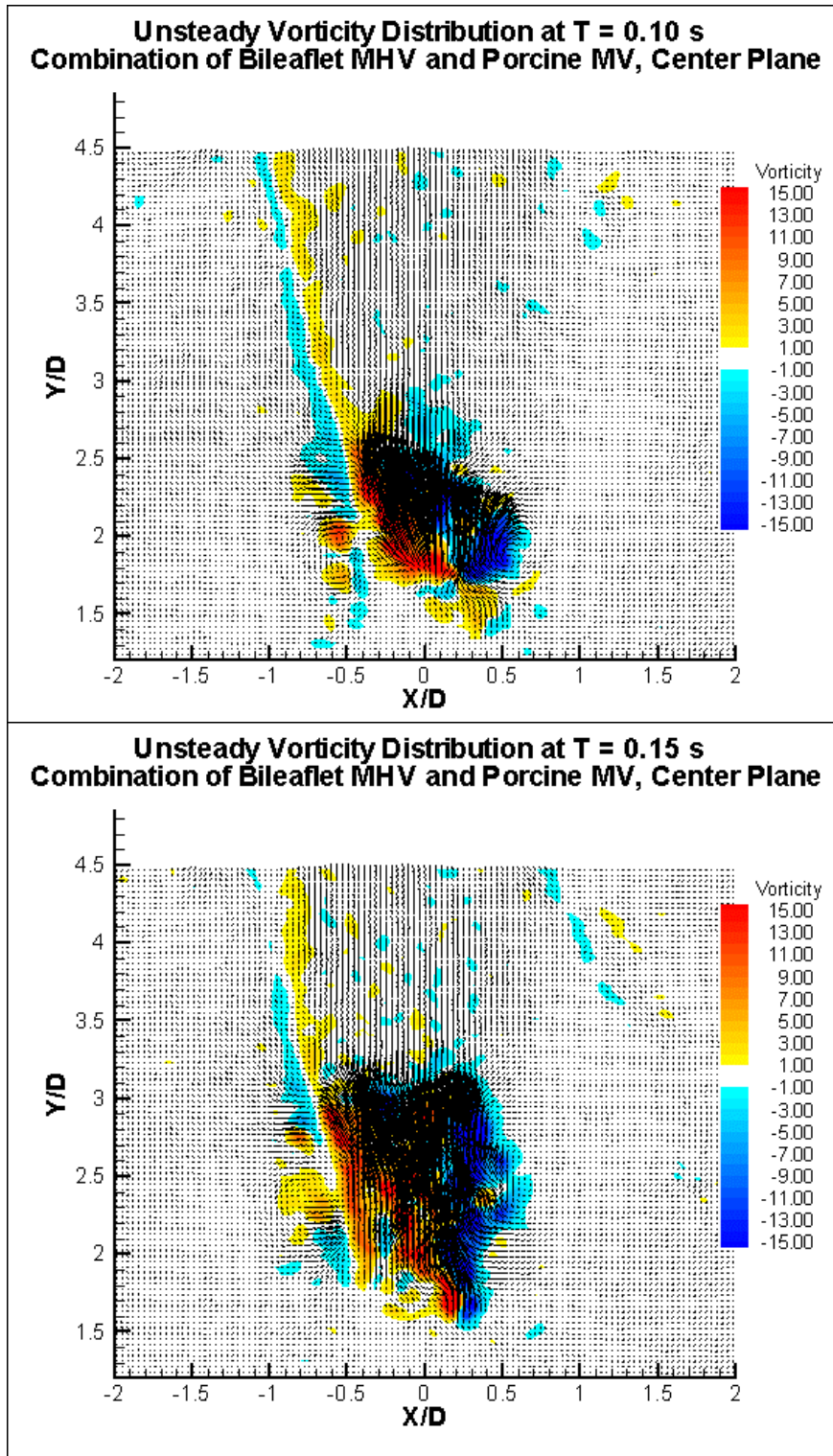


Figure 4.9: Unsteady Vorticity Distributions for the chordal preservation case at two time instants, T = 0.10 s and T = 0.15 s.

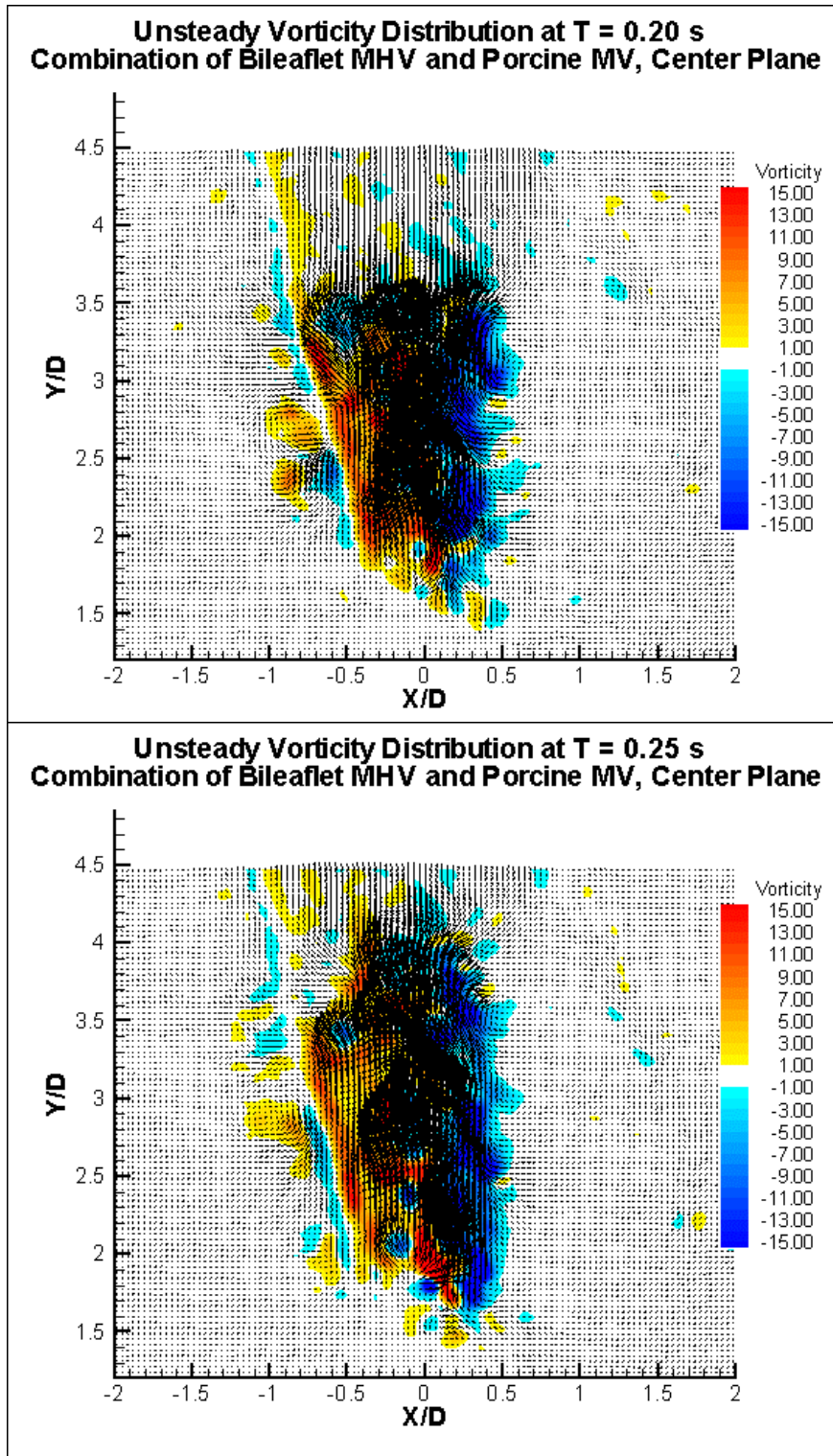


Figure 4.10: Unsteady Vorticity Distributions for the chordal preservation case at two time instants, T = 0.20 s and T = 0.25 s.

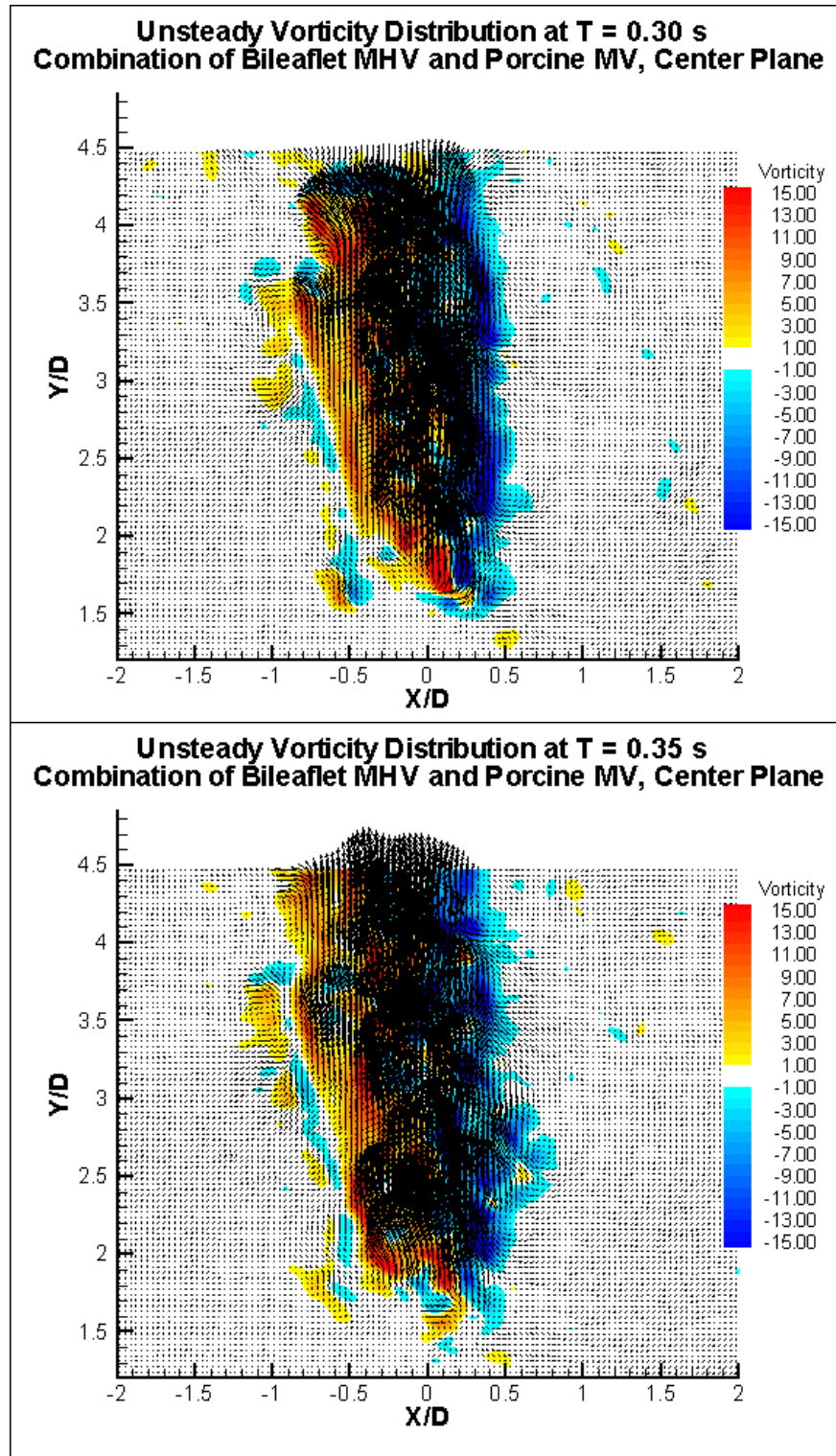


Figure 4.11: Unsteady Vorticity Distributions for the chordal preservation case at two time instants, T = 0.30 s and T = 0.35 s.

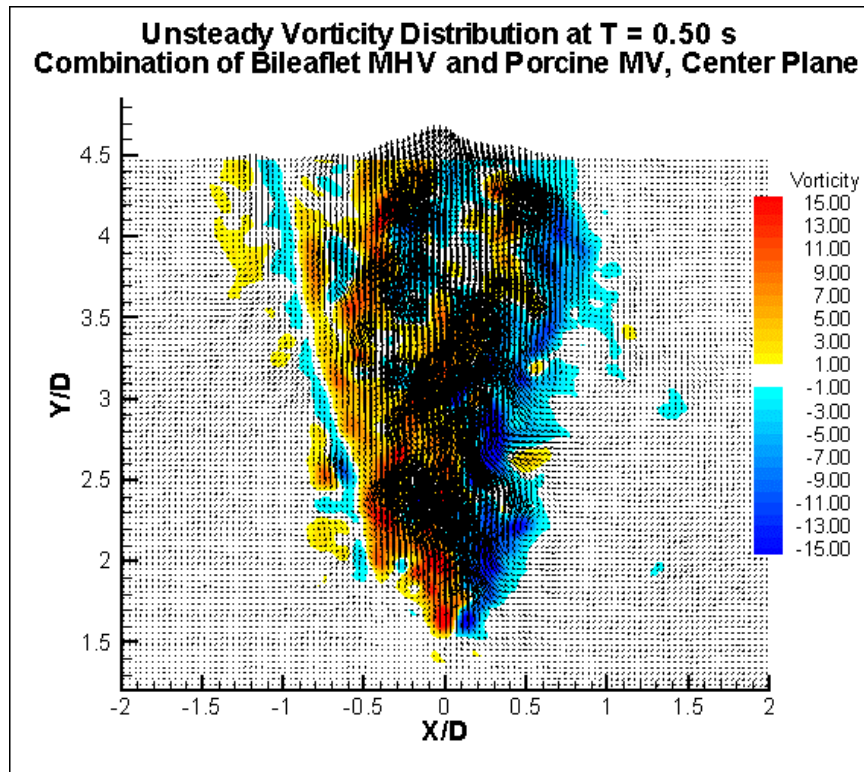


Figure 4.12: Unsteady Vorticity Distributions for the chordal preservation case at one time instant, T = 0.50 s.

4.2 Time-averaged Results

4.2.1 Velocity and Vorticity

Time-averaged velocity and vorticity distributions for the center planes of all three cases are shown in Figure 4.13 and 4.14. These measurements were obtained by averaging the values over one heart cycle. It can be seen that each of the cases tested have similar levels of vorticity. For the bileaflet valve, the skewness due to the asynchronous leaflet motion can clearly be seen as the jet from the right leaflet produces stronger velocity and vorticity components as shown by the large red and blue regions to the right of the image. This jet issuing from the outer orifice dominates the flow field over time. Directly after the mitral valve, the alternating red and blue regions of vorticity are indicative of the strong shear layers induced from the mechanical leaflets.

For the porcine valve, we see a narrower band consisting of two large regions of positive and negative vorticity, both approximately equal in strength. The left vorticity region is slightly larger than the right. There are distinct regions of dense velocity vectors in the center of the porcine and combination jets that are not present in the MHV case. In both of these cases, two thin bands of clockwise vorticity are present to the left of the jet. These regions are a result of the flow interaction with the sutures that secure the papillary muscles. From the start, both jets with the leaflets and CT have more narrow widths, which immediately influences their levels of dispersion. Overall, the porcine jet is the most contained, generating the least amount of lateral dispersion, but the addition of the natural valve to the MHV provides a significant improvement over the MHV alone.

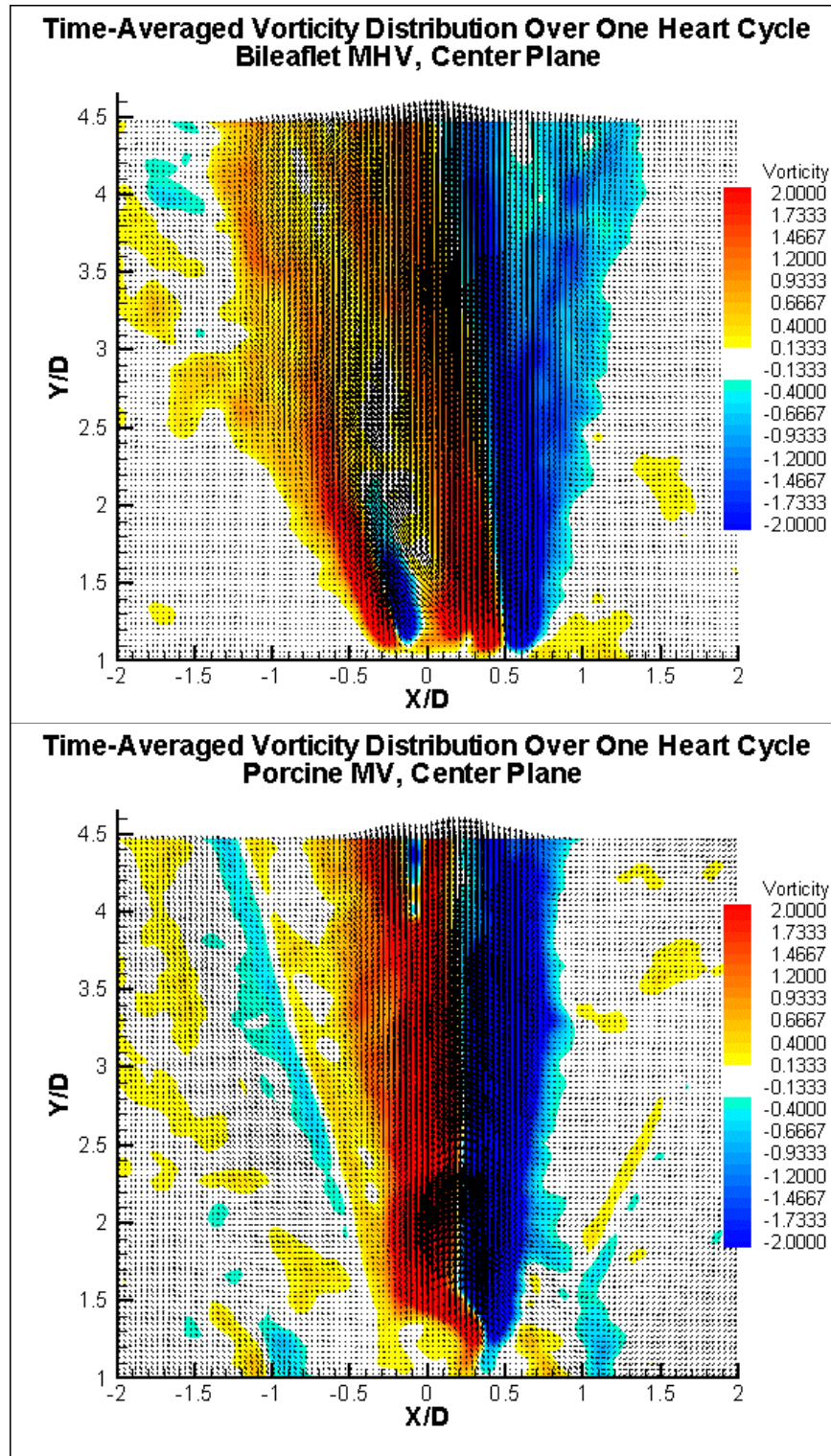


Figure 4.13: Time-averaged vorticity distributions for the bileaflet MHV and porcine valve cases.

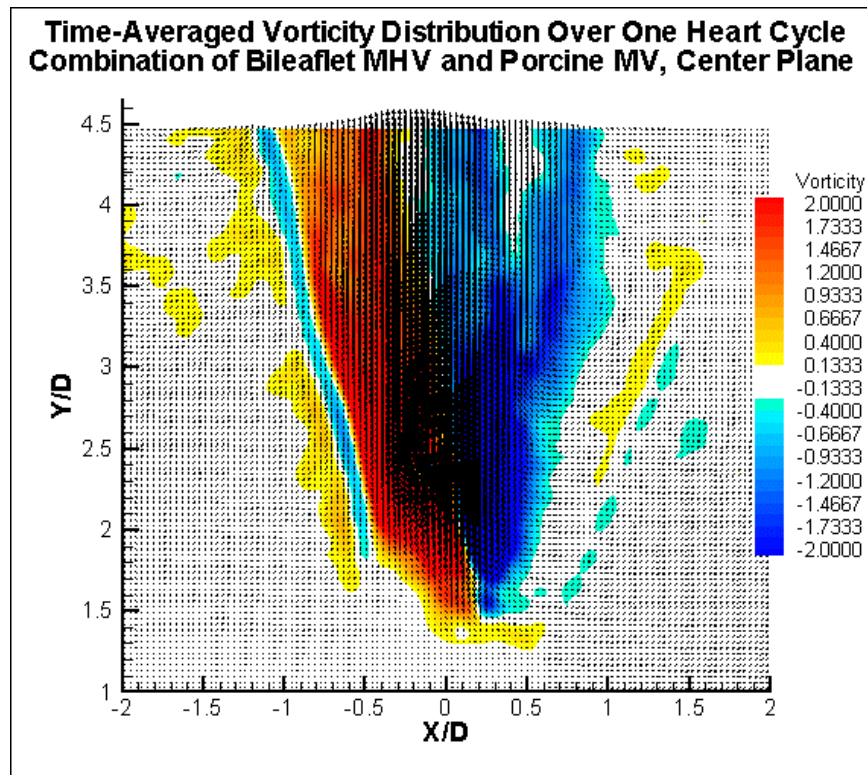


Figure 4.14: Time-averaged vorticity distribution for the chordal preservation case.

4.2.2 Additional Planes of Data

By making measurements in other planes across the volume of the left ventricular chamber, it is possible to gain insight into the three-dimensional characteristics of the flow fields for each of the configurations tested. Vorticity distributions from two other planes along with the center plane data can be seen in Figures 4.15 through 4.17. These figures display planes corresponding to $x = 0, 15,$ and 30 -mm across the valve diameter. For the CP case, only two planes are shown for $x = 0$ and $x = 15$ as it was not possible to process the remaining data file.

With increasing distance from the center plane of the valve, the size of vorticity fields decrease in each of the test cases. Though the regions containing vorticity diminish in size, there are areas of high intensity vorticity present in all of the planes. For the MHV at $x = 15$, the regions of vorticity alternate between clockwise and counterclockwise rotation as shown by the red and blue bands, but at $x = 0$, one of the blue bands in the wake of the left leaflet is no longer present. The distribution at $x = 15$ also reveals the asynchronous leaflet behavior as the right orifice jet is dominant. Near the leaflets of the MHV at $x = 15$, there are two small pockets of clockwise vorticity which are not visible at $x = 0$. Overall, it appears that the vorticity generated from the left leaflet diminishes at a faster rate than that produced by the right leaflet.

In the porcine case, at $x = 0$, the two opposing red and blue regions of vorticity dominate the flow field. At $x = 30$, most of the vorticity in the flow field has diminished with only small regions present due to the sutures. Also in Figure 4.16, there are two bands of positive and negative vorticity in the bottom corners of the flow field, which grow stronger at $x = 15$ and then lessen at $x = 30$. This region could be attributed to the jet interacting with the flow exiting through the aortic outflow pipe.

The most important conclusion to be made from the sets of data concerns the coherence of the jet in the out-of-plane direction. The data presented in section 4.1 clearly shows that the porcine and combination jets are more contained than the bileaflet jet in the

plane perpendicular to the pivot axis of the leaflets. It is important to determine the behavior of the jet in the direction parallel to the pivot axis as well. For the bileaflet case, at $x = 15$, the vorticity field closely resembles the $x = 0$ plane in that the intensity of the vorticity remains relatively the same between the two planes. This information indicates that the jet is expanding freely in the out-of-plane direction. For the porcine and combination cases, however, the data reveals otherwise. In the $x = 15$ planes, the regions of vorticity are not only smaller in size, but they are also less intense in comparison to the center plane. This suggests that the mitral jet is constricted by the native leaflets and chordae tendineae in the direction parallel to the pivot axis of the leaflets. MRI studies have shown that with a bileaflet MHV, the mitral jet flow is not redirected toward the aortic valve but rather loses its coherence and disperses within the ventricle [32]. These three-dimensional results provide evidence that the natural mitral tissue tends to guide the flow along a preferred pathway since the flow is constricted in planes both parallel and perpendicular to the pivot axis of the leaflets.

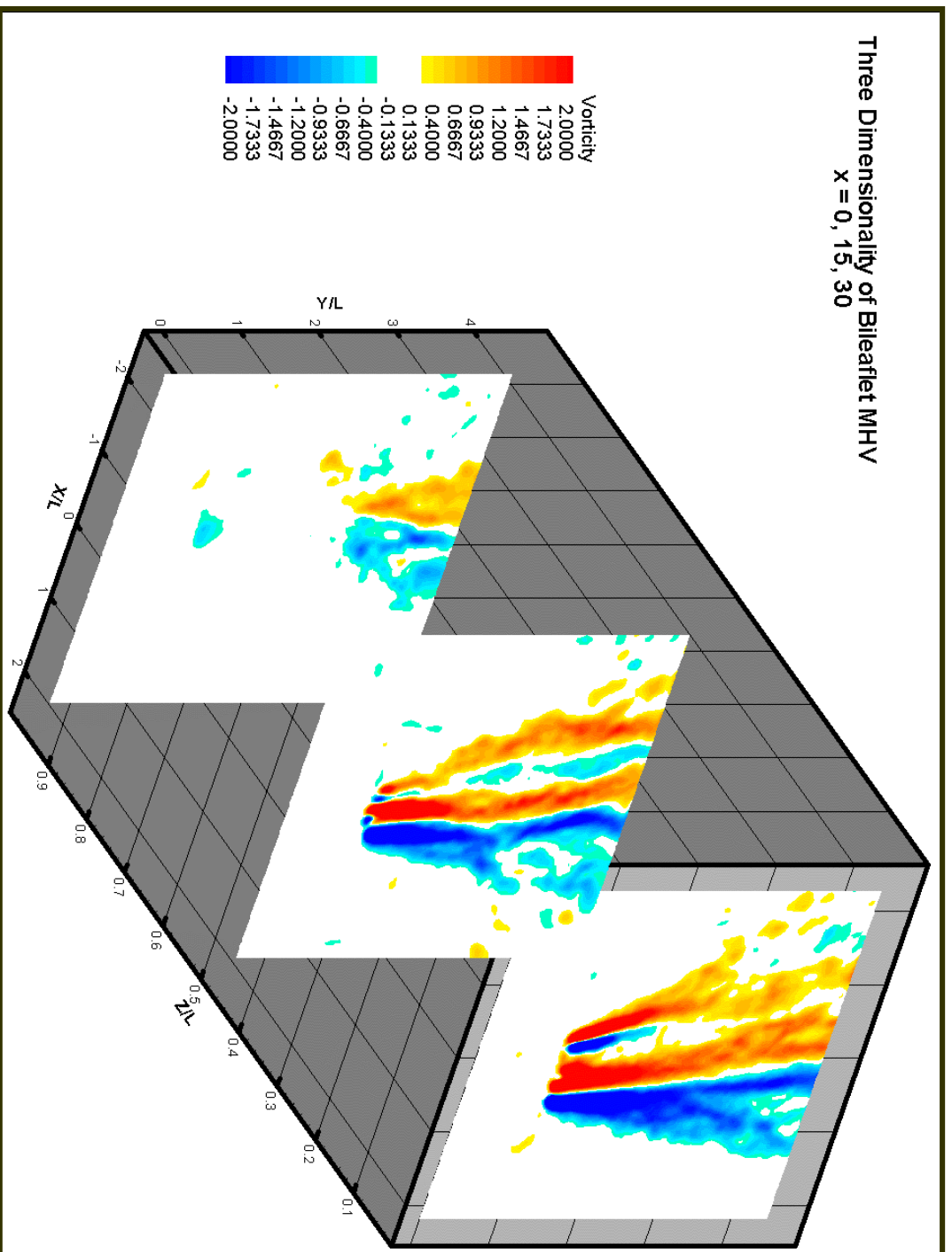


Figure 4.15: Time-averaged vorticity distributions for three planes, bileaflet MHV, $x = 0, 15$, and 30 .

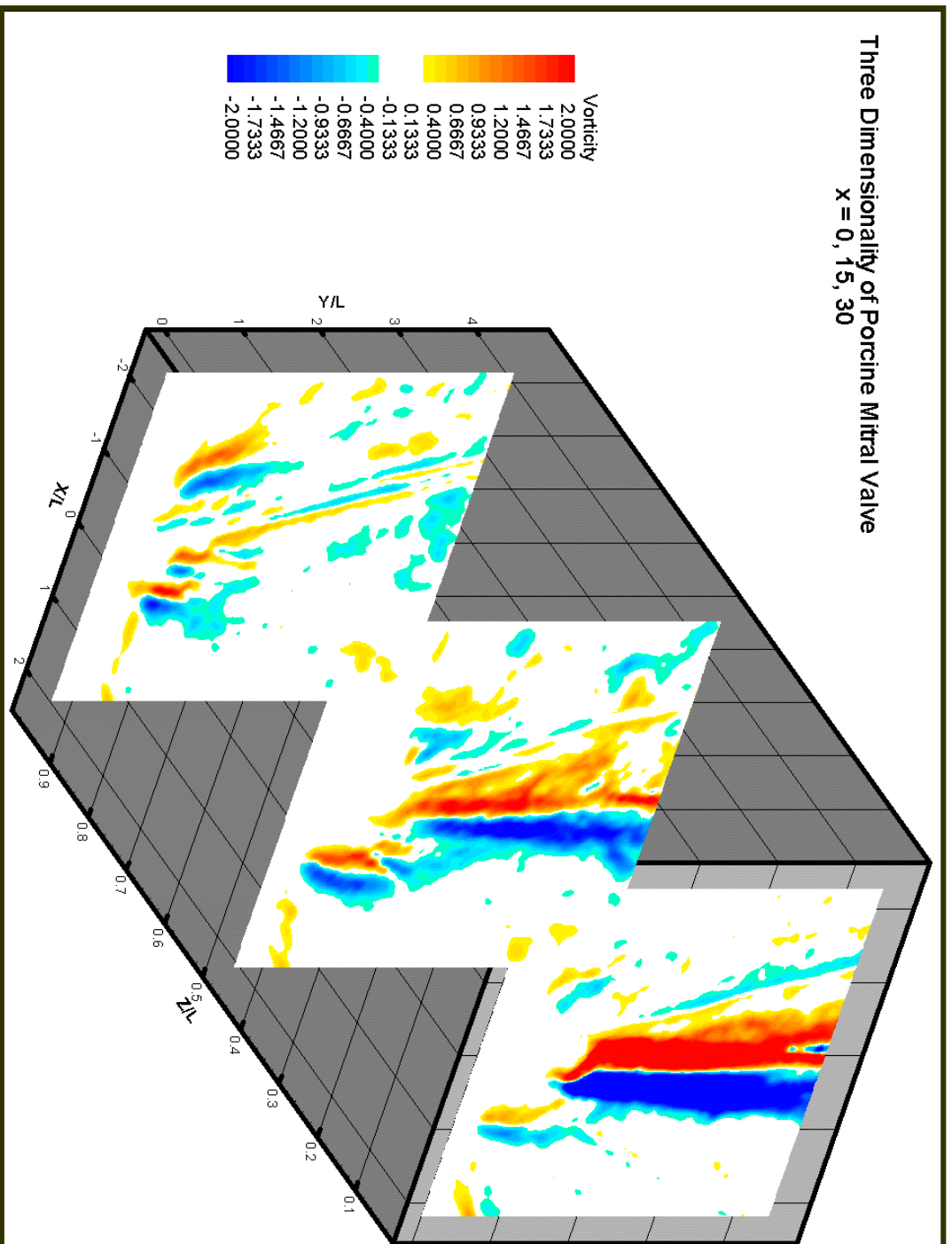


Figure 4.16: Time-averaged vorticity distributions for three planes, porcine mitral valve, $x = 0, 15,$ and 30 .

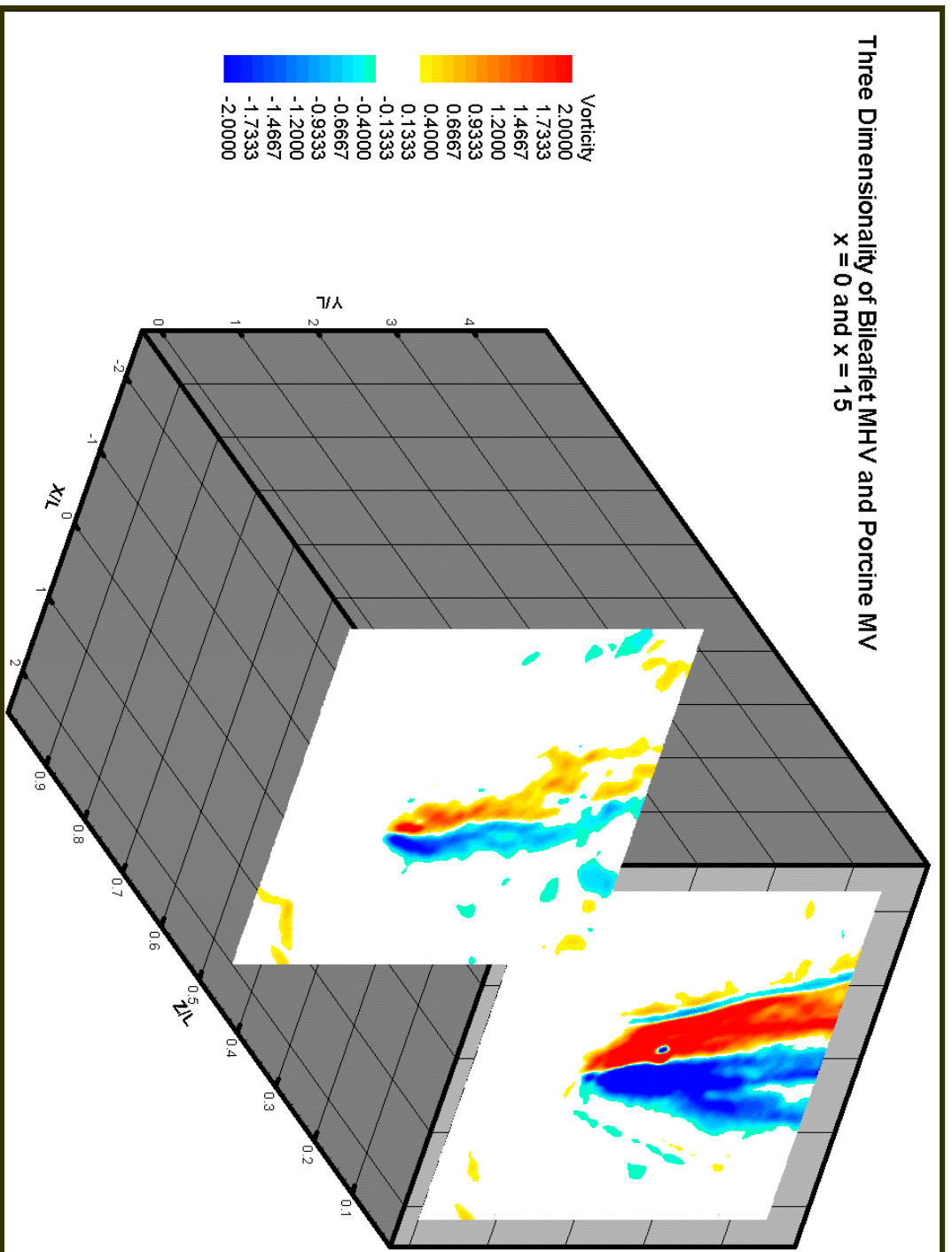


Figure 4.17: Time-averaged vorticity distributions for two planes, chordal preservation, $x = 0$ and 15.

4.2.3 Turbulent Kinetic Energy

Turbulent kinetic energy (TKE) measurements provide valuable information about the random character of the flow. Turbulent motions tend to be the most detrimental to the formed elements of blood. In cardiovascular flows such as those in this experiment, if data were averaged over the entire heart cycle, inherent error would be introduced in the calculation of turbulent kinetic energy by the fact that the flow itself is pulsatile. In order to best quantify the TKE, these data were calculated by averaging over a series of 100, 200, and 500 consecutive frames within each cycle at a point just after the valve has completely closed. Throughout these sequences of frames, the mean velocity is negligible as little forward motion is occurring due to the propagation of the jet, but what does remain are the random motions associated with the flow itself. By averaging in this way, the inherent error introduced by the pulsatility of the flow is omitted.

Figures 4.18 through 4.23 display the TKE distributions averaged over 100, 200, and 500 frames, respectively, for each of the configurations tested. Results for the bileaflet MHV show a large region of TKE present distal to the valve that is not present in the other two cases. The lowest TKE levels are observed when 100 frames are averaged, and as the number of frames averaged is increased from 100 to 500, it is obvious that the randomness occurring within the field also increases. The bright red regions in Figure 4.19 indicate these high levels of TKE. The two frames in Figure 4.18, averaged over 100 and 200 frames, respectively, show higher regions of TKE downstream from the left leaflet while averaging over 500 frames displays the most TKE distal to the right leaflet.

For both the porcine and combination cases, the frames shown for each are very similar in their size, shape, and levels of TKE. In contrast to the MHV, the areas of TKE present downstream of these two valve configurations are dramatically smaller, and the TKE levels are also much less. This is most likely due to the presence of the native tissue that guides and contains the flow. By increasing the number of frames averaged, we observe that the TKE levels decrease, which is opposite of what occurs for the bileaflet MHV.

The information presented here provides some basic insight into the random character of the flow for the three configurations tested; however, a solid understanding of the role of turbulence downstream of the valves has not been achieved. These complex flow fields require further data analysis and review.

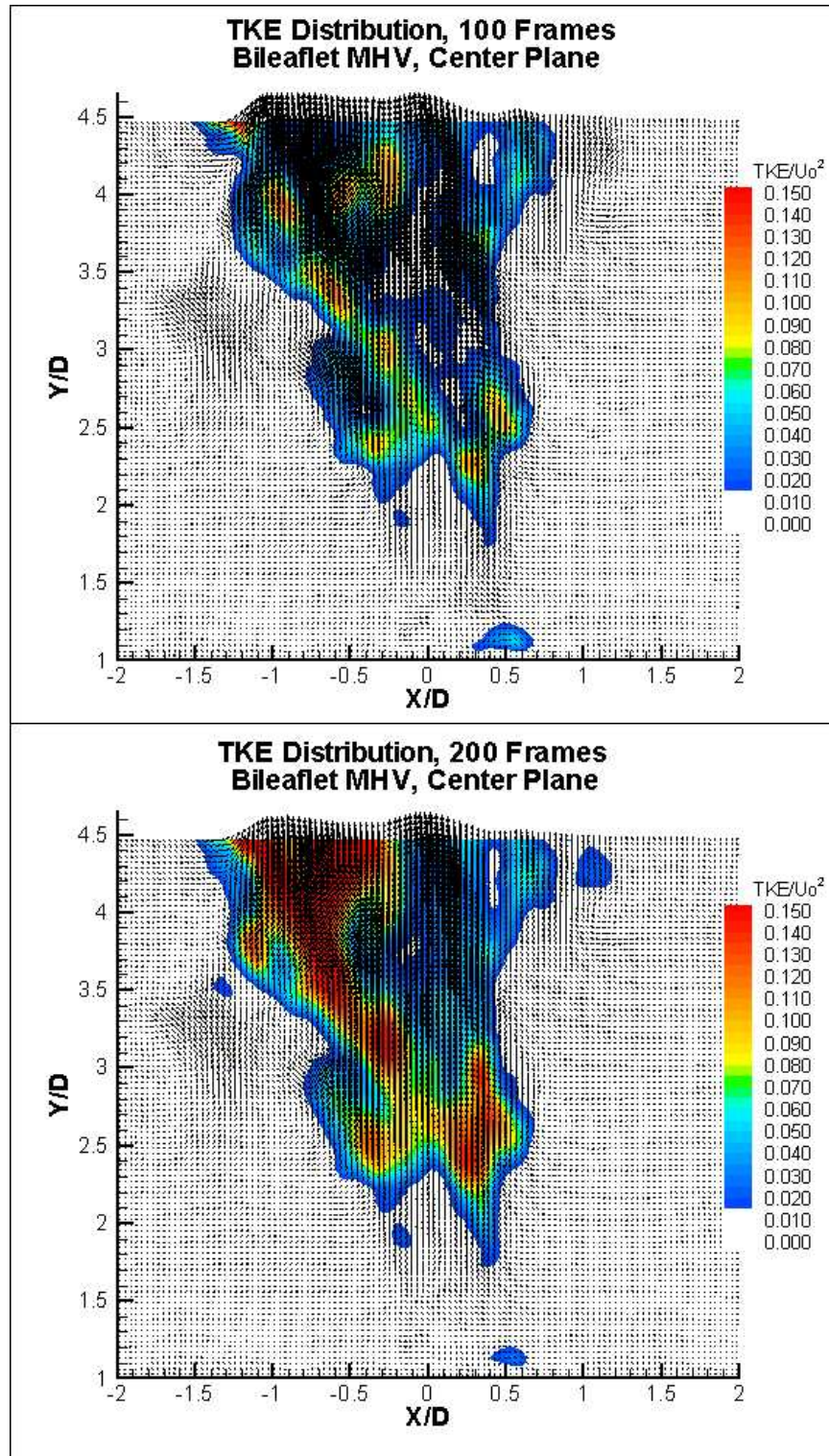


Figure 4.18: Time-averaged turbulent kinetic energy distributions for the bileaflet MHV averaged over 100 frames (top) and 200 frames (bottom).

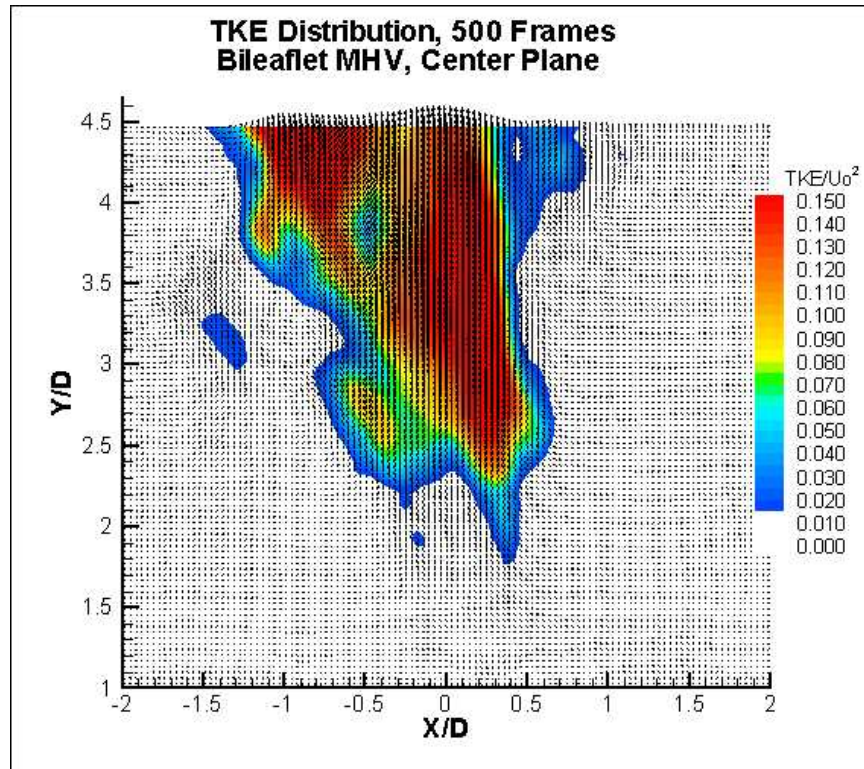


Figure 4.19: Time-averaged turbulent kinetic energy distributions for the bileaflet MHV averaged over 500 frames.

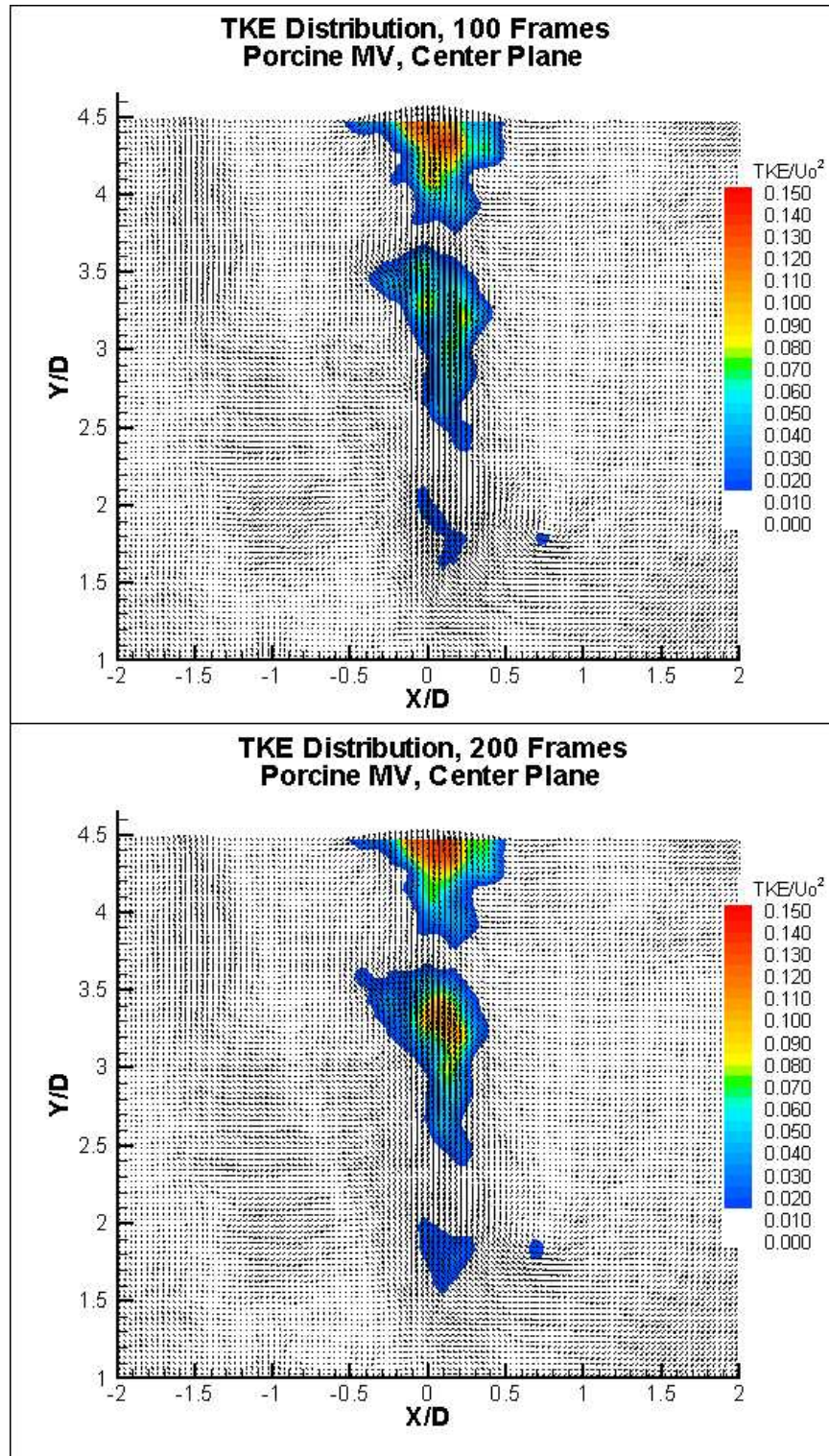


Figure 4.20: Time-averaged turbulent kinetic energy distributions for the porcine valve averaged over 100 frames (top) and 200 frames (bottom).

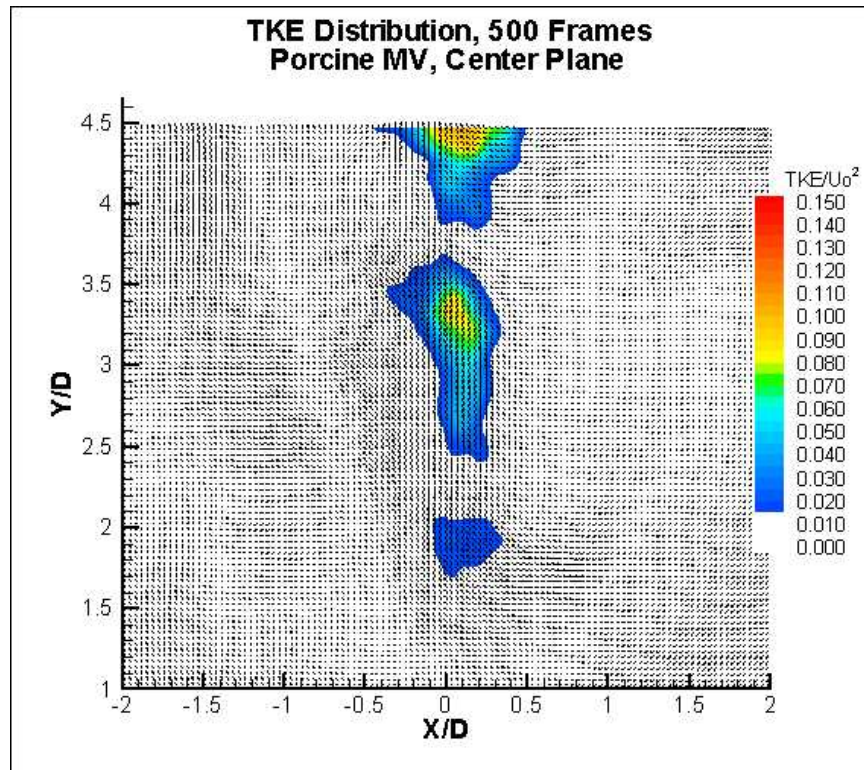


Figure 4.21: Time-averaged turbulent kinetic energy distributions for the porcine valve averaged over 500 frames.

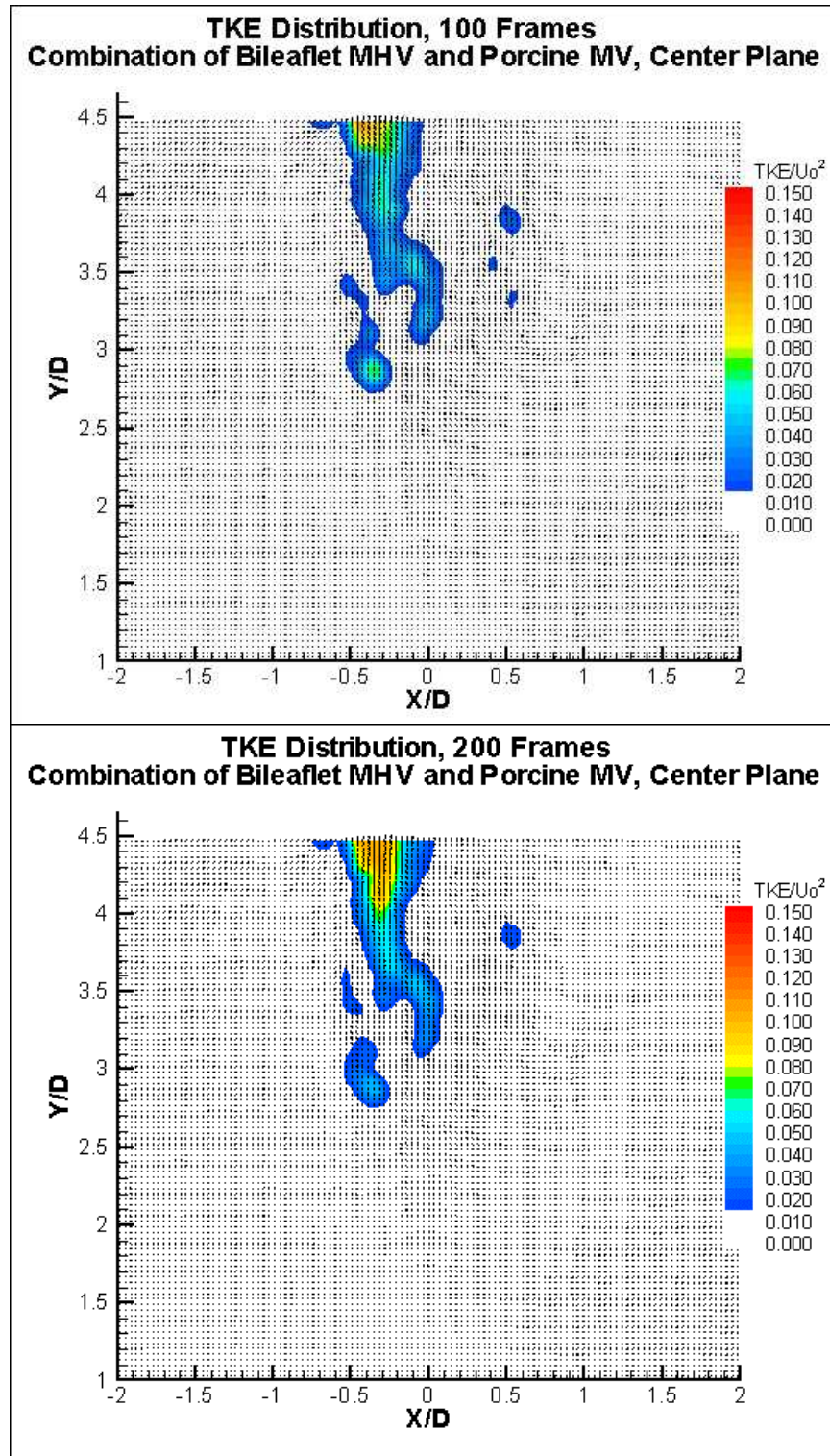


Figure 4.22: Time-averaged turbulent kinetic energy distributions for the chordal preservation case averaged over 100 frames (top) and 200 frames (bottom).

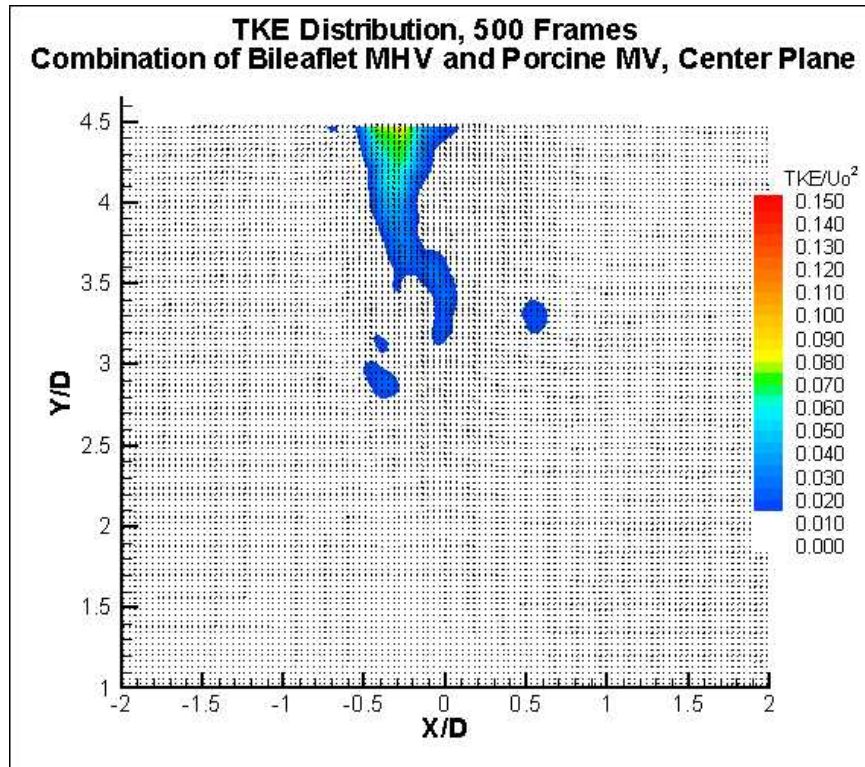


Figure 4.23: Time-averaged turbulent kinetic energy distributions for the chordal preservation case averaged over 500 frames.

4.2.4 Velocity Profiles Distal to the Valves

Velocity profiles were generated at certain distances away from the plane of the valves for the purpose of viewing how the jet velocity behaves as it enters and develops within the chamber in a time-averaged sense. For the configurations studied, the elevations in the y direction along which the profiles were calculated are shown in Figure 4.24.

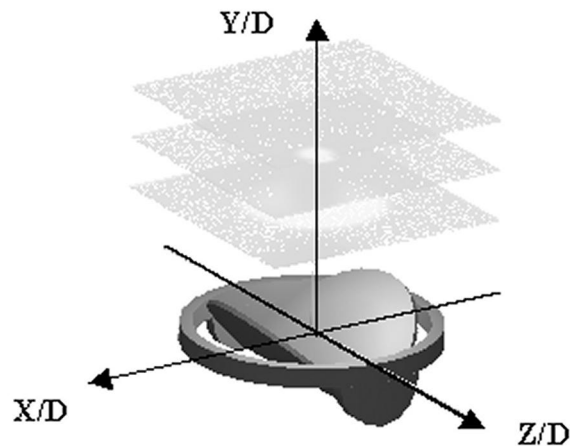


Figure 4.24: Illustration of MHV orientation and typical Y/D locations where the velocity profiles are calculated

Figures 4.25 and 4.26 display the time-averaged velocity profiles at five Y/D levels distal to the valve. The asynchronous leaflet motion is again clearly evident for the bileaflet MHV as the first few profiles closest to the jet inlet have two individual peaks, the right one being higher than the left. As the flow develops further downstream, the profiles level off, as indicated by the last two Y/D levels. The dispersion of the jet is also apparent as the profiles grow laterally with increasing Y/D. In addition to the jet dispersion, we also observe that the velocity profiles shift laterally to the left as the jet further penetrates the chamber.

In Figure 4.25, the profiles show that the porcine jet is more constricted, since the width of the individual profiles does not greatly increase with Y/D . Though the jet spreads somewhat, it does not shift much laterally. The peak average velocity of the porcine jet is much higher than the bileaflet case with values of 2.08 m/s and 1.20 m/s, respectively. The combination case falls between the other two cases, having a peak average velocity of 1.46 m/s. This jet is constrained by the presence of the mitral leaflets and CT and also shifts slightly to the left as it develops. Figure 4.26 allows for a comparison of all three jets on one set of axes at $Y/D = 2.5$. It is clear that the addition of the leaflets and CT to the MHV offers a significant reduction in dispersion but not quite enough to match the level of the porcine valve (at this specific location).

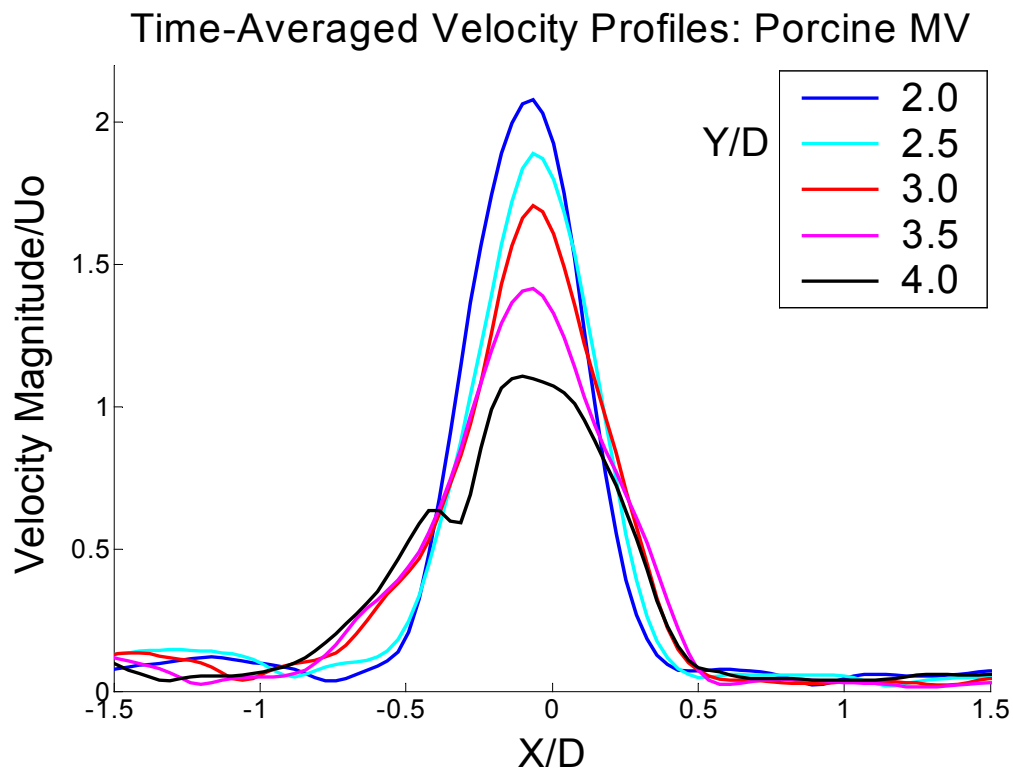
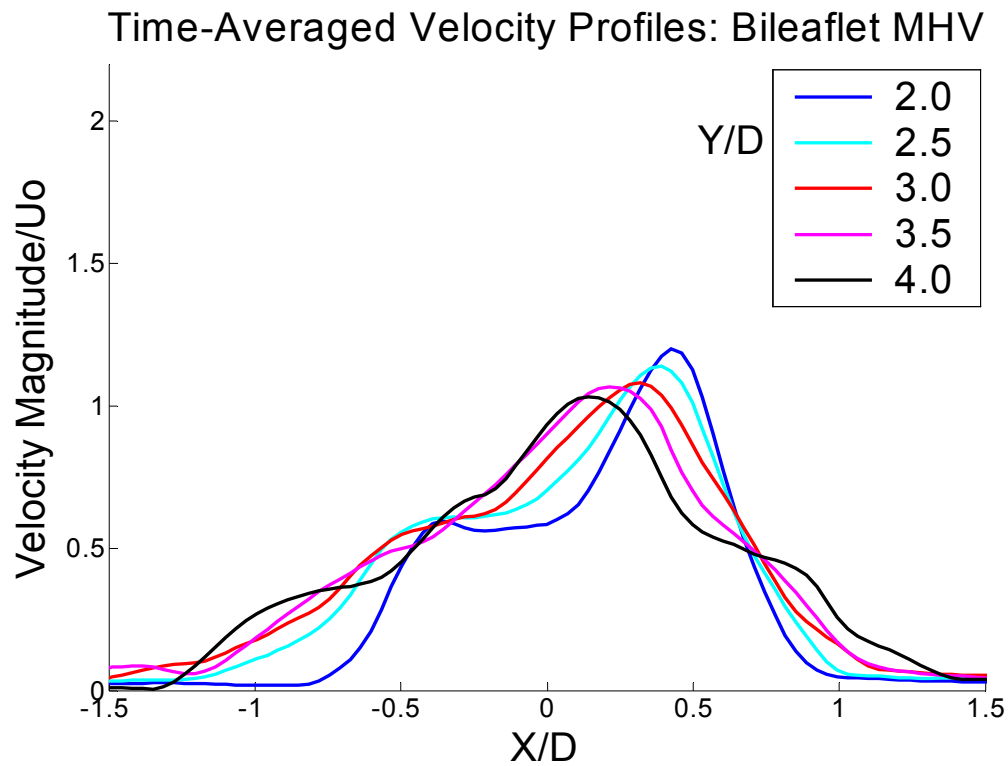


Figure 4.25: Time-averaged velocity profiles for five Y/D locations distal to the bileaflet MHV (top) and porcine mitral valve (bottom)

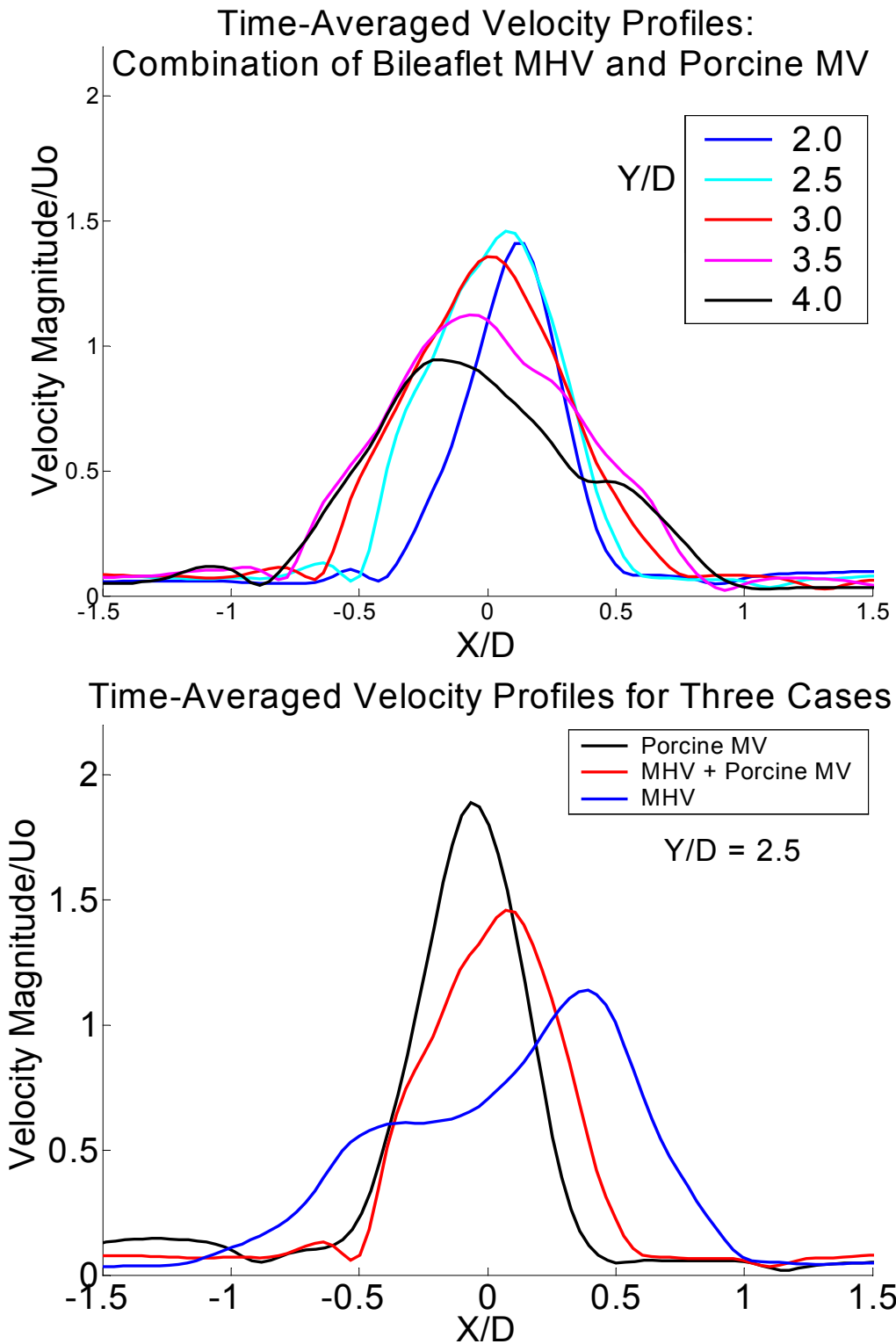


Figure 4.26: Time-averaged velocity profiles for five Y/D locations distal to the combination case (top) and profiles at $Y/D = 2.5$ for three test cases (bottom)

4.3 Discussion

4.3.1 Leaflet motions

The flow field results presented clearly show that the leaflet motions of the bileaflet MHV are repeatedly asynchronous. The flow visualization images presented in Figures 4.27 and 4.28 allow for a comparison to be made between symmetric and asymmetric leaflet opening. Although the angle of the jet entry into the chamber causes interaction with the wall of the ventricular simulator, valuable information can still be obtained from the images. Here the two outer orifice jets enter just before the central jet emerges into the chamber. While the two outer jets peel into vortices immediately, the central jet appears to gain strength as it develops. Because the mechanical leaflets open simultaneously, we do not observe the same flow conditions as discussed above. While the overall jet is composed of three individual orifice jets, they enter the chamber “simultaneously” in comparison to the asynchronous case. In the first three instants shown, the vortices formed are symmetric and virtually identical to each other. In the remaining images, though the jet is not exactly mirrored around its centerline, it is much more balanced and symmetric than the other bileaflet case tested. The extent of vortex shedding is less than what was observed with the asynchronous leaflet opening. Here we see two distinct vortices from the two outer orifice jets develop and propagate downstream, whereas in the other MHV case, we observe the presence of four vortices due to the time delay between the leaflet openings.

Other researchers have suggested that asynchronous leaflet motion negatively affects the flow development distal to the valve. It appears that this type of motion seems to induce higher rates of shear. Instantaneous velocity and vorticity distributions, as shown in Figure 4.29, provide for a comparison between the flow fields for the two bileaflet cases at $T = 0.20$ s in the heart cycle. The results confirm what was observed in the flow visualization images in that the normal opening of the leaflets gives rise to a much more symmetric jet. By examining the intensity of the colored vorticity contours, we see a marked difference between the two MHV flow fields. It is clear that the vorticity levels in the asynchronous opening case are much higher, indicating levels of higher shear. The same conclusion can be made when looking at the time-averaged vorticity distributions, shown in Figure 4.30.

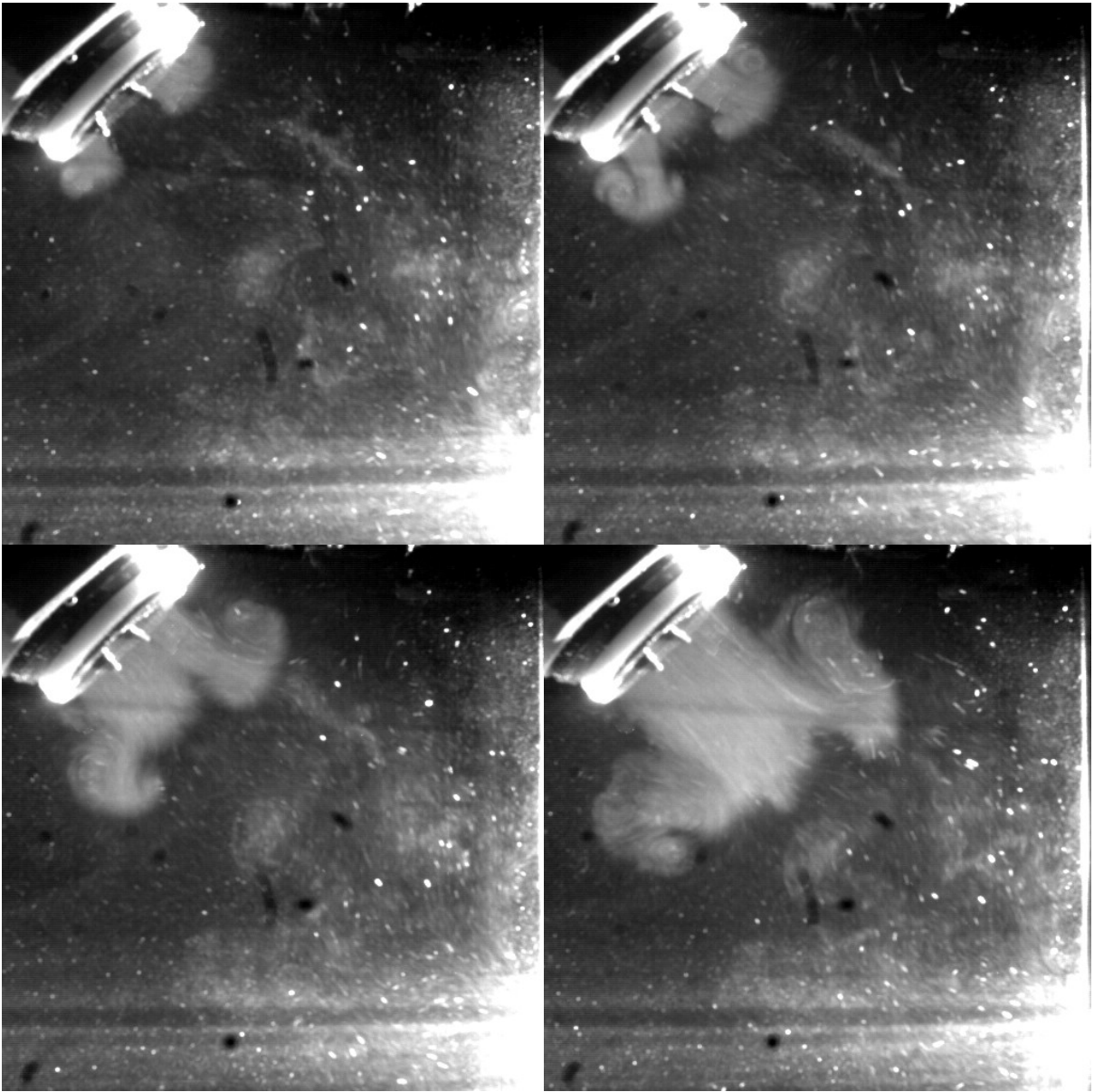


Figure 4.27: Flow visualization images illustrating mitral jet development in a case with symmetric mitral leaflet opening.

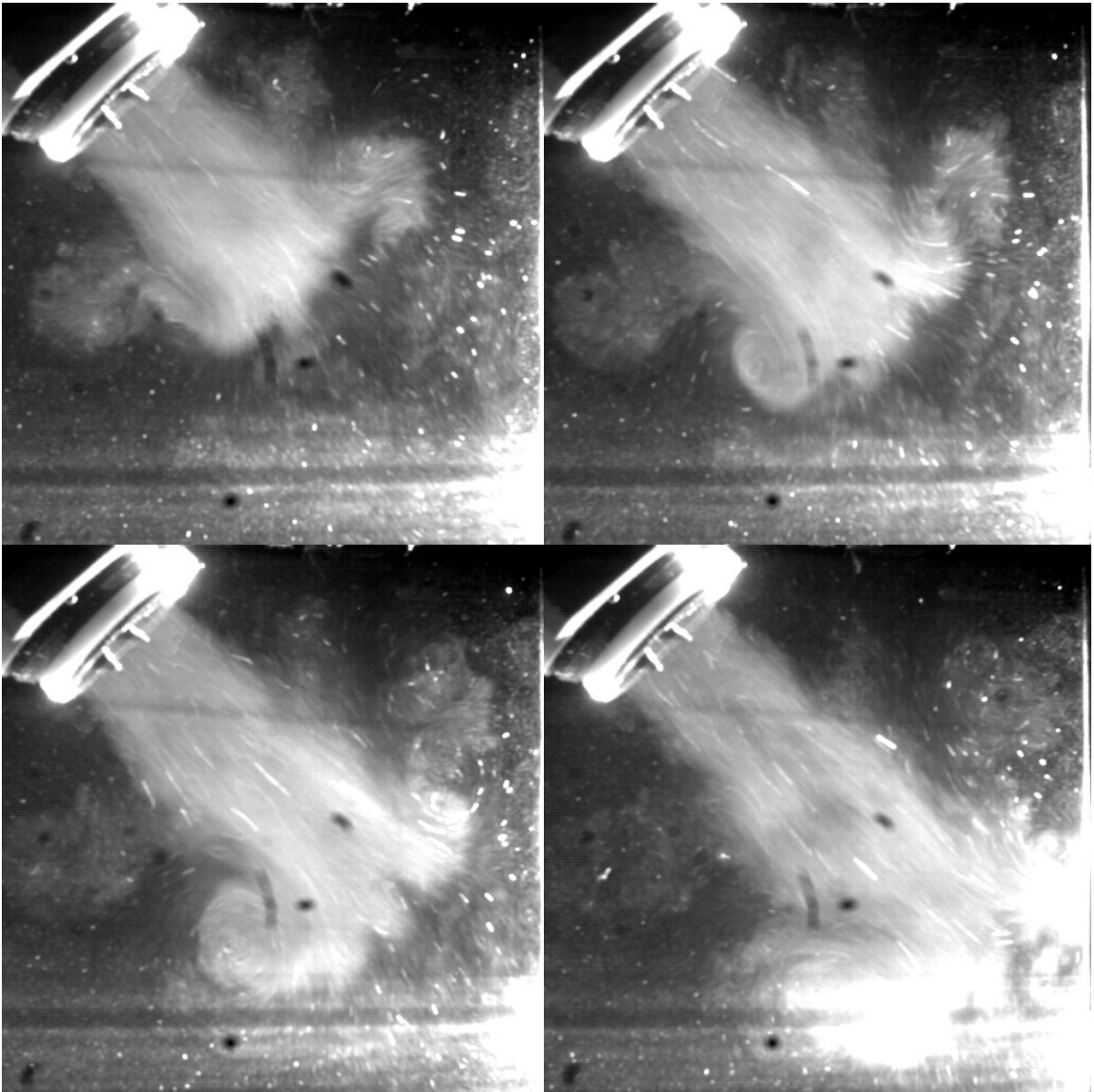


Figure 4.28: Flow visualization images illustrating mitral jet development in a case with symmetric mitral leaflet opening.

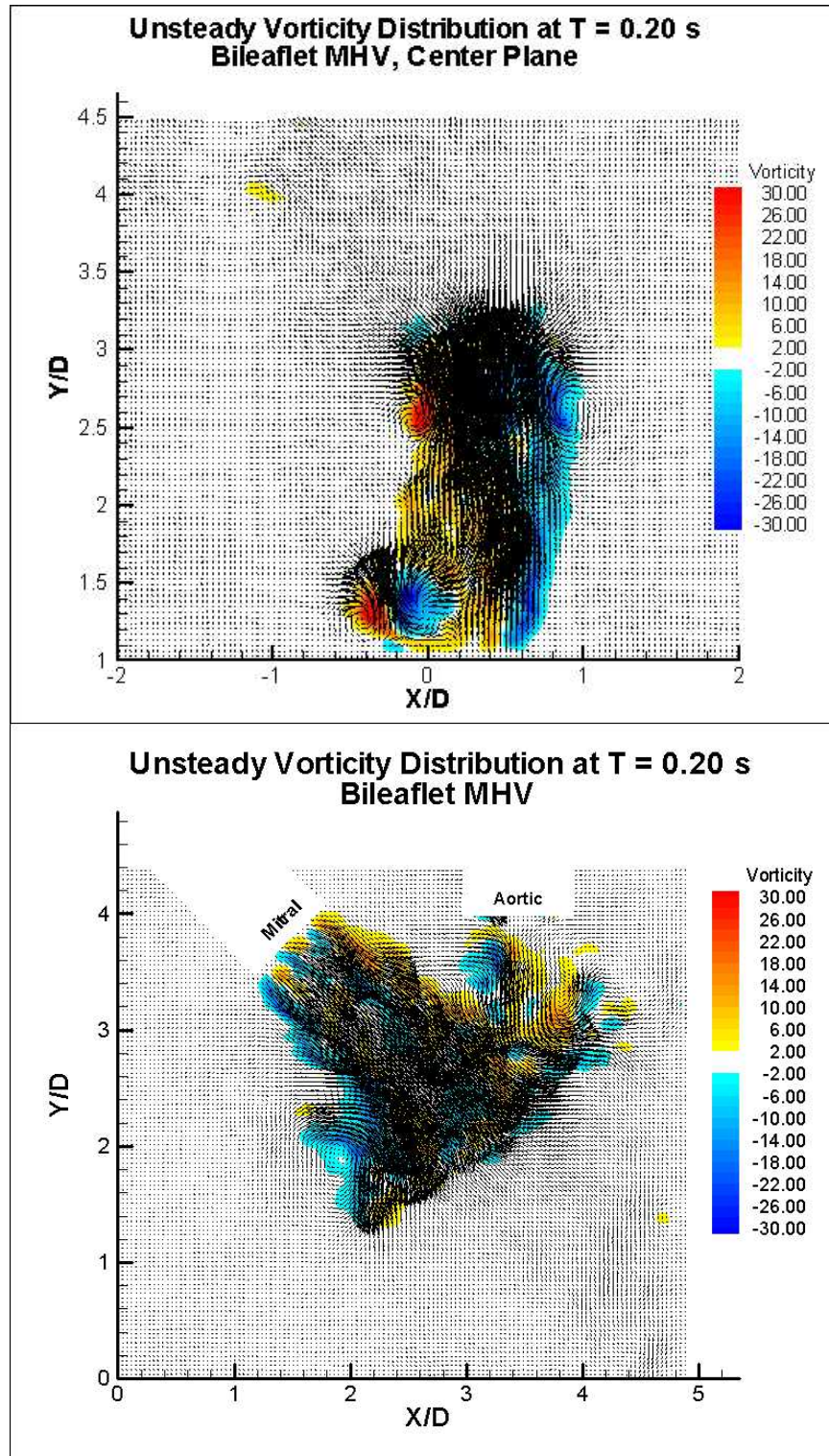


Figure 4.29: Unsteady Vorticity Distributions for two bileaflet MHVs at T = 0.20 s: asymmetric leaflet opening (top) and symmetric leaflet opening (bottom).

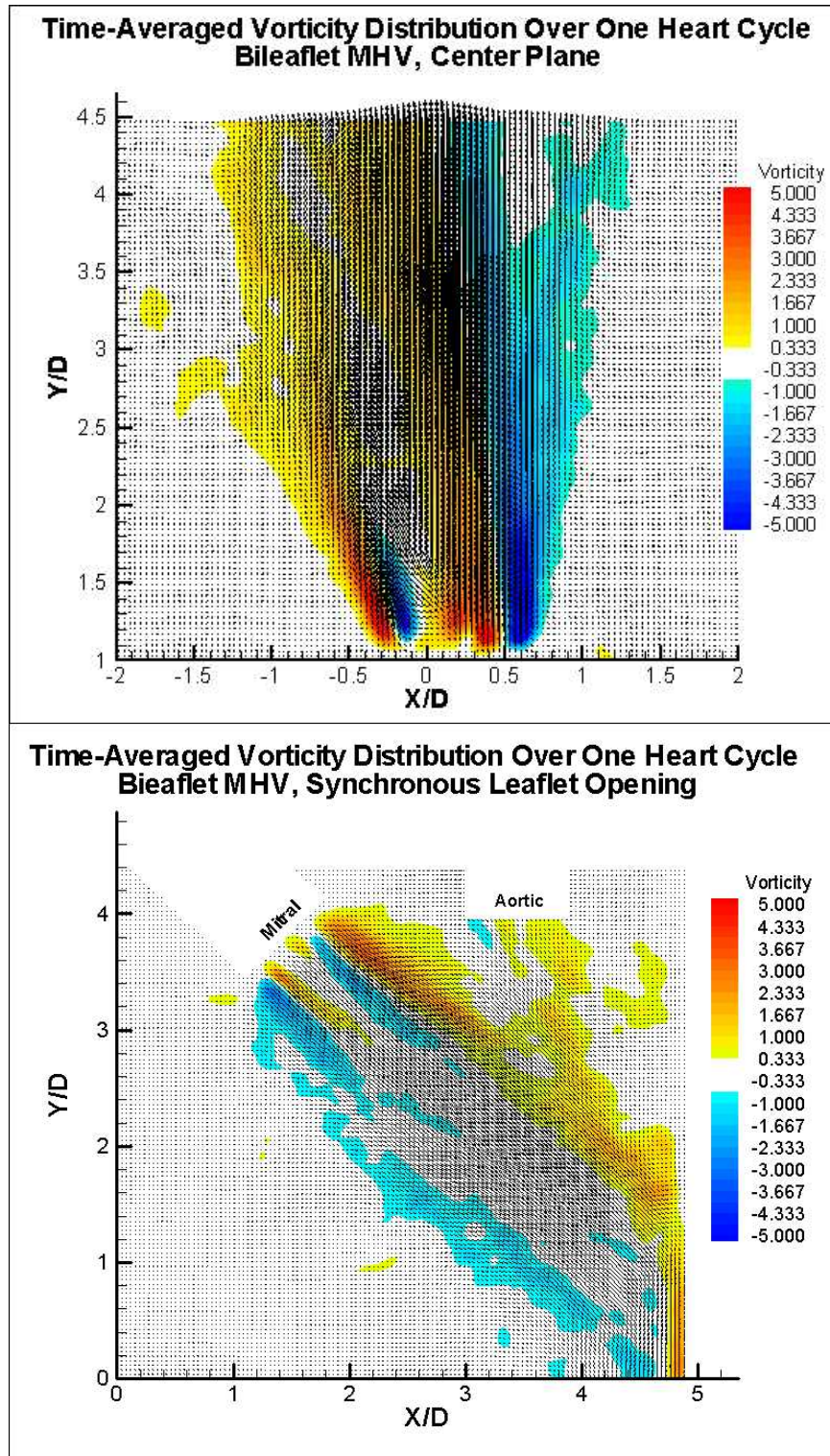


Figure 4.30: Time-averaged Vorticity Distributions for two bileaflet MHVs: asymmetric leaflet opening (top) and symmetric leaflet opening (bottom).

In addition to affecting the levels of shear distal to the leaflets, the presence of two jets issuing into the chamber separately allows for further dispersion of the jet than if the leaflets opened with symmetric motions. The levels of dispersion for both the symmetric and asymmetric leaflet openings can easily be seen by comparing the jets in Figures 4.1-4.4 with those of Figures 4.29 and 4.30. Each of the jets grows laterally, causing them to lose their uniformity. Energy, which cannot be recovered, is dissipated within the vortical structures; therefore, the left ventricle must work harder to pump the blood through to the rest of the body. These effects are far more pronounced in the case with asynchronous opening.

The mechanism behind the greater dispersion can be better understood by looking at a well-known physics principle called the Law of Biot-Savart (equation below). In fluid mechanics, this law relates the velocity induced by a vortex filament to its strength and rotation. The vortex shed from the second jet (left leaflet) affects the initial jet (right leaflet) as it issues into the chamber by inducing a leftward velocity component, thus shifting flow from the right jet to the left as shown in Figure 4.31.

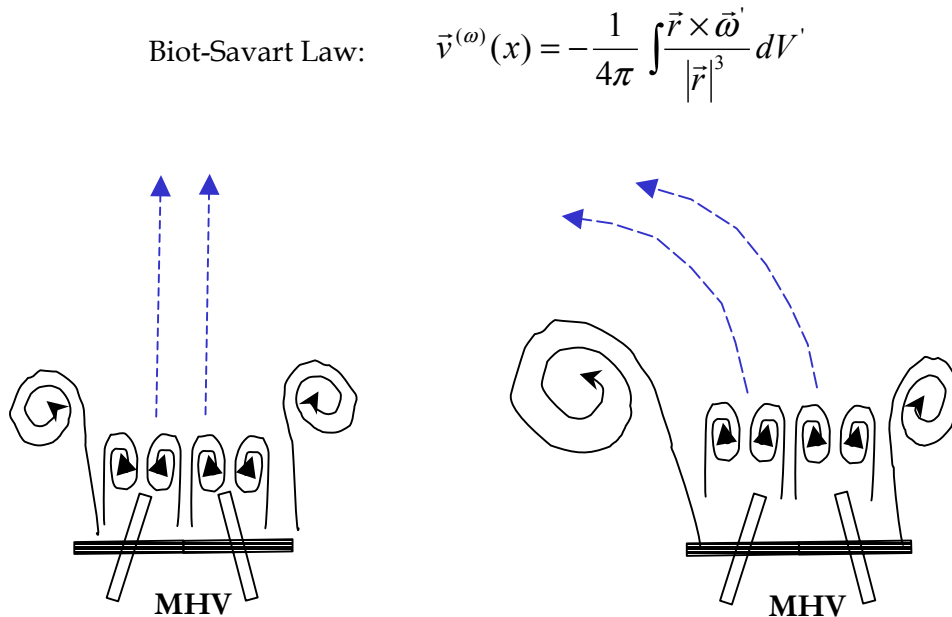


Figure 4.31: Illustration of the effect of the vortex shed from the left leaflet on the mitral jet behavior.

One way to observe the Biot-Savart mechanism discussed above is to examine the actual behavior of the jet as it propagates downstream. This allows us to understand how the shed vortices interact with one another distal to the leaflets. As shown in Figure 4.32, lateral shifting occurs in two of the cases studied due to the influence of the induced velocities from the shed vortices as discussed above. The level of shifting was determined by finding the horizontal X/D location of the maximum velocity points at various Y/D s distal to the valves. In this way, it is possible to track the lateral motion of the jet front as it moves distal to the valve configurations. The porcine jet, as indicated by the red line, remains along the same path and then shifts slightly between $Y/D = 3.5$ and $Y/D = 4.5$. For the bileaflet case, the jet is initially further to the right due to the fact that the right leaflet opened before the left. The jet consistently moves to the left as it progresses in the chamber. Due to the constriction imposed by the leaflets and CT, the chordal preservation jet is initially closer to the porcine jet, and then follows a shifting pattern similar to the bileaflet MHV.

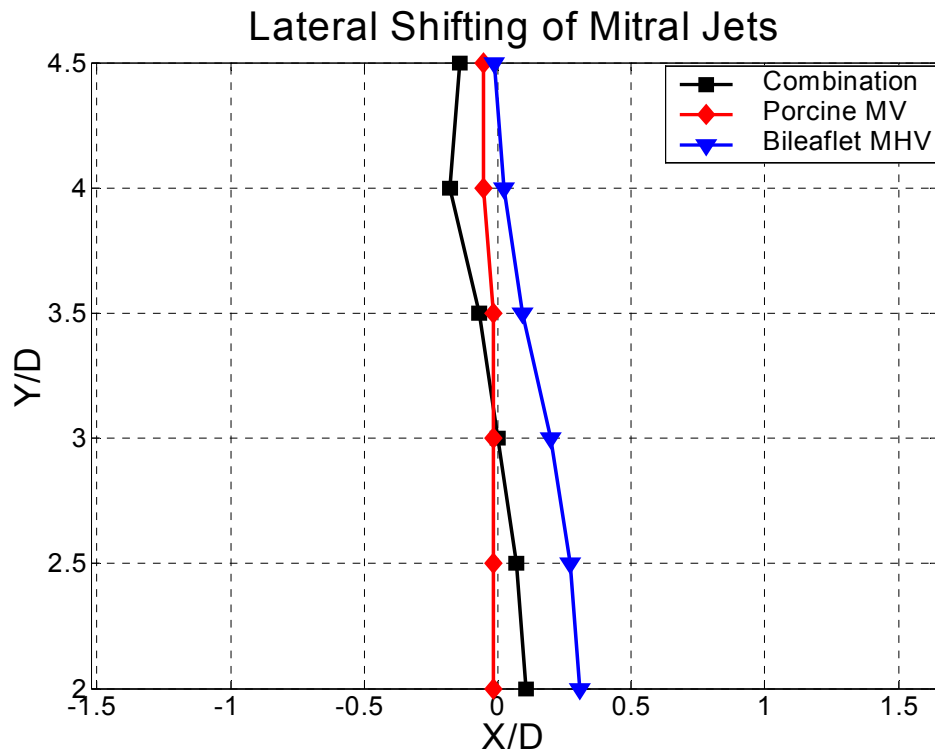


Figure 4.32: Maximum velocity points at various Y/D levels illustrate how the mitral jets shift laterally.

4.3.2 Vortex Shedding

In all three test configurations, some degree of vortex shedding is present distal to the mitral valves. Ideally, a MHV would mimic the flow patterns produced downstream from the natural mitral valve, but the evidence shown here indicates that this is not the case. Although studies have shown vortices within the normal human LV, they do not appear to have a negative effect on the flow constituents or the function of the LV. Vortices are shed in the flow past MHVs as a result of the generation of shear layers induced by the accelerating jets past the valve leaflets. The shear layers are prone to roll up into vortices that may encounter instabilities that cause them to become turbulent. The high level of vortex formation and propagation as seen in the bileaflet MHV, both with symmetric and asymmetric leaflet opening, is far from the ideal conditions. The presence of the native mitral leaflets and CT suppresses the vortex formation to a point further downstream, making the overall flow closer to that in the normal LV. By limiting the vortex shedding from the leaflets, the coherence of the jet is preserved, allowing it to remain on its “preferred” pathway through the LV. Since these vortices often break down to turbulence, delaying their development may also minimize energy lost as the jet redirects itself toward the aortic valve. In future studies, if the native tissue were incorporated into a flexible left ventricular model, flow conditions may be even further advanced to more closely mimic the natural mitral inflow and outflow jets.

In spite of the anticoagulant therapy that MHV recipients must follow, complications involving thrombus formation occur all too often. The activation of platelets is the primary culprit responsible for the thrombogenicity of all MHVs. Typically, initial damage to platelets occurs in the highest regions of shear stress, which are located along the mechanical leaflets, especially in those that generate regurgitant jets. High rates of shear and deformation, flow stagnation, and turbulence are all fluid mechanical factors that influence thrombus formation. In the center of a vortex, both velocity and pressure is low. If a blood element were to enter into the vortex, depending on its composition and density, it would either be ejected into the rest of the flow or be pulled to the center. It is known that in regions of low pressure and recirculation, platelet aggregation and clot formation are

more prone to occur. There are no distinct regions of ongoing recirculation present in the fields investigated here. These areas of recirculation are more prone to develop very close to the leaflets, and in this work, the area of interrogation was more focused on the flow distal to the valve and not directly upon the leaflets themselves. However, there are coherent vortices within the field that remain organized and propagate downstream. As Bluestein et al. [6] have shown in studies of a valve in the aortic position, platelets exposed to the highest shear stresses, i. e., damage, are often trapped in the vortices shed from the leaflets. After being exposed to these flow conditions, the activated platelets trapped in the vortices will release their granule constituents and produce procoagulant phospholipid surfaces likely to start the positive feedback reactions of coagulation.

In the mitral position, results show extensive vortex formation distal to the leaflets of the bileaflet MHV, especially when the mechanical leaflets do not open synchronously. The vortices shed from the leaflets, which remain coherent and propagate throughout the cycle, could possibly trap blood elements and convect them downstream in the same way that Bluestein et al. have postulated. Figures 4.33 and 4.34 show instantaneous vorticity distributions for the bileaflet MHV with the black, arrowed lines representing the streamlines at three specific time instants in the cycle, $T = 0.20$ s, $T = 0.30$ s, and $T = 0.35$ s. With the addition of the streamlines to the flow, it is easier to visualize how a blood element could become trapped in the vortex and be carried downstream. For example, if a platelet were damaged along the leaflet and became entrapped in the leftmost vortex located at $Y/D = 1.3$ in Figure 4.33, by the next time instant shown, it would have traveled to $Y/D = 2.2$ while remaining in a region of lower pressure and shear. As this vortex interacts and disperses laterally, the damaged element is still exposed to these flow conditions as it progresses to $Y/D = 2.4$, shown in Figure 4.34. The shear stresses associated with vortex shedding are unlikely to damage elements in the blood due to their large spatial scales. These large vortical structures, however, may cascade into smaller and smaller structures, giving rise to turbulent stresses that could damage blood cells. The TKE results found in this experiment show that there are definitely turbulent motions associated with the bileaflet MHV flow field. In addition to the initial trauma associated with entry through the

mitral valve, the platelets may then be subjected to further stresses as they exit through the aortic valve. This scenario would be especially significant to a patient who undergoes double valve replacement with both valves being mechanical.

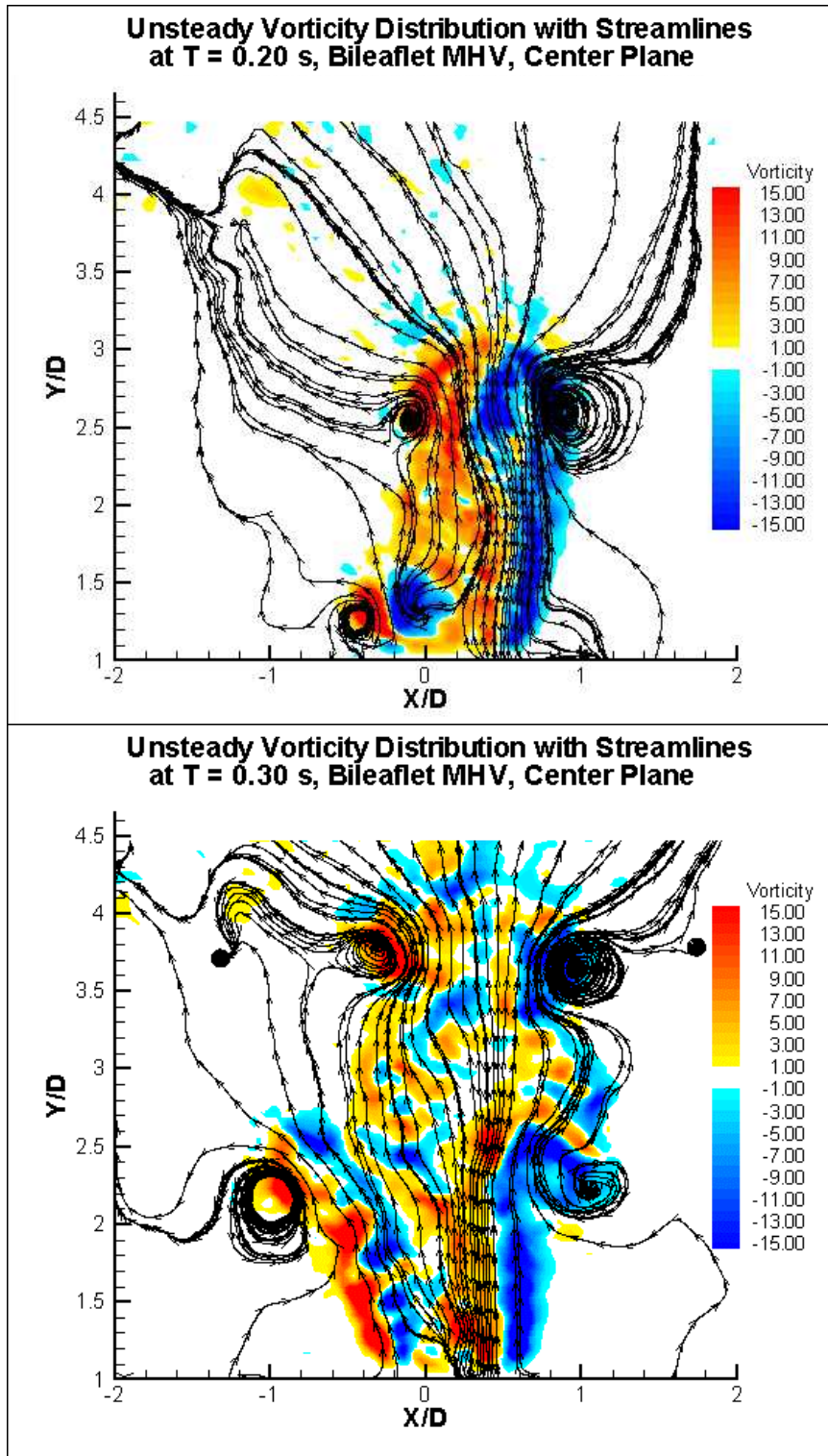


Figure 4.33: Unsteady Vorticity Distributions with streamlines at two time instants, T = 0.20 s and T = 0.30 s.

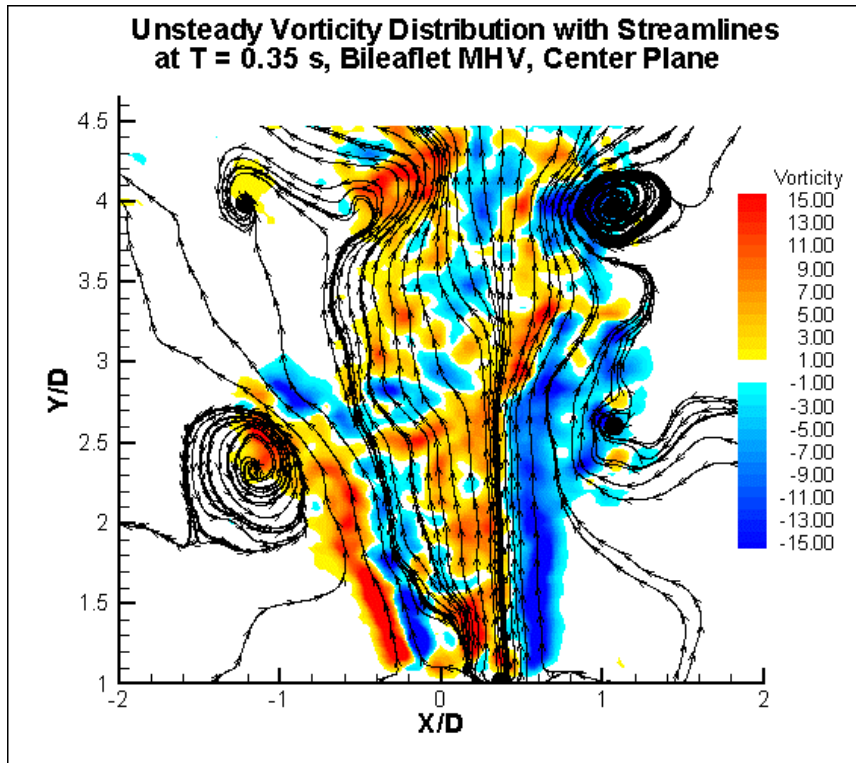


Figure 4.34: Unsteady Vorticity Distributions with streamlines at $T = 0.35$ s.

4.3.3 Mitral Jet Dispersion

Following the suggestion of Kilner et al. [31] and Laas et al. [32], we anticipate that a more efficient mitral jet would sustain its momentum and minimize its spreading, so that the flow would remain on its “preferred” pathway. This would allow the flow to be redirected towards the aortic valve to facilitate ventricle emptying. In this process, the leaflets and/or chordae of a biological valve, like the porcine valve tested here, play a role by reducing the amount of jet dispersion downstream. The native tissue itself forms a “tunnel” which guides the jet by inhibiting the flow perpendicular to the forward moving flow. When the entering stream is able to freely flow normal to the preferred direction, the jet loses its coherent structure, thus preventing it from being smoothly redirected toward the aortic valve. This behavior was observed here in the bileaflet MHV results as well as in the work of Laas et al [32].

By measuring the widths of the time-averaged velocity profiles at different Y/D locations distal to the valves, it was possible to establish a level of dispersion for each of the configurations tested. The width of the jet was determined by locating the two X/D positions where the slope of the velocity magnitude maintains a level of zero. Figure 4.35 illustrates the relationship between the widths of the three jets versus the distance downstream from the valve. The MHV case shows the highest dispersion at an average level of 2.54 as seen in Figure 4.36. In this sense, the addition of the natural mitral tissue to the MHV (chordal preservation) reduces the spreading to the level of the porcine valve alone, 1.538. Compared to the MHV, this represents a reduction of 61 percent. The levels of spreading in the out-of-plane direction are also reduced as shown previously by the three-dimensional results. These findings agree with the MRI results of Laas et al. [32] who showed that the mitral jet issuing from the bileaflet MHV greatly diffused into the LV. In addition to the other positive results of the chordal preservation technique, it is also then advisable for surgeons to utilize this technique, either total or partial, so that the corresponding flow conditions in the LV would be nearer to that of the natural valve.

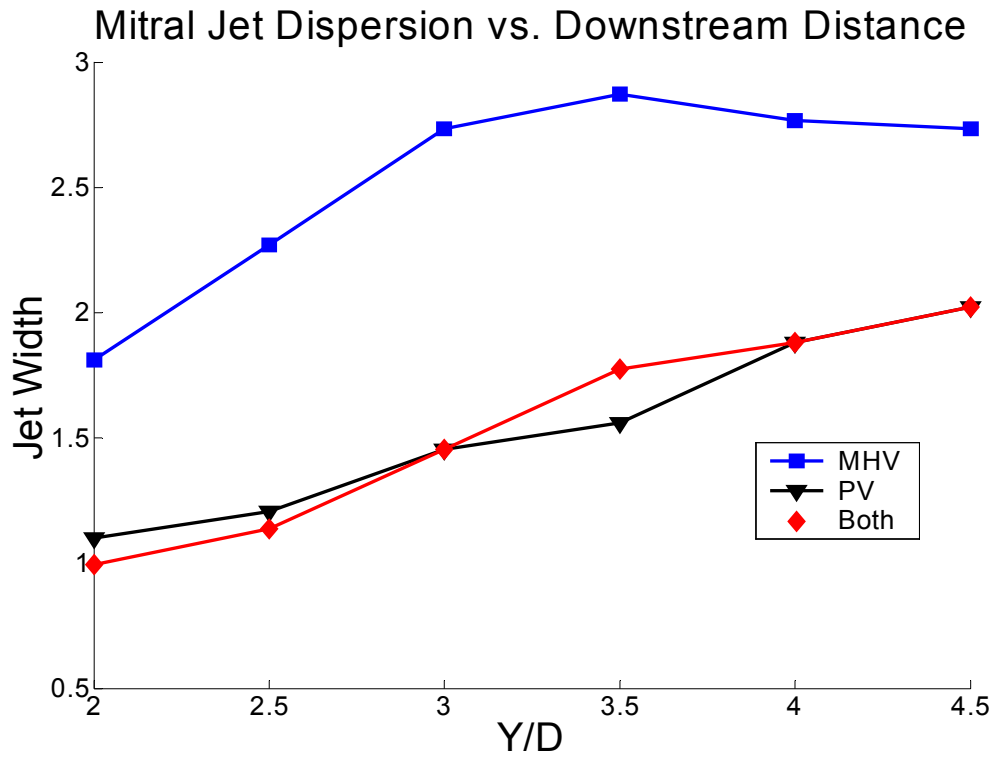


Figure 4.35: Dispersion of the mitral jets for the test cases studied.

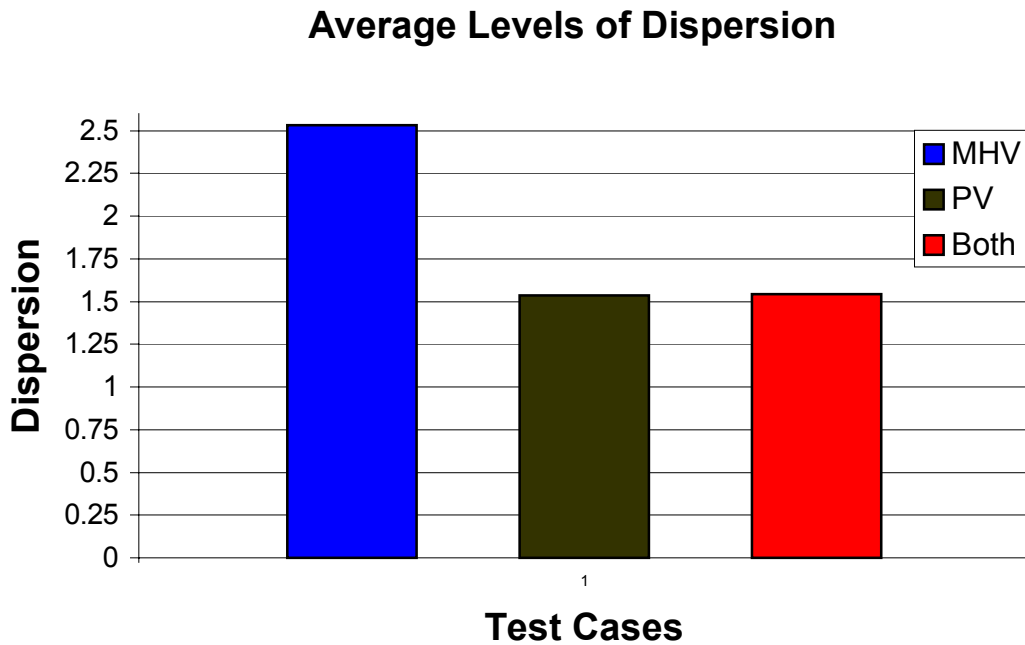


Figure 4.36: Average mitral jet dispersion levels based on six Y/D levels.

Chapter 5

5 Conclusions and Future Work

In the present work, the downstream flow characteristics distal to three valve configurations were studied using a high frequency Time-Resolved Digital Particle Image Velocimetry (TRDPIV) system. Information regarding the flow character was obtained and included insights into vorticity levels, vortex shedding, jet dispersion, and leaflet motions for a bileaflet MHV, a porcine MV, and a combination of both types of valves. Overall, the results presented provide insight on the hemodynamic characteristics of natural and MHVs, reveal the detrimental character of asynchronous leaflet opening, document the mechanism of vortex formation and interaction distal to the valve, and illustrate the importance of chordal preservation. Instantaneous velocity fields and vorticity maps were presented along with time-averaged velocity, vorticity, and turbulent kinetic energy measurements. Asynchronous leaflet behavior was observed in both of the cases that incorporated the bileaflet MHV. Extensive vortex formation and propagation occurred distal to the MHV, which led to high levels of jet dispersion. The porcine mitral jet exhibited lateral oscillatory behavior and less vortex development overall, and its levels of dispersion were markedly less than those of the MHV. In the MHV/porcine combination system, the jet behavior was greatly affected by the chordal preservation technique. The presence of the native leaflets and chordae tendineae limited vortex propagation and jet dispersion. Levels of vorticity among the cases were comparable while the turbulent kinetic energy levels were highest distal to the MHV. Three-dimensional results also showed a restrained mitral jet in the out-of-plane direction, indicating that the leaflets and tendineae may act to guide the incoming jet along a pathway into the left ventricle. Based on the findings from this and other works, valve performance could be improved by implementing a design that directed the incoming mitral jet along its preferred pathway. In this way, flow would more closely mimic the

natural heart's flow patterns. These results also support the use of the chordal preservation technique during mitral valve replacement.

While this work provides new information about the flow past both mechanical and natural mitral valves as well as the technique of chordal preservation, further studies must be performed to improve, expand upon, and validate the results presented here. This research may also serve as a steppingstone for new paths of related study. With regard to the experimental setup, future work includes the utilization of a second generation testing machine that allows for the incorporation of a left atrium model as well as an aortic arch. The simulator is no longer gravity fed; its chambers are controlled independently by a high precision computer controlled pumps and control valves. By using this new machine, more accurate waveforms may be inputted into the system and pressures and flow rates may be controlled in an easier manner. In order to examine flow characteristics such as levels of circulation and kinetic energy, more cycles of data must be taken to further assess the signals. Synchronizing the signals for each data set will also improve the analysis process and corresponding results. Applying improved imaging processing techniques would allow for less light to be reflected from the native mitral tissue and sutures. In this way, more details of the flow closer to the valves, i. e. very close to or within the leaflets and chordae tendineae, could be investigated. Other paths of future work also include studying the flow distal to the native leaflets without the chordae tendineae as well as examining the effects of valve tilting and orientation in each of the three configurations.

References

1. Adrian, R. J. Particle-imaging techniques for experimental fluid mechanics. *ARFM*. 23:261-304,1991.
2. Affeld, K. Cardiac valves and cardiac assist systems. Proc. of Fluid Dynamics and Biological Flows. Humboldt University: Berlin, Germany. March 1998.
3. Anatomy and Physiology Related to Valve Repair. St. Jude Medical. 2000. <<http://www.sjm.com/products/repairanatomyphysiology.shtm>>.
4. Bellhouse, B. J. and F. H. Bellhouse. Fluid mechanics of the mitral valve. *Nature*. 224: 615-616, 1969.
5. Bellhouse, B. J. "Fluid mechanics of a model mitral valve". In: *The Mitral Valve. A Pluridisciplinary Approach*, edited by D. Kalmanson. London: Edward Arnold, 1976, pp.99-110.
6. Bluestein, D., E. Rambod, and M. Gharib. Vortex shedding as a mechanism for free emboli formation in mechanical heart valves. *J. Biomech. Eng.* 122: 125-134, 2000.
7. Browne, P., A. Ramuzat, R. Saxena, and A. Yoganathan. Experimental investigation of the steady flow downstream of the St. Jude bileaflet heart valve: a comparison between laser doppler velocimetry and particle image velocimetry techniques. *Annals of Biomedical Engineering*. 28:39-47, 2000.
8. Brucker, C. Dual-camera DPIV for flow studies past artificial heart valves. *Experiments in Fluids*. 22:495-506, 1997.
9. Bruss, K. H., H. Reul, J. V. Gilse, and E. Knott. Pressure drop and velocity fields of four mechanical heart valve prostheses: Bjork-Shiley Standard, Bjork-Shiley Concave-Convex, Hall-Kaster and St. Jude Medical. *Life Support Sys.* 1:3-22, 1983.
10. Camp, J. P., M. Smith, and M. Szurgot. Lessons of the Bjork-Shiley heart valve failure. Dec. 1997. <<http://www.me.utexas.edu/~uer/heartvalves/index.html>>.
11. Chandran, K. B., R. Schoepfoerster, and K. C. Dellesperger. Effect of prosthetic mitral valve geometry and orientation on d in a model of human left ventricle. *J. Biomechanics*. 22: 51-65, 1989.

12. Cohen, L. H., R. L. Reis, and A. G. Morrow. Left ventricular function after mitral valve replacement. *J. Thorac Cardiovasc Surg.* 56:11-15, 1968.
13. David, T. E., H. D. Strauss, E. Mesher, et al. Is it important to preserve the chordae tendineae and papillary muscles during mitral valve replacement? *Can. J. Surg.* 24:236-239, 1981.
14. David, T. E., D. E. Uden, and H. D. Strauss. The importance of the mitral apparatus in left ventricular function after correction of mitral regurgitation. *Circulation.* 68:76-82, 1983.
15. David, T. E., R. J. Burns, C. M. Bacchus, and M. N. Druck. Mitral valve replacement for mitral regurgitation with and without preservation of chordae tendinae. *J. Thorac. Cardiovasc. Surg.* 88:718-725, 1984.
16. Donnerstein, R. L. and H. D. Allen. Asynchronous leaflet closure in the normally functioning bileaflet mechanical heart valve. *Am Heart J.* 119:694-697, 1990.
17. Edwards Lifesciences Corporation, Irvine, CA. Our History. 2002. <<http://www.edwards.com/AboutUs/WhoWeAre/OurHistory.aspx>>.
18. Edmunds, L. Henry, Jr. Thrombotic and bleeding complications of prosthetic heart valves. *Ann Thorac Surg.* 44:430-445, 1987.
19. Fontaine, A. A., H. Shengqiu, R. Stadter, et al. In vitro assessment of prosthetic valve function in mitral valve replacement with chordal preservation techniques. *J. Heart Valve Dis.* 5:186-198, 1996.
20. Gams, E., S. Hagl, H. Schad, W. Himisch, N. Mendler, and F. Sebening. Importance of the mitral apparatus for left ventricular function: an experimental approach. *Eur. J. Cardio-thorac. Surg.* 6:17-24, 1992.
21. Garitey, V., T. Gandelheid, J. Fusezi, et al. Ventricular flow dynamic past bileaflet prosthetic heart valves. *Int. J. Artificial Organs.* 18: 380-391, 1995.
22. Gross, J. M., C. D. Shermer, and N. H. C. Hwang. Vortex shedding in bileaflet heart valve prostheses. *ASAIO Transactions.* 34: 845-850, 1988.
23. Hansen, D. E., P. D. Cahill, G. C. Derby, and C. D. Miller. Relative contributions of the anterior and posterior mitral chordae tendineae to canine global left ventricular systolic function. *J. Thorac Cardiovasc Surg.* 93:45-55, 1987.

24. Hansen, D. E., G. E. Sarris, M. A. Niczyporuk, et al. Physiologic role of the mitral apparatus in left ventricular regional mechanics, contraction synergy, and global systolic performance. *J. Thorac. Cardiovasc. Surg.* 97: 521-533, 1989.
25. Hasselinc, L. Digital image processing in flow visualization. *ARFM.* 20:421-485, 1988.
26. Heart Valve Disease and Therapy. St. Jude Medical. 1997. <<http://www.sjm.com/stjude/patients/htm/tocdis.htm>>.
27. Hennein, H. A., J. A. Swain, C. L. McIntosh et al. Comparative assessment of chordal preservation versus chordal resection during mitral valve replacement. *J. Thorac. Cardiovasc. Surg.* 99:828-837, 1990.
28. Hetzer, R., G. Bougioukas, M. Franz, and H. G. Borst. Mitral valve replacement with preservation of papillary muscles and chordae tendineae - revival of a seemingly forgotten concept. I. Preliminary clinical report. *Thorac. Cardiovasc. Surg.* 31:291-296, 1983.
29. Huang, H. T., D. Dabiri and M. Gharib. On errors of digital particle image velocimetry. *Meas. Science and Technology.* 8:1427-1440, 1997.
30. Hung, T. C., R. M. Hochmuth, J. H. Joist, and S. P. Suter. Shear-induced aggregations and lysis of platelets. *Trans. ASAIO.* 22:285-290, 1976.
31. Kilner, P. J., G. Z. Yang, A. J. Wilkes et al. Asymmetric redirection of flow through the heart. *Nature.* 404:759-761, 2000.
32. Laas, J., M. Perthel, A. Aiken, and D. Kivelitz. Intraventricular flow in the normal heart and after mitral valve replacement. Kurt Singelmann, Videostudio MHH, 2000.
33. Lillehei, C. W., M. J. Levy, and R. C. Bonnabeau, Jr. Mitral valve replacement with preservation of papillary muscles and chordae tendineae. *J. Thorac. Cardiovasc. Surg.* 47:532-543, 1964.
34. Maymir, J. C., R. S. Deutsch, R. S. Meyer, D. B. Geselowitz, and J. M. Tarbell. Mean velocity and reynolds stress measurements in the regurgitant jets of tilting disk heart valves in an artificial heart environment. *Annals of Biomed. Eng.* 26:146-156, 1998.
35. Miki, S., K. Kusuhara, U. Yuichi et al. Mitral valve replacement with preservation of chordae tendineae and papillary muscles. *Ann. Thorac. Surg.* 45:28-34, 1988.

36. Miller, D. W., D. D. Johnson, and T. D. Ivey. Does preservation of the posterior chordae tendineae enhance survival during mitral valve replacement? *Ann Thorac Surg.* 28:22-27, 1979.
37. Okita, Y. et al. Analysis of left ventricular motion after mitral valve replacement with a technique of preservation of all chordae tendineae: Comparison with conventional mitral valve replacement or mitral valve repair. *J Thorac Cardiovasc Surg.* 104:786-795, 1992.
38. Pierrakos O., P. P. Vlachos, A. R. Mace, and D. P. Telionis. Vorticity and turbulence characteristics inside a transparent flexible left ventricle. BED-Vol. 51, Bioengineering Conference, ASME 2001.
39. Ramstack, J. M., L. Zuckerman, and L. F. Mockros. Shear-induced activation of platelets. *J. Biomechanics.* 12:113-125, 1979.
40. Ranganathan, N., M. D. Silver, and E. D. Wigle. "Recent advances in the knowledge of the anatomy of the mitral valve." In: *The Mitral Valve. A Pluridisciplinary Approach*, edited by D. Kalmanson. London: Edward Arnold, 1976, pp.3-13.
41. Rastelli, G. C. et al. Cardiac performance after replacement of the dog mitral valve with Starr-Edwards prosthesis with and without preservation of the chordae tendineae. *Surg Forum.* 17:178-179, 1966.
42. Rastelli, G., J. W. Kirklin, and J. L. Titus. Fate of papillary muscles after prosthetic replacement of mitral valve. *Mayo Clin Proc.* 42:210-217, 1967.
43. Rastelli, G. C. et al. Exercise tolerance and hemodynamic studies after replacement of canine mitral valve with and without preservation of the chordae tendineae. (*Suppl*) *Circulation.* 35:I34-I41, 1967.
44. Reif, T. H., T. J. Schulte, and N. H. Hwang. Estimation of the rotational undamped natural frequency of bileaflet cardiac valve prostheses. *ASME J. Biomech. Eng.* 112:327-332, 1990.
45. Reul, H., N. Talukder, and E. W. Muller. Fluid mechanics of the natural mitral valve. *J. Biomechanics.* 14:361-372, 1981.
46. Rouleau, C. A., R. L. Frye, and F. H. Ellis. Hemodynamic state after open mitral valve replacement and reconstruction. *J Thorac Cardiovasc Surg.* 58:870-878, 1969.

47. Rushmer, R. F. Initial phase of ventricular systole: asynchronous contraction. *Am. J. Physiol.* 194:188-194, 1956.
48. Schoepfoerster, R. T. and K. B. Chandran. Velocity and turbulence measurements past mitral valve prostheses in a model left ventricle. *J. Biomechanics.* 24:549-562. 1991.
49. Seidel, W. and W. Gross. Experimental investigations on the function of papillary muscles after prosthetic mitral valve replacement. *Surgery.* 61:802-807, 1967.
50. Spence P. A., C. M. Peniston, T. E. David, et al. Toward a better understanding of the etiology of left ventricular dysfunction after mitral valve replacement: an experimental study with possible clinical implications. *Ann. Thorac. Surg.* 41:363-371, 1986.
51. Subramanian, A., H. Mu, J. R. Kadambi, et al. Particle image velocimetry in the investigation of intravalvular flow fields of a bileaflet mechanical heart valve in a pulsatile flow. *J. Heart Valve Dis.* 9: 721-731, 2000.
52. Texas Heart Institute. The Heart. March 2002. <<http://www.tmc.edu/thi/anatomy.html>>.
53. Tsakiris, A. G., D. A. Gordon, Y. Mathieu, and I. Lipton. "Time-motion of both mitral leaflets early in diastole." In: *The Mitral Valve. A Pluridisciplinary Approach*, edited by D. Kalmanson. London: Edward Arnold, 1976, pp.27-32.
54. Walker, P. G., E. M. Pedersen, S. Oyre, et al. Magnetic resonance velocity imaging: a new method for prosthetic heart valve study. *J. Heart Valve Dis.* 4:296-307, 1995.
55. Westerweel J. *Digital Particle Image Velocimetry, Theory and Application*. Delft University Press, 1993.
56. Wiggers, C. J. and L. N. Katz. The contour of the ventricular volume curves under different conditions. *Am. J. Physiol.* 58:439-475, 1922.
57. Willert C. E. and M. Gharib. Digital particle image velocimetry. *Experiments in Fluids.* 10:181-193, 1991.
58. Williams, A. R. Release of serotonin from human platelets by acoustic microstreaming. *J. Acoust. Soc. AM.* 56:1640-1643, 1974.
59. Woo, Y. and A. P. Yoganathan. In vitro pulsatile flow velocity and shear stress measurements in the vicinity of mechanical mitral heart valve prostheses. *J. Biomechanics.* 19:39-51, 1986.

60. Yacoub, M. "Anatomy of the mitral valve chordae and cusps." In: *The Mitral Valve. A Pluridisciplinary Approach*, edited by D. Kalmanson. London: Edward Arnold, 1976, pp.15-20.
61. Yoganathan, A. P., J. T. Ellis, T. M Healy, and G. P. Chatzimavroudis. Fluid dynamic studies for the year 2000. *J. Heart Valve Dis.* 7:130-139, 1998.

Vita

On June 23, 1978, Amber Rae Phillips was born the only child to Bradley R. and Deborah D. Phillips in Parkersburg, West Virginia. As a child, she loved to talk with others and most enjoyed reading and playing softball. She attended Parkersburg High School where she received many honors and graduated 1st in the class of 1996. She earned her Bachelor of Science Degree, Summa Cum Laude, in Engineering Science and Mechanics from Virginia Polytechnic Institute and State University in August 2000. On March 10, 2001, she became Amber Rae Mace when she was united in marriage to Kevin Michael Mace in Parkersburg, West Virginia. She defended her thesis on December 16, 2002 and graduated with her Masters Degree in Engineering Mechanics in May 2003. In the spring of 2003, Kevin and Amber joyfully welcomed a baby girl, Charis Rae, into the world.